

ELECTROMIGRATION INDUCED INTERFACE REACTION  
IN CU-WIRE/AL-PAD DIFFUSION COUPLE

By

PATRICIA ARACELLY RODRIGUEZ-SALAZAR

DISSERTATION

Submitted in partial fulfillment of the requirements  
For the degree of Doctor of Philosophy at  
The University of Texas at Arlington  
December, 2016

Arlington, Texas

Supervising committee:

Choong-Un Kim, Supervising Professor  
Nancy Michael  
Harry Tibbals  
Yaowu Hao  
Kyung Suk Yum

## ABSTRACT

### ELECTROMIGRATION INDUCED INTERFACE REACTION IN CU-WIRE/AL-PAD DIFFUSION COUPLE

PATRICIA ARACELLY RODRIGUEZ-SALAZAR, PhD

The University of Texas at Arlington, 2016

Supervising Professor: Choong-Un Kim

This dissertation presents experimental observations that may assist the understanding of electromigration (EM) failure mechanism active in Cu wire and Al thin film pad (wire bond). This study is motivated by an ongoing industrial effort to adapt Cu as wire bonding material for interconnection. Traditional material used for the wire bond has been Au; however, its high cost combined with its susceptibility to reliability failure caused by excessive growth of IMCs (IMC) makes Cu to be an attractive replacement. Though, since an application of Cu to wire bond technology is relatively new, many of reliability failure mechanisms are unknown especially the ones related to EM reliability as it is increasingly serious in limiting useful life of wire bond. This makes the investigation on EM failure mechanism in Cu to be necessary.

One of the most challenging difficulties of EM study is the isolation of the EM from any other effects on the failure process such as an increase in temperature by Joule heating. The Joule heat effect is of particular concern because it is expected to be considerable at wire bond configuration, making failure by EM to proceed concurrently with other failure mechanisms. Our

investigation then begins with design of test structure that can prove that wire bond failure is indeed induced by EM, and progresses towards understanding microscopic mechanism by which wire bond becomes failure prone by EM.

Therefore, this study proposes the use of a special configuration sample where two interfaces can be tested at the same temperature and current density conditions. The design of the sample includes a two-level interconnect structure pattern on Si substrate where a short strip conductor allows flow of test current from one pad to another. The short distance combined with heat-conduction through Si substrate assists the minimization of temperature gradient between the two interfaces. This design helps to isolate the EM effect over other factors that could contribute to the interface degradation such as Joule heating.

The samples are then subjected to various testing conditions of temperature and current density and it is indeed found that there exists a difference in the failure kinetics when the interfaces are compared: the pad where current flows from pad to wire (mass flow is from the wire to pad) always fails faster than the opposite case. If it is considered that both interfaces have been tested at the same temperature and current density, the only factor contributing to this difference will be the EM because it is directional.

The dependence of failure rate on the pad in respect to the direction of current flow is also found in Au-Al wire bond which is also tested for comparison purpose. This result indicates that the A-Al and Cu-Al wire bond shares the same failure mechanism when electric current is applied and provides further evidence that EM plays a critical role in inducing degradation in the interface integrity. When the EM failure kinetics of the first failing pad of samples are collected, and analyzed, they are found to follow the classic "Black's equation" that relates the failure rate to current density and test temperature; the failure rate shows current density dependence with

exponent close to 2 for both Cu-Al and Au-Al wire bonds and temperature dependency with an activation energy of  $\sim 1.2\text{eV}$  for Cu-Al and  $0.9\text{eV}$  for Au-Al. While Au-Al and Cu-Al wire bonds do not show typically different EM failure parameters, overall life of Cu-Al wire bond is notably higher (nearly one order of magnitude). This suggests that EM life enhancement in Cu-Al is mainly due to slower diffusion rate of species at the interface, which is consistent with other observations reporting slower IMC growth rate in Cu-Al than in Au-Al wire bond interface.

In order to understand the EM mechanism leading to failure, microstructure of the interface is closely inspected after EM testing. This study shows that the growth of IMC is enhanced at the failing pad where EM forces IMC to grow into Al pad. Both Cu-Al and Au-Al shows the same trend, that is that the growth of IMC is substantially enhanced by EM when it is directed from the wire to the Al pad. This is consistent with a common expectation that the growth of IMC layers leads to the interface failure and EM makes the failure to be accelerated by speeding up their growth. However, it is noticed that there exists a distinctive difference in failure morphology between Au-Al and Cu-Al wire bond interface. The difference is that the damage at Au-Al interface appears as an extended voiding, while such voiding is absent in case of Cu-Al interface. Instead, it appears that the damage proceeds by the growth of cracks. It is believed that slow interdiffusion rate in Cu-Al interface makes the Kirkendall voiding to be suppressed from its formation while other factors like interface strain becomes primary factor responsible for interface failure.

Although EM failure mechanism in Cu-Al wire bond interface is microscopically understood by the use of the theory that EM forces IMC growth to be accelerated when it directs atomic flux towards Al pads where short-circuit diffusion path is available, the difference in activation energy between EM failure and thermal growth rate of IMC phases appears to disagree



with the theory. However, EM failure involves multiple processes such as crack initiation and growth in addition to IMC growth, it is possible that its activation energy may not necessarily be the same to that of thermal IMC growth. It is our belief that the cracking is delayed at higher temperature because of active stress relaxation process while such process is suppressed at lower temperature. This can make the activation of EM failure to be higher than that of IMC growth.

On the other hand, the microscopic mechanism of EM failure established in this study also provides a reasonable explanation on an abnormal failure behavior at the interface. As is indicated, the failure always occurs faster at the pad where EM flux is directed toward Al pad. However, the rate of failure development is actually the opposite in the beginning EM testing. Initially, the failure rate measured by the interface resistance change is higher at the pad where EM flux is directed toward wire. With progressing of EM, its rate decreases and is eventually slower than the opposite case. This crossover in failure rate does not appear in case of Al-Au wire bond interface but is unmistakably existing in Cu-Al wire bond. This is found to be related to the interplay between the type of IMC phase forming at given time and its contribution to the interface resistance. In the pad where EM is directed toward Cu wire, the growth of high resistance  $\gamma - Cu_9Al_3$  phase is initially more active because EM flux is against the direction of Cu diffusion. As EM progresses, with slow migration of Cu into Al pad, the growth of IMC phases in Al pad is generally suppressed, leading to slower increase in interface resistance. This agrees well with the microstructural mechanism found in our study.

So as to better understand EM mechanism, the growth of IMC phases without EM load is investigated by subjecting the samples to only thermal condition. This study is done to compare IMC growth behaviors with and without EM, and also to determine the fundamental mechanism of IMC growth in Cu-Al; wire bond. This study leads to the conclusion that there are three IMC

phases possible to grow at interface, and they are  $\alpha_2 - Cu_3Al$ ,  $\gamma - Cu_9Al_4$  and  $\theta - CuAl_2$ . Interdiffusion makes the  $CuAl_2$  phase to form first in Al pad because Al provides fast diffusion path for Cu due to abundant grain boundaries. This gradually consumes Al pad while a portion of  $CuAl_2$  is replaced for  $Cu_9Al_4$ . Finally, Cu rich phase,  $Cu_3Al$ , forms at Cu wire side but its growth is very sluggish due to lack of diffusion short-circuit. As consequence, the three IMC layers form at the interface, mostly consuming Al pad with time. The growth rate of the total IMC layer thickness, all phases combined, follows an ideal diffusion controlled growth kinetics showing  $(t)^{1/2}$  dependence. The activation energy for the growth is observed to be  $\sim 0.5$  eV, which is far lower than that of EM failure.

While our investigation has yielded reasonably self-consistent EM failure mechanism active in Cu-Al wire bond, there still exists a number of subjects that await further investigation. Among many, the question as to the type of IMC phases possible to form at Cu-Al interface requires careful and extensive investigations. The source of stress that initiates the cracking and the type of IMC phase affecting such progress is an unanswered but critical question not only for understanding the fundamental mechanism of interface structure but also for finding ways to improving EM reliability of Cu/Al wire bonds.

Copyright © by

Patricia Aracelly Rodriguez-Salazar

2016

## ACKNOWLEDGMENTS

First and above all, I praise God, the almighty for providing me this opportunity and granting me the capability to proceed successfully. This dissertation appears in its current form due to the assistance and guidance of several people. I would, therefore, like to offer my sincere thanks to all of them.

I offer my sincerest gratitude to my supervisor, Dr. Choong-Um Kim, who has supported me throughout this pathway with his patience and knowledge whilst allowing me the room to work in my own way. I attribute the level of my Ph.D. degree to his encouragement and effort and without him, this dissertation would not have been completed or written. I simply could not wish for a better supervisor. My deep gratitude also goes to my committee members Dr. Yaowu Hao, Dr. Kyung Suk Yum, Dr. Harry Tibbals and especially Dr. Nancy Michael for their suggestions and advice.

In my daily work, I have been blessed with a friendly and cheerful group of fellow students and group members: Dr. Mingyoung Kim, Dr. Lianshan Chen, Dr. Huili Xu, Codie Mishler, Yang Li, Po-Cheng Lu, Huandi Gu, Eunmee Kim, Himanshu Naik, and Valery Ouvarov-Bancalero.

I will be always grateful to Kermit Beird, Sam Williams, Jennifer Standlee and Beth Robinson because without their help and wise advice any project I have been involved in, would not have the expected results.

I cannot forget the moral support received from very good friends I met when I arrived here and old friends that I left behind: Antonio Alanis, Gladys Rojas, Paula Umbarila, Julián Lizarazu, Ximena Zuñiga, Luz María Jiménez, Eduardo Arteaga, Gabriel and Michelle Colorado,

Derek and Winnie Wong, Teresita Mina, Paulina Yacelga, María Isabel Chavez, Ana Lucía Herrera, Tania Torres and José Luis Rivadeneira.

Finally, I would like to thank my beloved parents, Galo and Rosita, my sisters Gaby and Cris, my brother Pablo, and my brother and sister in law Danny and Ely for supporting me throughout my studies and believe in me, but special thanks go to my granny Milita who is the pillar of my life, without her guidance, patience, love and advice I could not have reached this or any other goal.

December, 2016

## TABLE OF CONTENTS

1. INTRODUCTION .....	1
1.1 Overview .....	1
1.2 Au/Al system vs. Cu/Al system in the wire bonding process .....	3
1.3 Factors affecting wire bonding reliability .....	10
1.4 Objectives of this study .....	10
2. BACKGROUND .....	12
2.1 Wire bonding .....	12
2.2 Diffusion .....	14
2.2.1 Hume-Rhotery rules .....	17
2.2.2 Diffusion paths .....	18
2.2.2.1 Lattice diffusion .....	20
2.2.2.2 Grain boundary diffusion .....	23
2.2.2.3 Dislocation pipe diffusion .....	31
2.2.2.4 Surface diffusion .....	34
2.3 Intermetallic compounds .....	35
2.3.1 Mechanisms of diffusion in intermetallic compounds .....	36
2.3.2 Intermetallic formation in binary systems .....	39
2.3.3 Intermetallic compounds in Au-Al systems .....	41
2.3.4 Intermetallic formation in Cu-Al systems .....	45
2.4 Electromigration .....	48
2.4.1 Failure by elecromigration .....	49
2.4.2 Electromigration and current density: Black's equation .....	51

3. EXPERIMENTAL METHODS.....	53
3.1 Test chip .....	53
3.2 Sample package .....	54
3.3 Electromigration testing .....	56
3.4 Test conditions.....	57
4. ELECTROMIGRATION FAILURE KINETICS AND MECHANISM .....	59
4.1 Characteristics of electromigration failure in wire bond .....	60
4.2 Electromigration failure kinetics .....	66
4.3 Intermetallic phase growth by aging .....	71
4.4 Intermetallic compound formation in Cu-Al diffusion couple.....	76
4.5 Failure mechanism analysis.....	82
4.5.1 Effect of electromigration on the intermetallic compound growth mechanism ...	82
4.5.2 Mechanism of failure rate change in Cu-Al wire bond interface.....	85
4.6 Summary and discussion .....	91
4.6.1 IMC formation in Cu-Al system.....	91
4.6.2 Failure mechanism by electromigration.....	97
5. SUMMARY AND CONCLUSIONS .....	99
6. REFERENCES .....	101
7. BIOGRAPHICAL INFORMATION.....	113

## LIST OF FIGURES

Figure 1: The virtuous circle of the semiconductor industry .....	2
Figure 2. (a) Feature size scaling trend , (b) Current density .....	3
Figure 3. Au-Al phase diagram.....	4
Figure 4. World copper and gold production and forecast .....	5
Figure 5. Copper and gold price comparison .....	5
Figure 6. Cu-Al phase diagram ' .....	8
Figure 7. Wire bonding process .....	13
Figure 8: Transition path.....	16
Figure 10: Diffusivity paths .....	18
Figure 11: Diffusion spectrum of metals .....	19
Figure 12: Grain boundary: (a) tilt, (b) twist .....	24
Figure 13: (a) Low angle tilt boundary, (b) Low angle twist boundary: ○ atoms in a crystal below the boundary, • atoms in a crystal above the boundary .....	25
Figure 14: Random high-angle grain boundary .....	25
Figure 15: Variation of grain boundary energy with misorientation (schematic) .....	26
Figure 16: Left: coherent twin boundary, right: incoherent twin boundary .....	26
Figure 17: Twin boundary energy as a function of the grain boundary orientation .....	27
Figure 18: Fisher model of an isolated grain boundary .....	27
Figure 19: Diffusion regimes in a polycrystal according to Harrison classification .....	30
Figure 20: Smoluchowski model of a dislocation pipe .....	32
Figure 21: Various points and line defects on a vicinal crystal/vapor surface .....	34
Figure 21. Schematic comparison between IMCs and standard alloys .....	35



Figure 22. Schematic diagram showing the sequence in phase formation in the Au-Al thin film according to Majni et.al. ....	44
Figure 23. Schematic illustration showing the IMC evolution during aging at 150°C, 175°C, 250°C and 350°C. The time axis is in log scale .....	47
Figure 24. Electromigration representation .....	48
Figure 25: Thermal acceleration loop during electromigration .....	50
Figure 26. Schematic representation of the two-level test structure .....	53
Figure 27. Cu(Au)-wire/Al-pad wire bonded sample .....	55
Figure 28. Short wire (left) and long wire (right) internal configuration .....	56
Figure 29. Test schematics.....	57
Figure 30. Failure signal from S-Au samples: (a) S1 failure signal, (b) S2 failure signal and (c) Sample temperature .....	61
Figure 31. Failure signal for L-Cu samples .....	63
Figure 32. Failure signal for S-Cu samples .....	63
Figure 33. Failure signal for wire bonded samples (a), (c), (e) Cu-Al system, (b), (d), (f) Au-Al system .....	65
Figure 34. Cumulative probability: (a) S-Au, (b) L-Cu and (c) S-Cu .....	66
Figure 35. Activation energy based on MTTF.....	68
Figure 36. Current exponent based on MTTF .....	68
Figure 37. SEM micrographs that according to failure criteria: (a) and (b) not failed sample, (c) and (d) failed sample.....	70
Figure 38. Series of SEM micrographs showing Cu-Al wire bond interface microstructure as a function of aging at 160°C .....	71

Figure 39. Series of SEM micrographs showing Cu-Al wire bond interface microstructure as a function of aging at 180°C .....	72
Figure 40. Series of SEM micrographs showing Cu-Al wire bond interface microstructure as a function of aging at 190°C .....	72
Figure 41. Series of SEM micrographs showing Cu-Al wire bond interface microstructure as a function of aging at 200°C .....	73
Figure 42. Time exponent based on aging time .....	74
Figure 43. Plot showing the kinetic constant k of IMC phase growth as a function of aging temperature .....	75
Figure 44. IMC formation: (a) as received sample, (b) interface aged at 160°C and (c) EM tested S2 interface for 1600h at 160°C and 1.75A .....	77
Figure 45. Cross-sectional microstructure of Cu/Al interface .....	78
Figure 46. X-ray diffraction for a sample aged at 400°C .....	79
Figure 47. Enlarged view of Figure 46 near $\theta$ -CuAl <sub>2</sub> .....	79
Figure 48. X-ray diffraction of a sample aged at 450°C .....	80
Figure 49. IMC phases in a sample aged at 450°C .....	81
Figure 50: Schematics of S1 and S2 after wire bonded process .....	82
Figure 51. Schematic representation of intermetallic compound growth under electromigration	84
Figure 52: Signal obtained from S1 and S2 under EM conditions .....	85
Figure 53: Wire bonded interfaces at t = 0 .....	86
Figure 54: Wire bonded interfaces at a time t1 between 0 < t < tc .....	88
Figure 55: Wire bonded interfaces at a time t2 between 0 < t < tc .....	88
Figure 56: Wire bonded interfaces at a time t3 between 0 < t < tc .....	88

Figure 57: Wire bonded interfaces at a time $t > t_c$ .....	89
Figure 58. Magnified image of intermetallic formation in S1 and S2. EM testing conditions: 160°C and 1.75A .....	89
Figure 59: SEM micrographs, the arrow shows the direction of the electron flow. EM testing conditions: 160°C and 1.75A .....	90
Figure 60. As received Cu-Al wire bonding sample.....	92
Figure 61. Capillary .....	93
Figure 62. Schematic of residual stress distribution .....	94

## LIST OF TABLES

Table 1. Comparison of wire bonding material properties .....	6
Table 2. Comparison of heats of formation between Cu-Al and Au-Al IMCs .....	7
Table 3. Structural information for the IMC formed in the Cu-Al system.....	9
Table 4. Properties of Cu-Al IMCs found at temperatures below 500°C .....	9
Table 5: Wire bonding technologies .....	14
Table 6. Al, Au and Cu characteristics .....	18
Table 7. Hume-Rothery rules for Al, Cu and Au.....	18
Table 8: Numerical factor q .....	31
Table 9: Diffusion in IMCs .....	37
Table 10: Structural information for the IMC formed in the Al-Au system.....	42
Table 11: List of interface transformations determined by Xu et.al. ....	43
Table 12: Formation enthalpies of the low-temperature Al-Au phases .....	45
Table 13. Electromigration conditions for different samples .....	59
Table 14. Aging test conditions for S-Cu samples .....	59
Table 15. Activation energy (Q) for IMC growth in Cu/Al bonds .....	75
Table 16. Cu-Al intermetallics characteristics .....	86
Table 17: Average thickness measured in an electromigration tested sample.....	91
Table 18. Interdiffusion coefficients based on Wagner's equation.....	91

## CHAPTER 1

### 1. INTRODUCTION

#### 1.1 Overview

It is apparent that microelectronics advent has opened doors to new horizons where integrated circuits have played an important role from the very beginning of their creation since the late 1950s, when Jack St. Clair Kilby, a Texas Instruments Engineer, decided to change the future, conceiving the first integrated circuit, where the components, passive as well as active, were placed over a piece of semi-conductive material (Germanium piece) that was half the size of a paper clip. The success of this element (called chip due to its small size) containing a few transistors, resistors, and capacitors, led to the Physics Nobel Prize for its inventor in 2000.

The design of an integrated circuit involves a development plan, where its functional characteristics and performance will define the elaboration of the logic circuit diagram. Once the diagram is finished, a series of simulations are executed to test the operation of the designed circuit; if no issues are encountered, a massive production plan is implemented. This manufacturing process has allowed the miniaturization of most of the devices used daily, translating to lower production costs. The manufacturing of IC devices consists of two major steps. The first is to produce IC circuits on Si wafer. The second is to assembly the device into a package so that it can be interface with outer circuits such as the system board. The typical packaging process involves the interconnection of the integrated circuit chips to the lead frames in order to connect them electrically; this connection is called bonding and it is usually made by using very thin wires<sup>1</sup> (wire bonding). Consequently, the practice of these modern fabrication processes has made possible the integration of massive quantities of electronic elements in tiny chips, which has

connoted an enormous advance in the technology field, meaning the beginning of increased complexity in the design of integrated circuits (Figure 1).

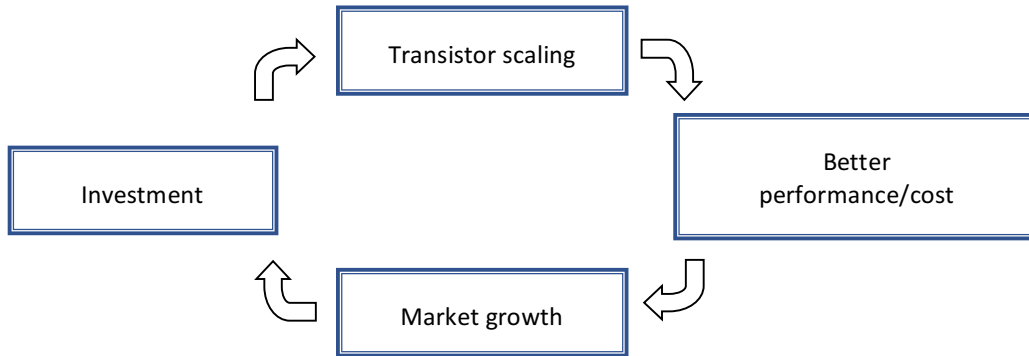


Figure 1: The virtuous circle of the semiconductor industry

However, this constant size reduction has also introduced phenomena that affect the reliability of the devices. Figure 2 (a) illustrates how miniaturization has evolved with time. Such miniaturization inevitably forces the devices to carry exponentially high current density as shown Figure 2 (b). The most seriously affected IC component by increased current density is the interconnects within the chip. However, the level of increase in the current density has reached to the point of affecting reliability beyond on-chip interconnects. Among various interconnects of such kinds, wire bond that connects IC circuit on Si and lead frame is emerging as one of the main reliability threats in recent years. It is the place where reliability failure can occur under high current density because Joule heating and EM combined can occur in a considerable magnitude.

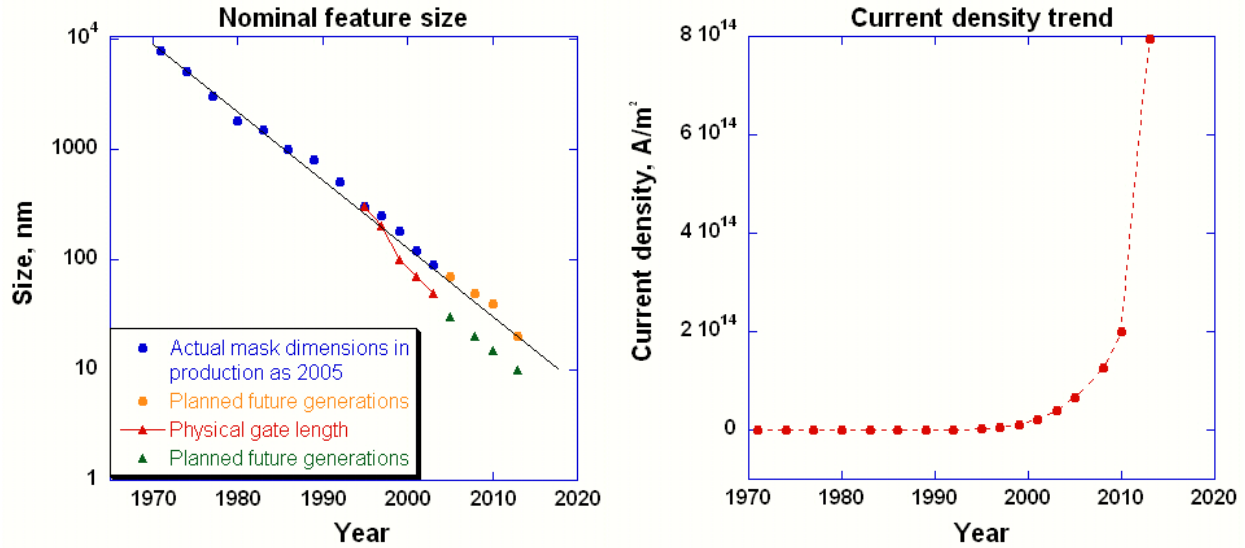


Figure 2. (a) Feature size scaling trend <sup>2</sup>, (b) Current density

## 1.2 Au/Al system vs. Cu/Al system in the wire bonding process

In the past, the use of Au-wire bonded to Al-pad on Si chip was widely used to interconnect the integrated circuits to the lead frame. The use of Au as wire bond material has offered various advantages as a package level interconnect. It is easy to wire bond to Al pad that is most common termination structure of IC interconnects. Further, Au is a material with an excellent electrical and thermal conductivity. However, such benefits are increasingly outweighed by two main factors, and they are poor reliability and high material cost. When the wire bond made by Au is exposed to thermal stress, a product of either Joule heating, high temperatures or both, metallurgical degradation as well as void formation occurs. It is known that such degradation process is triggered by the formation of IMC phases at Au-Al interface. Figure 3 shows the phase diagram of Au-Al system. As is shown, there are multiple IMC phase possible to form at interface by a process of interdiffusion. The formation of IMCs, mainly  $Au_5Al_2$  (aka white plague) and  $AuAl_2$  (aka purple plague) are known to induce interface failures (as a form of voiding) and limit the reliability of the

interconnection. This leads to Au wire bond systems unattractive for high power devices where current density is excessively high so that the device is likely to be operating at high temperature. In addition, another challenge emerged: Au price, its ever-increasing price (Figure 4) combined with poor reliability made it necessary to find an alternative material for the wire bond.

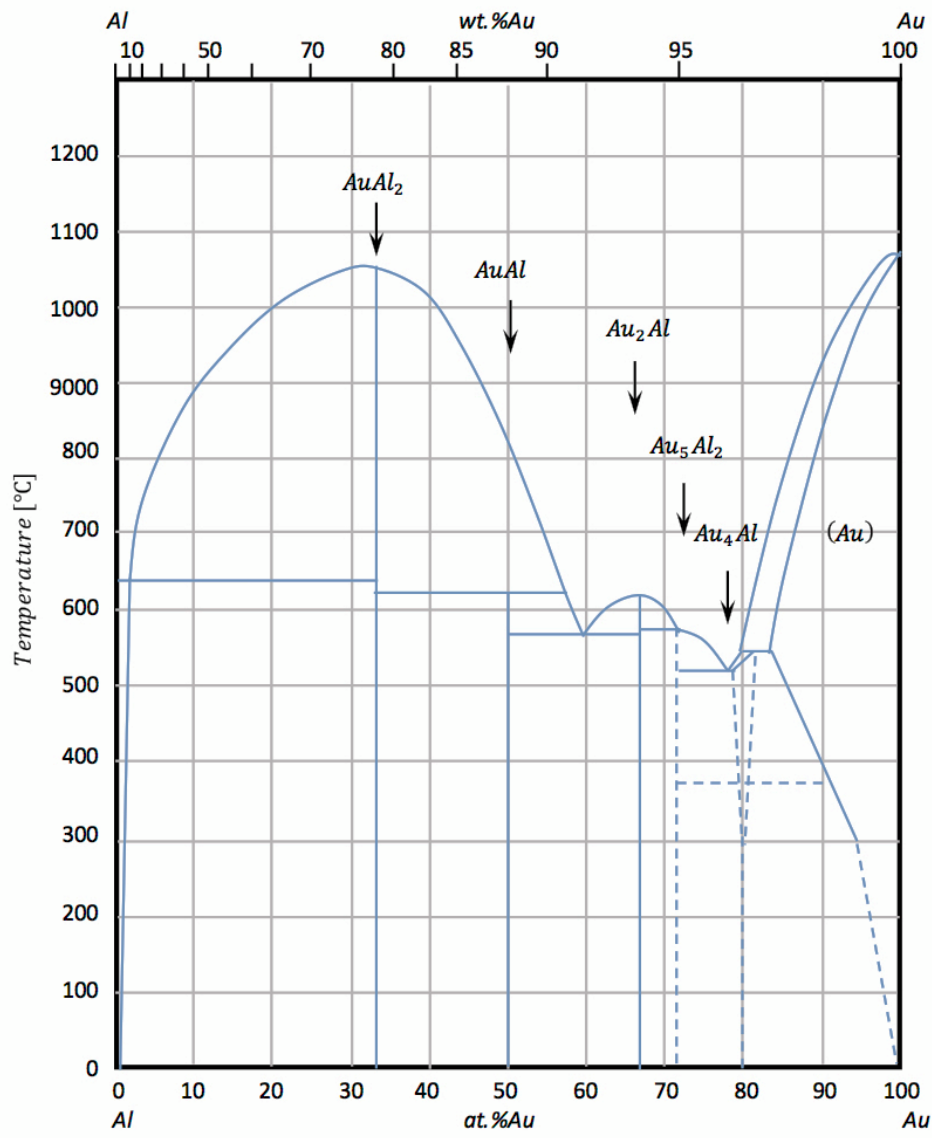


Figure 3. Au-Al phase diagram



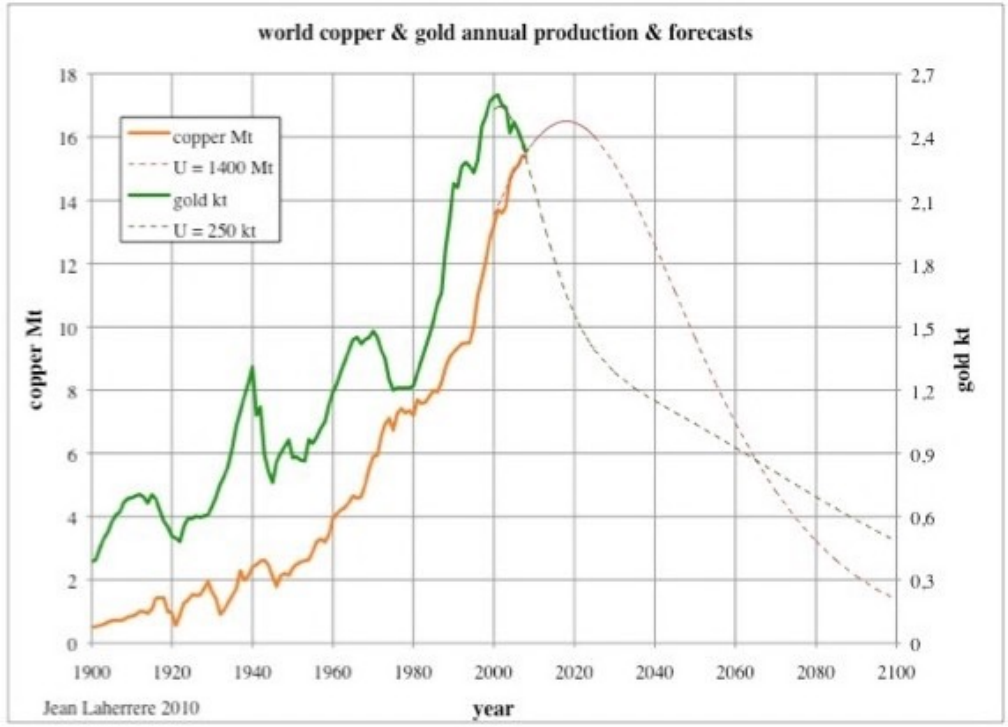


Figure 4. World copper and gold production and forecast <sup>3</sup>

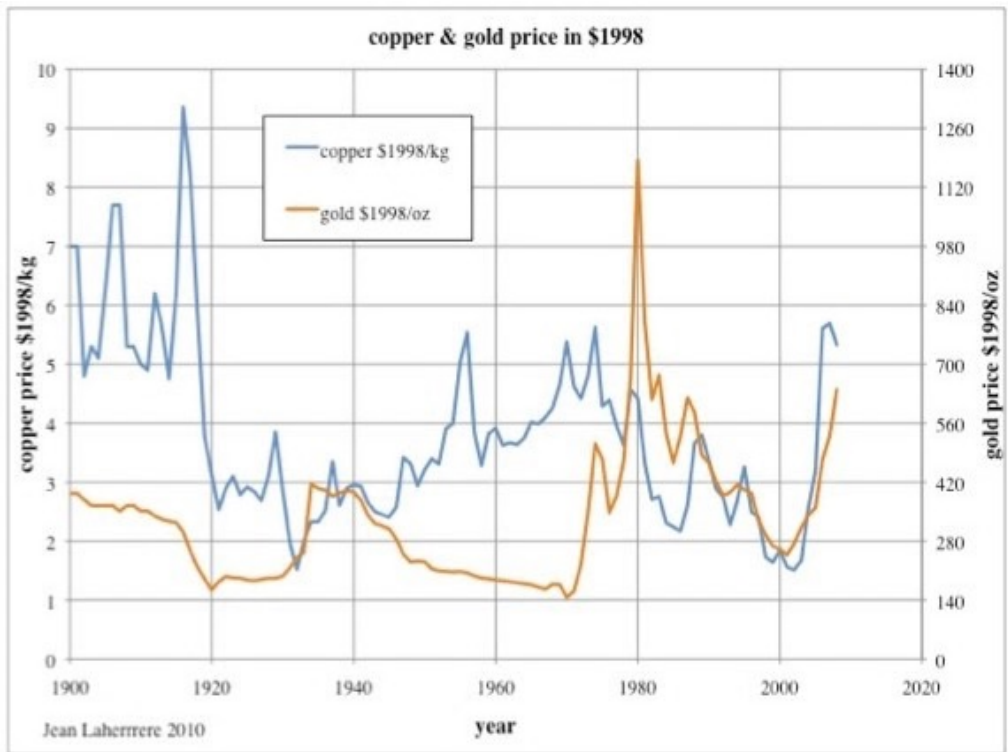


Figure 5. Copper and gold price comparison <sup>3</sup>

A search for an alternative material led to the development of Cu based wire bonding technology. Compared to Au, Cu is much cheaper as shown in Figure 5. Additionally, it provides better mechanical, electrical and thermal properties than Au. Table 1 presents comparison of Au and Cu properties.

Table 1. Comparison of wire bonding material properties

	Properties	Units	Cu	Au	Al
General	Atomic number	---	29	79	13
	Lattice structure	---	FCC	FCC	FCC
	Atomic radius <sup>4</sup>	pm	128	144	143
	Atomic mass <sup>5</sup>	g/mol	63.546	196.967	26.982
	Lattice constant <sup>6</sup>	Å	3.61	4.08	4.05
	Density @ 25°C <sup>4</sup>	g/cm <sup>3</sup>	8.92	19.30	2.70
Thermal and electrical	Melting point <sup>5</sup>	°C	1084.62	1064.18	660.32
	Thermal conductivity @ 25°C <sup>7</sup>	W/m-K	401.9	317.7	235.9
	Thermal expansion coefficient @ 25°C <sup>6</sup>	10 <sup>-6</sup> /K	16.5	14.2	23.1
	Electrical resistivity @ 20°C <sup>4</sup>	nΩ·m	16.78	22.14	28.2
	Electronegativity (Pauling scale) <sup>8</sup>	---	1.9	2.4	1.5
	Specific heat <sup>6</sup>	J/kg-K	384.4	129.1	904
Mechanical	Young's modulus <sup>6</sup>	GPa	130	78	70
	Tensile strength <sup>9</sup>	MPa	221-445	117.2	45
	Modulus of elasticity <sup>9,10</sup>	GPa	123	79	62
	Elongation in 50mm <sup>9,10</sup>	%	60	70	50
	Vickers hardness <sup>6</sup>	MPa	369	216	167
	Poisson ratio <sup>6,11</sup>	---	0.34	0.44	0.35

Furthermore, it is also noted that Cu has potentially better reliability against metallurgically driven interface failures. It is suggested that the growth rate of IMCs in the Cu-Al couple is about 1/10<sup>th</sup> of the growth rate for Au-Al at temperatures between 150°C and 300°C <sup>12, 13</sup>), which provides higher durability to Cu bond when compared to Au bond.

Slow growth of IMCs in Al-Cu may be attributed to two main reasons. The first is the fact that interdiffusivity in Al-Cu system is known to be far lower. In addition, there is a general tendency that IMC phase formation is more difficult in Al-Cu system. This can be seen from the heat of formation (HOF). Table 2 compares the heat of formation for the Cu-Al and Au-Al systems. Even though heat of is not a direct indicator for action kinetics, it does indicate the easiness of the reactions. The data shows that Au reacts more easily (more negative HOF) with Al than does Cu <sup>21</sup>.

Table 2. Comparison of heats of formation between Cu-Al and Au-Al IMCs <sup>21</sup>

<b>Au-Al system</b>		<b>Cu-Al system</b>	
Phase	Effective heat of formation [ <i>J/g atom</i> ]	Phase	Effective heat of formation [ <i>J/g atom</i> ]
<i>Au<sub>4</sub>Al</i>	-18.5	<i>Cu<sub>9</sub>Al<sub>4</sub></i>	-3.20
<i>Au<sub>5</sub>Al<sub>2</sub></i>	-20.0	<i>Cu<sub>3</sub>Al<sub>2</sub></i>	-4.25
<i>Au<sub>2</sub>Al</i>	-19.8	<i>Cu<sub>4</sub>Al<sub>3</sub></i>	-4.77
<i>AuAl</i>	-16.3	<i>CuAl</i>	-5.44
<i>AuAl<sub>2</sub></i>	-10.2	<i>CuAl<sub>2</sub></i>	-6.13
The negative sign implies that the formation of an IMC from its elements usually is an exothermic process.			

With the implementation of Cu wire bonding technology, the reaction between Al pad and Cu wire bonding has been investigated in recent years. These studies indicate that Cu wire bond on Al pad also promotes the formation of IMC phases. This is a natural consequence of thermodynamically driven process because Al and Cu also forms numerous IMC phases. These phases can be seen from the phase diagram shown in Figure 6, where equilibrium phases are shown as a function of Al content in Cu and temperature. It can be seen that various IMC phases form as Al content increases. A detailed description of the structural information in the Cu-Al IMC phases may be found in

Table 3, and the mechanical and electrical properties of the phases found below 500°C are listed in Table 4 (except  $\alpha_2 - Cu_3Al$ ).

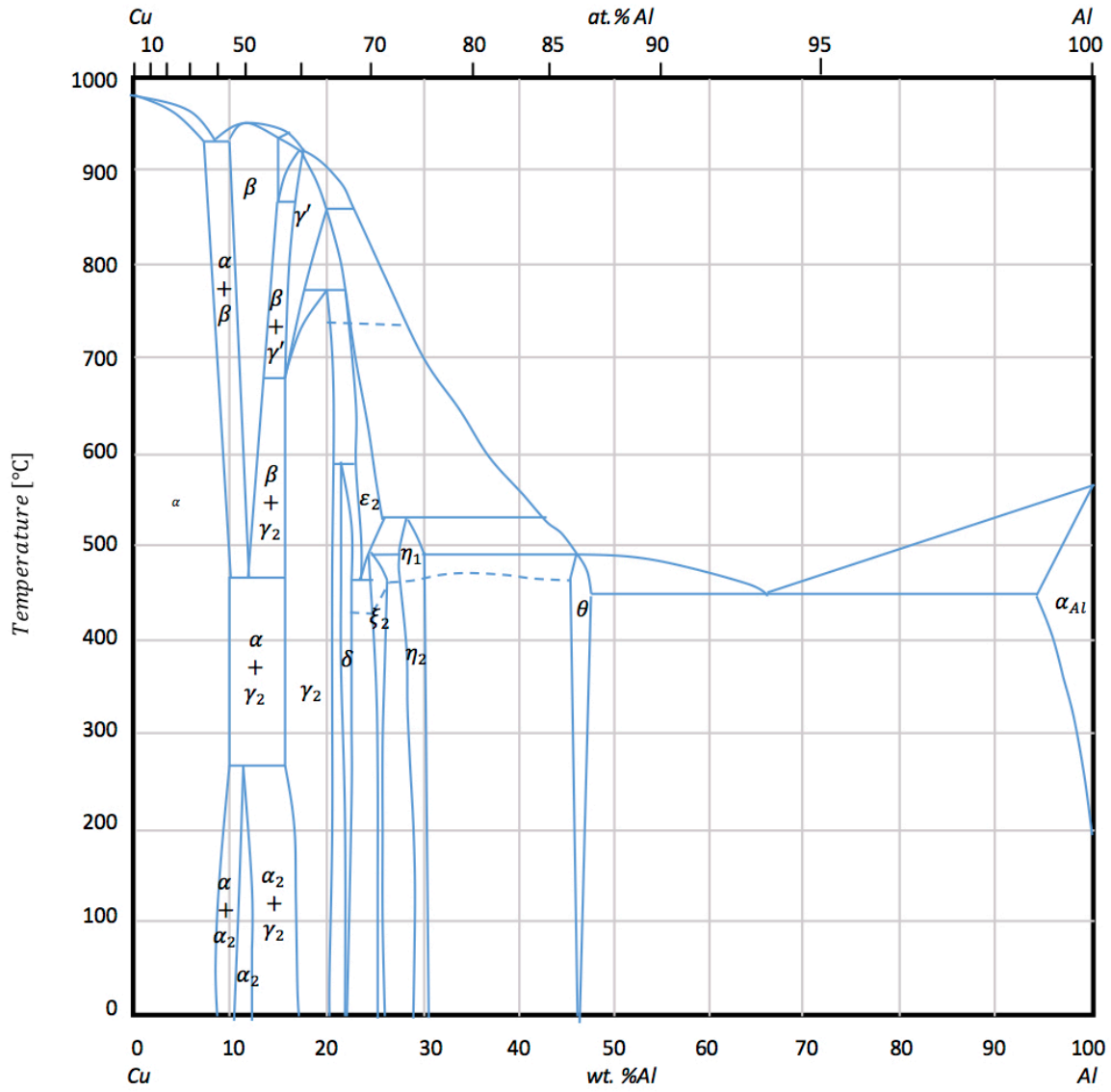


Figure 6. Cu-Al phase diagram<sup>14, 15</sup>

Table 3. Structural information for the IMC formed in the Cu-Al system

Phase	at. % Cu	Space group <sup>16</sup>	Crystal structure <sup>17</sup>	Lattice parameter
(Al)	0 – 2.84 <sup>16</sup>	Fm-3m	Cubic	$a = 4.05\text{\AA}^{16}$
$\theta - CuAl_2$	31.9 – 33.0	I4/mcm	Tetragonal	$a = 6.07\text{\AA}, c = 4.87\text{\AA}^{18}$
$\eta_1$	49.8 – 52.4 <sup>16</sup>	Cmmm	Orthorhombic	$a = 4.09\text{\AA}, b = 12.00\text{\AA}, c = 8.64\text{\AA}^{16}$
$\eta_2 - CuAl$	49.8 – 52.3 <sup>16</sup>	C2/m	Monoclinic	$a = 12.07\text{\AA}, b = 4.11\text{\AA}, c = 6.91\text{\AA}^{16}$ $\beta = 55.04^\circ^{16}$
$\xi_1 - Cu_4Al_3$	55.2 – 59.8 <sup>16</sup>	Fmm2	Orthorhombic	$a = 8.14\text{\AA}, b = 14.49\text{\AA}, c = 9.99\text{\AA}^{16}$
$\xi_2 - Cu_{4-\delta}Al_3$	55.2 – 56.3 <sup>16</sup>	Imm2	Orthorhombic	$a = 4.09\text{\AA}, b = 7.03\text{\AA}, c = 9.98\text{\AA}^{16}$
$\varepsilon_1$	59.4 – 62.1 <sup>16</sup>	Unknown	Unknown	---
$\varepsilon_2$	55.0 – 61.1 <sup>16</sup>	P6 <sub>3</sub> /mmc	Hexagonal	$a = 4.15\text{\AA}, c = 5.06\text{\AA}^{16}$
$\delta - Cu_3Al_2$	60.5 – 62 <sup>19</sup>	R3m	Rhombohedral	$a = 8.71\text{\AA}^{16}, \alpha = 89.74^\circ^{16}$
$\gamma_0$	59.8 – 69.0 <sup>16</sup>	I – 43m	Cubic	---
$\gamma_1 - Cu_9Al_4$	65 – 68.0 <sup>19</sup>	P – 43m	$\gamma$ – brass	$a = 8.71\text{\AA}^{16}$
$\beta_0$	67.6 – 70.2 <sup>16</sup>	Unknown	Unknown	---
$\beta$	70.6 – 82.0 <sup>16</sup>	Im-3m	Cubic	$a = 2.95\text{\AA}^{16}$
$\alpha_2 - Cu_3Al$	88.0 – 91.0 <sup>20</sup>	---	Cubic	$a = 3.65\text{\AA}^{20}$
(Cu)	91.0 – 100	Fm-3m	Cubic	$a = 3.61\text{\AA}^{16}$

Table 4. Properties of Cu-Al IMCs found at temperatures below 500°C

Phase	$CuAl_2$ ( $\theta$ )	$CuAl$ ( $\eta_2$ )	$Cu_4Al_3$ ( $\xi_2$ )	$Cu_3Al_2$ ( $\delta$ )	$Cu_9Al_4$ ( $\gamma_2$ )
Resistivity <sup>21</sup> , [ $\mu\Omega \cdot m$ ]	7.0 – 8.0	11.4	12.2	13.4	14.2 – 17.3
CTE <sup>21</sup> , [ $ppm/^\circ C$ ]	1.61	1.19	1.61	1.51	1.76
Density <sup>21</sup> , [ $g/cm^2$ ]	4.36	2.7	NA	NA	6.85
Young's modulus <sup>22</sup> , [ $MPa$ ]	123.5±6.6	180.2±12.5	180.2±12.5	174.4±19.5	186.8±9.0
Fracture toughness <sup>22</sup> , [ $MPa\sqrt{m}$ ]	0.27±0.66	0.20±0.03	0.21±0.05	0.68±0.15	0.67±0.10
Specific heat density <sup>22</sup> [ $J/kg \cdot K$ ]	@ 20°C	---	537	---	498
	@ 100°C	---	560	---	498
Thermal diffusivity <sup>22</sup> [ $m^2/s$ ]	@ 20°C	---	$3.0 \times 10^{-5}$	---	$8.4 \times 10^{-6}$
	@ 100°C	---	$2.3 \times 10^{-5}$	---	$1.0 \times 10^{-5}$
Thermal conductivity <sup>22</sup> [ $W/m \cdot K$ ]	@ 20°C	---	87	---	26
	@ 100°C	---	69	---	33

### 1.3 Factors affecting wire bonding reliability

It is known that IMC formation and growth plays a very important role in the wire bonding process because they form the metallurgical bond between the wire and the pad materials to provide the electrical interconnection, however, if the thickness of the IMC exceeds a critical thickness, the properties of the interface may degrade, due to two main reasons:

- Over a critical thickness, the IMC layer makes the bond to be subjected to failure by fracture because IMC layer is brittle and the bond interface is likely to under high thermal stress due to thermal expansion difference.
- High temperature by joule heating, exacerbated by poor thermal conduction of IMC layer, consequently, the growth and linkage of Kirkendall voids are possible.

Extended growth of IMC increases likelihood of Kirkendall void. Kirkendall void is a result of mass flux divergence during interdiffusion and it forms when the accumulation of vacancies (by depletion of mass) reaches a critical point. It should be noted that the IMC formation and growth can be significantly affected by EM. Under operation condition of devices, the Cu-wire/Al-pad interface, depending on the electrical current density and direction, and the working temperature, the reaction leading to IMC formation and mechanism may be affected by the presence of EM, can either promote or suppress the IMC formation and growth, and thus affect functionally the performance of the wire bonded interconnection and its physical reliability.

### 1.4 Objectives of this study

Even though there exist several studies investigated the IMC formation and growth in the Cu-Al system, most of them just take two factors affecting the bonding reliability into account: temperature and time. There is almost no comprehensive study on effect of EM on the bond

reliability especially with relation to metallurgical process occurring at interface. Therefore, this study aims to investigate the IMC growth mechanism in Cu-Al wire bond interface with a weighted emphasis on the mechanism by which IMC growth is affected by EM. Also aimed is to obtain engineering data that compares the kinetics of EM failure between Au-Al and Cu-Al.

The stated objective may appear simple but it poses a number of challenges and requires collaborated investigative strategies, starting from test sample structure and metallurgical analysis. To overcome such challenges and for successful investigations, we carry out the investigation with specified objectives:

- 1) First prove that EM is clearly affecting the failure kinetics beyond any doubt. This requires a sample structure that can compare EM failure rate with current direction because directional dependence is the hallmark evidence for EM involvement.
- 2) Conduct EM testing on number of samples with variation in current and temperature so that failure kinetics can be analyzed by the use of commonly adapted engineering process. This data can provide leads to understanding the metallurgical failure mechanism.
- 3) Compare EM failure kinetics of Cu-Al and Au-Al. This comparison provides information not only useful for engineering purposes but also for understanding the failure mechanism.

Characterize the IMC formation forming at interface with and without current. Comparison of type and kinetics of IMC formation at interface on those conditions can provide critical information required for identifying failure mechanism active at interface.

## CHAPTER 2

### 2. BACKGROUND

The aim of this study is to understand the EM induced failure mechanism in Al-Cu wire bonding interface in comparison with that in the Au-Al. The study requires understanding of multiple background subjects, starting from the process of wire bonding to mechanisms leading to failure. For this reason, this chapter presents a brief description of background information.

#### 2.1 Wire bonding

There exist several processes that provide the connection that makes possible the power supply and distribution signal between chip and substrate, such as flip chip soldering or solder bumps, among others; however, wire bonding is still the most common, being currently responsible for more than 90% of today's chip interconnects <sup>23</sup>. The wire bonding process is described in Figure 7:

- 1) Electric flame off (EFO) fires forming a ball.
- 2) Tool descends to form the first bond.
- 3) Force applied to form the ball bond on chip side connection.
- 4) Tool ascends to top of loop.
- 5) Formation of the loop.
- 6) Tool descends and forms the wedge bond on the lead frame.
- 7) Tool ascends to start the wire bonding cycle again.



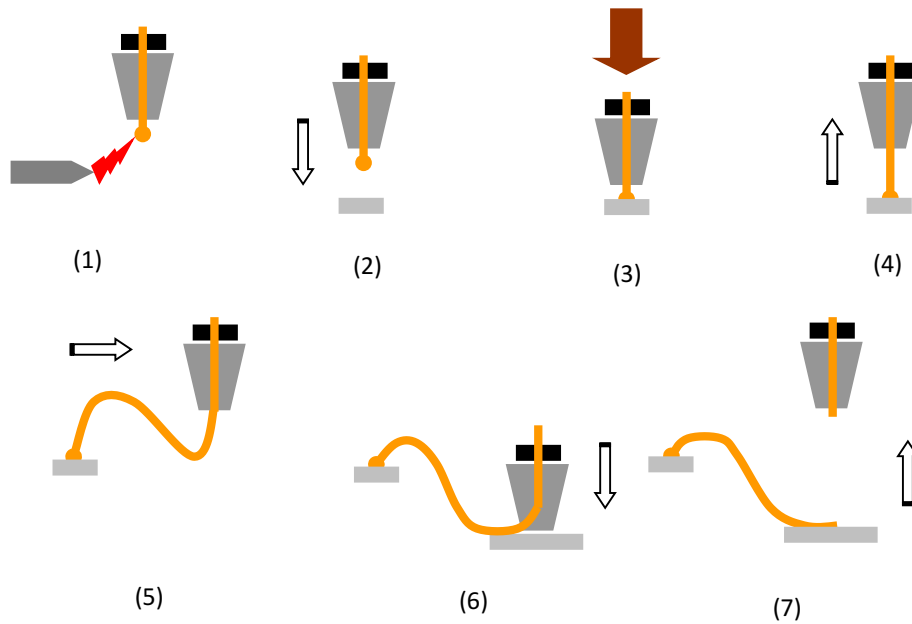


Figure 7. Wire bonding process

There are three different technologies used in wire bonding processes: thermo-compression (TC), ultrasonic (US) and thermo-sonic (TS). Thermo-compression technology requires a relatively high force to reach the bonding as well as high interface temperatures (above 300°C<sup>24</sup>) combining basically heat and force to plastically deform the joint points, therefore, it is sensitive to surface contaminants a reason by which it requires clean surfaces. Ultrasonic technology, unlike thermo-compression, does not require high temperatures and in fact, is performed at room temperature and relatively low forces; its operating frequency is a function of the size of the structure to be soldered, i.e. higher the frequency smaller the components. While thermos-sonic technology combines ultrasonic energy and heat<sup>4</sup> to produce the bonding, the temperatures used by this technology typically fluctuate between 125°C and 220°C and like the ultrasonic technology it requires low forces to form the bonding.

Table 5 shows a summary of the characteristics of the wire bonding technologies.

Table 5: Wire bonding technologies <sup>25</sup>

<b>Wire bonding</b>	<b>Thermo-compression</b>	<b>Thermo-sonic</b>	<b>Ultrasonic</b>
Ultrasonic power	No	Yes	Yes
Bonding force	High	Low	Low
Temperature	300 – 500°C	120 – 220°C	Room temperature
Bonding time	Long	Short	Short
Contamination	Strongly affected	Middle	Middle

Among the mentioned technologies, it is the thermo-sonic technology the one used in the fabrication of the samples provided in this study, because it minimizes the cratering damage to the semiconductor chip when the bonding force is applied.

Each method mentioned above has its own advantages and disadvantages. However, when it comes to an issue of reliability, there is a general commonality that IMC formation plays a key role. The formation of IMC is essential because it enables stable and strong metallurgical bond between the pad and substrate. However, its excessive growth is detrimental to the reliability because IMC layers makes the interface to be prone to mechanical failure because of their brittleness <sup>26</sup> and also the process leading to its growth can result in interface cracks and/or voids. It is therefore important to understand how IMC phase forms and grows under thermal and electrical conditions in order to find a way to manage the reliability of the bond to a proper level <sup>27</sup>.

## 2.2 Diffusion

In a perfect crystal lattice, there are no defects and therefore, atomic movement is restricted to thermal vibration about their stable positions. However, in a normal crystal lattice there exist a number of defects that allow movement of atoms over a distance over time. This process of atomic transportation is called diffusion. Several diffusion mechanisms are possible to exist depending on the defect present in the material and on the site where the diffusing atoms occupy in the host

crystal lattice. Point defects, such as vacancies, impurities, and interstitial ions promote lattice (bulk or volume) diffusion, while along the line and surface defects, for example, dislocations, grain, and twin boundaries, etc. occur a diffusion process known as short-circuit diffusion. In general, linear, planar and surface defects provide a high diffusivity path for atomic diffusion because their activation energies are lower compared to that one required when diffusion occurs through point defects.

In principle, diffusion consists of two components: driving force and kinetics. The driving force for diffusion can be understood by using the framework of thermodynamics; the equilibrium state of a system can be predicted through the calculation of the driving force ( $\Delta G$ ) for a transformation from a metastable state (initial state) to a stable equilibrium state (final state). If a transition from a metastable to the equilibrium state is considered, the transformation between the initial and final states involves rearrangement of atoms, which imply that the system should go through a transformation (or reaction) path. Since the initial and final states could be metastable or stable, the energy of the system decreases along any transformation path between them as seen in Figure 8:

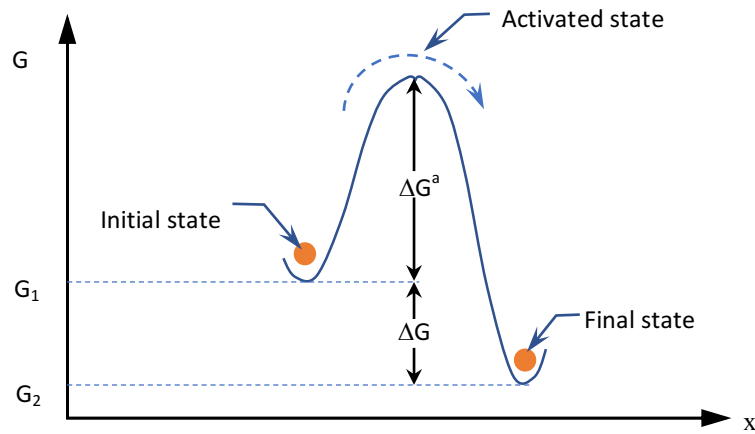


Figure 8: Transition path

In Figure 8,  $G_1$  and  $G_2$  are the Gibbs free energies of the initial and final states of the system, respectively,  $\Delta G^a$  is the activation free energy barrier, while the driving force is given by:

$$\Delta G = G_2 - G_1$$

Most kinetic processes in materials comprise diffusion, it is so that inhomogeneous materials can become homogeneous by diffusion as well as compositions of phases can change by diffusion. However, in order for diffusion to occur the system has to acquire enough energy to overcome the energy activation barrier; this energy can be obtained from thermal fluctuation, a process that is called thermal activation. So, the possibility of reaching this thermal fluctuation (rate at which process occurs), depends exponentially on temperature, phenomenon that can be described by the Arrhenius equation which is in general applied to thermally activated process:

$$rate \propto \exp\left(-\frac{G^a}{k_B T}\right)$$

Generally, the diffusion process requires a certain degree of miscibility between solute and the solvent, and the rules established by Hume-Rothery, factors that impact the solubility in a particular system.

### 2.2.1 Hume-Rhotery rules

Hume-Rhotery found two sets of rules that in most of the cases apply to interstitial and substitutional diffusion, which represents a strong guideline for intermetallic formation and system solubility prediction. According to Hume-Rhotery rules, in order for two elements to be soluble, there should meet specific conditions, otherwise, mixture of two elements would result in IMC phase formation. As previously stated, both Cu and Au wire bond on Al pad forms multiple IMC phases. Such IMC formation is inevitable and it is well predicted by the general rules established by Hume-Rhotery. According to Hume-Rhotery, a solute added to solvent matrix is completely soluble if they meet the following conditions:

#### Interstitial solute case

1. Solute atoms considerably smaller than solvent atoms in order to fit into the interstitial spaces of the crystal lattice.
2. Both solvent and solute must have similar electronegativity.

#### Substitutional solute case

1. The difference between the solute and solvent radii should not be greater than 15%.

$$\% \text{ difference} = \left( \frac{r_{\text{solute}} - r_{\text{solvent}}}{r_{\text{solvent}}} \right) \times 100\% \leq 15\%$$

2. Solvent and solute crystal structures must be identical.
3. A metal with higher valence will dissolve in another one with lower valence. Then, complete solubility is possible when both solvent and solute have the same valence.
4. If the difference of the electronegativity between solvent and solute is higher there is a high possibility of IMC formation instead solid solution.

Table 6. Al, Au and Cu characteristics

Element	Atomic radius [pm]	Electronegativity (Pauling scale)	Valence
Al	128	1.90	3
Au	143	1.61	2
Cu	144	2.54	5

When Cu-Al or Au-Al pair is considered, both systems belong to the substitutional case because atomic size of Cu, Au and Al is not different enough to have interstitial mixture. Table 6 enlist atomic size and electronegativities for Al, Au and Cu. According to Hume-Rothery rules for substitutional solute case (Table 7), the formation of IMCs between Al-Cu and Al-Au is higher:

Table 7. Hume-Rothery rules for Al, Cu and Au

	Radii % difference	Crystal structure	Solubility	Electronegativity difference
Al into Cu	11.11	FCC into FCC	Not possible	0.54
Cu into Al	12.50	FCC into FCC	Not possible	0.54
Al into Au	10.49	FCC into FCC	Not possible	0.29
Au into Al	11.72	FCC into FCC	Not possible	0.29

### 2.2.2 Diffusion paths

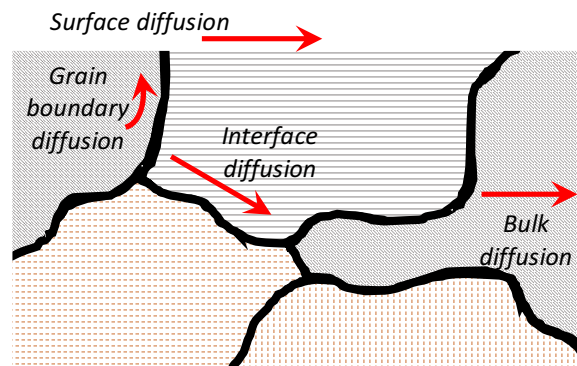


Figure 9: Diffusivity paths

As mentioned before, the diffusion process can take place through different paths in the crystal structures (Figure 9) and particularly for metals, the diffusion along dislocations, grain boundaries, and free surfaces are much faster than those along the crystal lattice. In Figure 10 is plotted the diffusion spectrum of metals (diffusivity paths) in a reduced temperature scale where  $T_m$  indicates the melting temperature. It has been experimentally demonstrated the diffusivity order as follows:

$$D \ll D_d \leq D_{gb} \leq D_s$$

where  $D_s$  = surface diffusivity

$D_{gb}$  = grain boundary diffusivity

$D_d$  = dislocation pipe diffusivity

$D$  = lattice or bulk diffusivity

Based on this asseveration the following statement corresponding to the activation energies holds:

$$\Delta Q > \Delta Q_d \geq \Delta Q_{gb} > \Delta Q_s$$

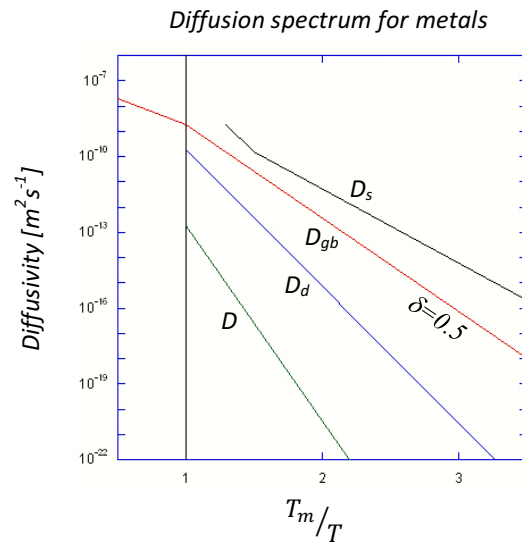


Figure 10: Diffusion spectrum of metals <sup>28</sup>

### 2.2.2.1 Lattice diffusion

In general, lattice diffusion, also known as bulk or volume diffusion, refers to the atomic movement within the crystal lattice and occurs by either interstitial or substitutional mechanisms of diffusion. Lattice diffusion relies on point defects whose concentration increases with temperature and therefore the diffusion coefficient (diffusivity) follows the Arrhenius equation:

$$D = D_0 \exp\left(-\frac{Q}{RT}\right)$$

where  $Q$  = activation energy for diffusion.

While the principle of diffusion is relatively simple to described, its prediction in a diffusion couple is considerably complex because it involves a second order partial differential equation. According to the Fick's diffusion rule, the atomic flux  $J$  is given by

$$J = -D \frac{\partial C}{\partial x}$$

where  $C$  represents the concentration, and the time variation of concentration is given by:

$$\frac{dC}{dt} = D \frac{\partial^2 C}{\partial x^2}$$

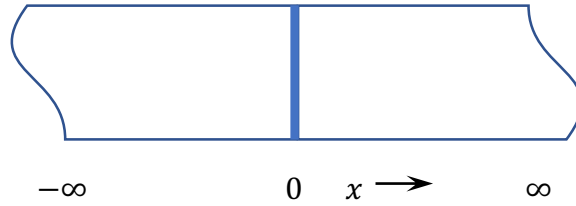
where concentration dependency of  $D$  is ignored.

There are several solutions found to particular cases of non-steady state diffusion problems under the assumption of constant diffusivity  $D$ , e.g. time  $t$  independent, at temperature  $T$  with penetration depth,  $x$ , and defined boundary or initial conditions, some cases and their particular solutions are described as follows:

*Thin-film solutions:*

- Instantaneous planar diffusion: this kind of diffusion problems comprise systems where a finite amount of solute spreads into adjacent semi-infinite solids.





Initial conditions:  $t = 0 \begin{cases} C = \infty; & x = 0 \\ C = 0; & x \neq 0 \end{cases}$

therefore, the process is subject to mass constraint for unit area:

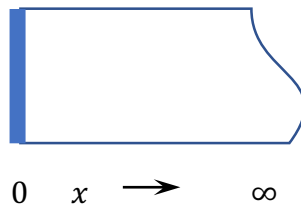
$$\int_{-\infty}^{+\infty} C(x, t) dx = M$$

where  $M$  = number of solute particles per unit area.

Solving the previous equation using Laplace transformation, the solution is as follows:

$$C(x, t) = \frac{M}{2\sqrt{\pi Dt}} \exp\left(-\frac{x^2}{4Dt}\right)$$

- Thin-film configuration: unlike the instantaneous planar diffusion this configuration includes systems where the solute is deposited initially onto the surface of a semi-infinite solid and diffuses into one-half space; in this case, the solution is mathematically similar to the previous configuration:

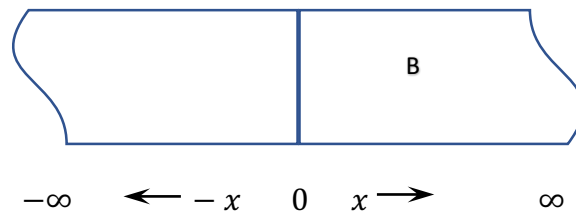


$$C(x, t) = \frac{M}{\sqrt{\pi Dt}} \exp\left(-\frac{x^2}{4Dt}\right)$$

*Extended initial distribution and constant surface concentration solutions*<sup>28</sup>:

In this case, the solute concentration is held constant at the surface of the solid. Such is the case of carburization or nitridation in metal surfaces, where the linearity of the concentration profile allows to apply the principle of superposition to find solutions for different geometric configurations.

- Semi-infinite diffusion couple:

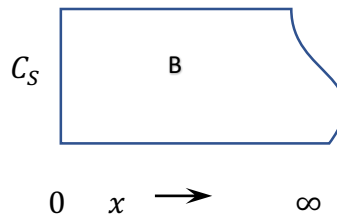


$$\text{Initial conditions: } t = 0 \begin{cases} C = C_0; & x < 0 \\ C = 0; & x > 0 \end{cases}$$

The solution for this case is given by the following equation:

$$C(x, t) = \frac{C_0}{2} \left[ \text{erf}(\infty) - \text{erf} \left( \frac{x}{2\sqrt{DT}} \right) \right] \equiv \frac{C_0}{2} \text{erf} \left( \frac{x}{2\sqrt{DT}} \right)$$

- Diffusion with constant surface concentration:

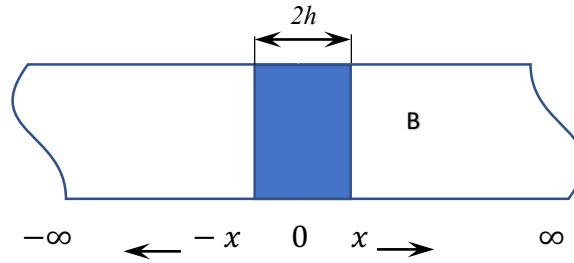


$$\text{Initial conditions: } t = 0 \begin{cases} C_s = C_0/2; & x = 0 \\ C = 0; & x > 0 \end{cases}$$

Therefore, the solution is expressed as follows:

$$C = C_s \text{erfc} \left( \frac{x}{2\sqrt{DT}} \right)$$

- Diffusion from a slab source



$$\text{Initial conditions: } t = 0 \begin{cases} C = C_0; & -h < x < h \\ C = 0; & x > h \text{ or } x < -h \end{cases}$$

The solution for this case is given by:

$$C(x, t) = \frac{C_0}{2} \left[ \operatorname{erf} \left( \frac{x+h}{2\sqrt{Dt}} \right) + \operatorname{erf} \left( \frac{x-h}{2\sqrt{Dt}} \right) \right]$$

It can be seen that the different solutions mentioned above, contain a common term  $\sqrt{Dt}$ , which is defined as the lattice diffusion characteristic length.

### 2.2.2.2 Grain boundary diffusion

A grain boundary is a two-dimensional homophase interface defect highly disordered generally few atoms diameter in thickness<sup>29</sup>, which separates two highly ordered single crystals of the same phase with different crystallographic orientations<sup>28, 30, 31</sup>, where there is interatomic bonding within the transition region. In polycrystalline materials without texture, grains are randomly oriented and therefore grain boundary nature depends on the misorientation of two neighboring grains and the orientation of the boundary plane relative to the grains<sup>28, 31, 32</sup>. Grain boundaries constitute the fastest diffusivity paths, and usually, their diffusivity follows an Arrhenius temperature dependence:

$$D_{gb} = D_{gb}^0 \exp \left( -\frac{\Delta H_{gb}}{k_B T} \right)$$

where  $\Delta H_{gb}$  = activation enthalpy

$D_{gb}^0$  = pre-exponential factor of grain boundary diffusion <sup>28</sup>

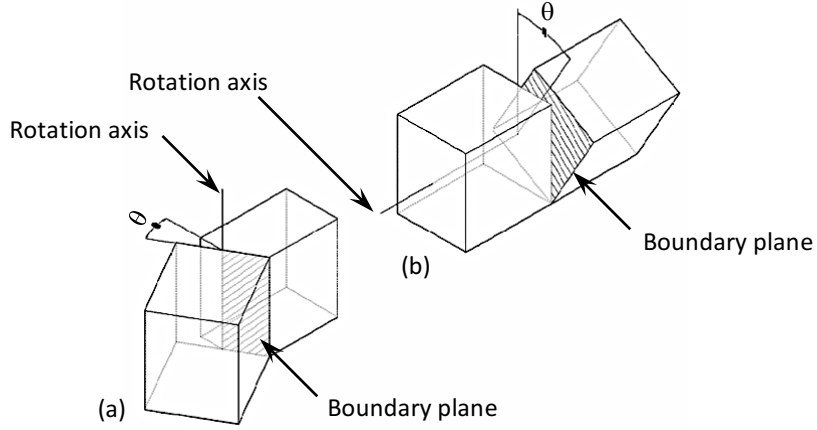


Figure 11: Grain boundary: (a) tilt, (b) twist <sup>28</sup>

Figure 11 shows the typical tilt (a) and twist (b) boundaries. The first one is created by the grain rotation around a rotation axis parallel to the boundary plane meanwhile the second one is formed due to the rotation of the grain around a rotation axis perpendicular to the boundary plane. At the same time, there are particular categories used to describe grain boundaries such as low and high angle grain boundaries as well as special boundaries. Low angle tilt boundary as well as low angle twist boundary (misorientation  $\leq 15^\circ$ ), can be considered as arrays of parallel edge dislocations <sup>32</sup> or planar network of screw dislocations <sup>28</sup> respectively (Figure 12). The energy of a low angle boundary depends on the spacing of the dislocations  $L_d$  and is given by:

$$L_d = \frac{b}{\sin \theta} \approx \frac{b}{\theta}$$

where  $b$  = dislocations Burgers vector

$\theta$  = misorientation angle

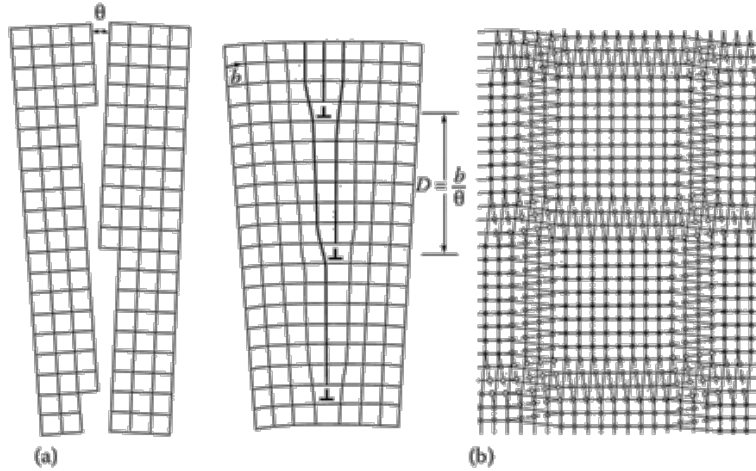


Figure 12: (a) Low angle tilt boundary, (b) Low angle twist boundary:  $\circ$  atoms in a crystal below the boundary,  $\bullet$  atoms in a crystal above the boundary<sup>32</sup>

As the misorientation angle increases ( $> 15^\circ$ ) the dislocation core in both cases, tilted and twisted boundaries, introduce a highly distorted fit in the crystal presenting a relatively open structure and resulting in high angle grain boundaries (Figure 13). At this stage, dislocations start to overlap, making it impossible to distinct individual dislocations and obtaining a grain boundary energy almost misorientation independent (Figure 14).

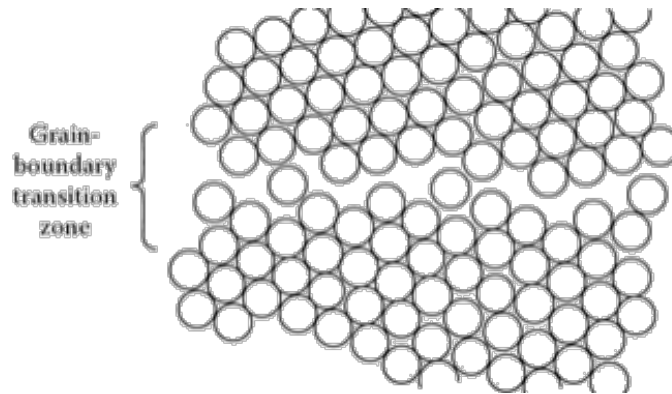


Figure 13: Random high-angle grain boundary<sup>28</sup>

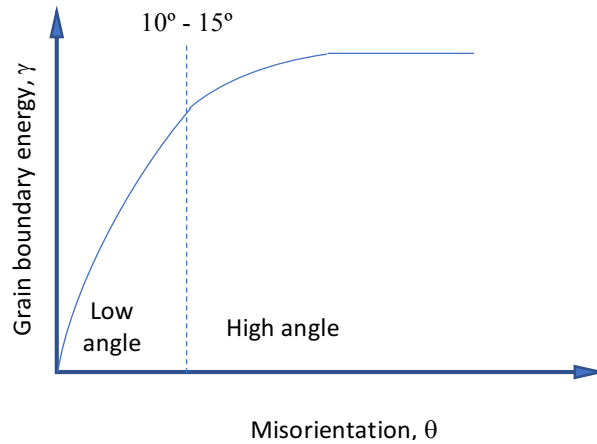


Figure 14: Variation of grain boundary energy with misorientation (schematic) <sup>32</sup>

There are special boundaries which are tilted in such way that their high angle boundaries have significantly lower energies due to the little distortion encountered along the boundary of the neighboring lattices. The simplest of these special boundaries is the twin boundary. The coherent boundary is the product of the alignment of the boundary and the twinning plane as seen in Figure 15-left. This boundary presents a symmetric tilt boundary between the twin-related crystals <sup>28</sup> which translates into a lower grain boundary energy which is opposite to the incoherent boundary energy as seen in Figure 16.

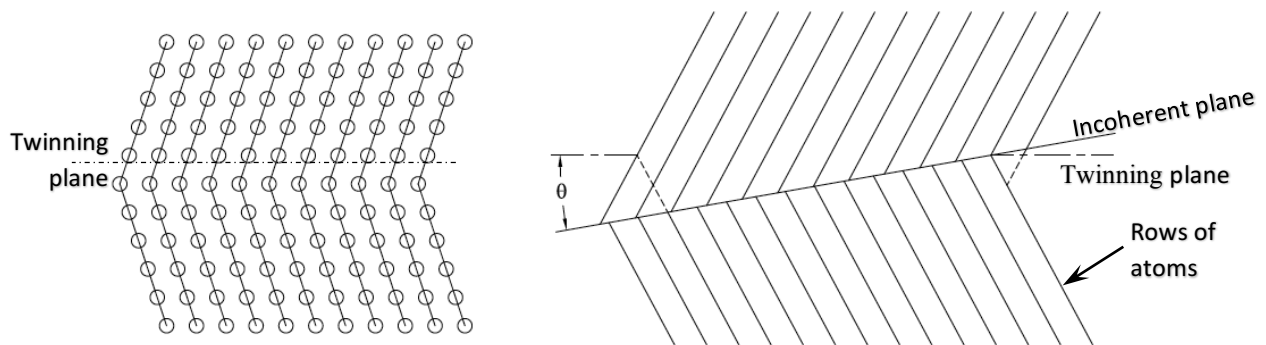


Figure 15: Left: coherent twin boundary, right: incoherent twin boundary <sup>32</sup>

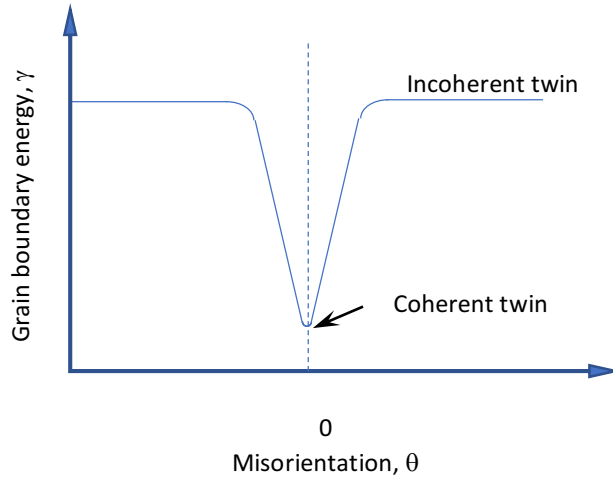


Figure 16: Twin boundary energy as a function of the grain boundary orientation<sup>28</sup>

In order to solve grain boundary diffusion problems, a model proposed by Fisher is often used. The model includes a free surface which carries the diffusion source, while the grain boundary is represented as a perpendicular slab to this surface, as seen in Figure 17. Here  $D$  and  $D_{gb}$  are the lattice and grain boundary diffusivity respectively, which are isotropic and independent of concentration, time and position, along with the grain boundary width  $\delta$ .

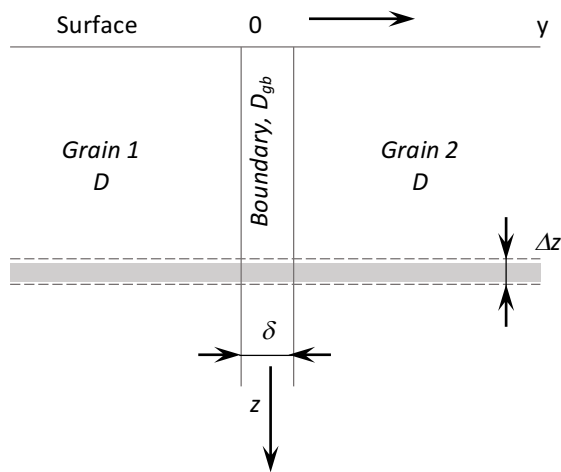


Figure 17: Fisher model of an isolated grain boundary<sup>28</sup>

Fisher's model assumes  $D \ll D_{gb}$  and that Fick's laws are observed into the grain as well as the grain boundary with a continuous solute flow at the boundary and a negligible variation of concentration through the width of the grain boundary which is very small ( $\delta \approx 0.5nm$ ). Therefore, mathematically a set of two simplified equations is given <sup>33</sup> :

$$\frac{\partial C}{\partial t} = D \left( \frac{\partial^2 C}{\partial y^2} + \frac{\partial^2 C}{\partial z^2} \right) \quad \text{for } |y| \geq \frac{\delta}{2}$$

$$\frac{\partial C_{gb}}{\partial t} = D_{gb} \frac{\partial^2 C_{gb}}{\partial y^2} + \frac{2D}{\delta} \left( \frac{\partial C}{\partial y} \right)_{y=\frac{\delta}{2}} \quad \text{for } |y| < \frac{\delta}{2}$$

In order to solve this system of equation it is required boundary conditions:

$$C \left( \pm \frac{\delta}{2}, z, t \right) = C_{gb} \left( \pm \frac{\delta}{2}, z, t \right)$$

$$D \left[ \frac{\partial C(y, z, t)}{\partial y} \right]_{|y|=\frac{\delta}{2}} = D_{gb} \left[ \frac{\partial C_{gb}(y, z, t)}{\partial y} \right]_{|y|=\frac{\delta}{2}}$$

Introducing normalized variables <sup>28</sup>, the mathematical solution is given as follows for the grain boundaries:

$$C(\xi, \eta, \beta) = C_1(\eta) + C_2(\xi, \eta, \beta)$$

while for the grains:

$$C_1(\eta) = C_{gb}(\eta)$$

where:

$$\xi \equiv \frac{y - \delta/2}{\sqrt{Dt}}, \quad \eta \equiv \frac{z}{\sqrt{Dt}}, \quad \beta \equiv \frac{(\Delta - 1)\delta}{2\sqrt{Dt}} \approx \frac{\delta D_{gb}}{2D\sqrt{Dt}}, \quad \Delta \equiv \frac{D_{gb}}{D}$$

- Constant source condition: where the solute concentration is kept constant by depositing a layer at the surface with a thickness  $h$  such that  $h \gg \sqrt{Dt}$  and zero everywhere else at  $t = 0$ .

Therefore, the initial conditions are:



$$C(y, z, t) = C_0; \quad z = 0, t > 0$$

$$C(y, z, t) = 0; \quad z > 0, t = 0$$

Solution:

$$C_1(\eta) = C_0 \operatorname{erfc}\left(\frac{\eta}{2}\right)$$

$$C_2(\xi, \eta, \beta) = \frac{C_0 \eta}{2\sqrt{\pi}} \int_1^{\Delta} \frac{\exp\left(-\frac{\eta^2}{4\sigma}\right)}{\sigma^{3/2}} \operatorname{erfc}\left[\frac{1}{2}\left(\frac{\Delta-1}{\Delta-\sigma}\right)^{1/2} \left(\xi + \frac{\sigma-1}{\beta}\right)\right] d\sigma$$

where  $\sigma$  = integration variable.

- Instantaneous source or thin layer condition: this condition was suggested by Suzuoka<sup>34</sup> and implies that  $h \ll \sqrt{Dt}$  when the initial layer of solute is completely consumed during the diffusion process<sup>33</sup>. The initial conditions are as follows:

$$t = 0 \begin{cases} C(y, z, t) = \infty; & z = 0 \\ C(y, z, t) = 0; & z \neq 0 \\ C(y, z, t) = 0; & z > 0 \end{cases}$$

$$C(y, z, t) = 0; \quad z = \infty, t \neq 0$$

$$\frac{\partial C(y, z, t)}{\partial z} = 0; \quad z = 0$$

Solution:

$$C_1(\eta) = \frac{M}{\sqrt{\pi Dt}} \exp\left(-\frac{\eta^2}{4}\right)$$

$$C_2(\xi, \eta, \beta) = \frac{M}{\sqrt{\pi Dt}} \int_1^{\Delta} \left[\frac{\eta^2}{4\sigma} - \frac{1}{2}\right] \frac{\exp\left(-\frac{\eta^2}{4\sigma}\right)}{\sigma^{3/2}} \operatorname{erfc}\left[\frac{1}{2}\left(\frac{\Delta-1}{\Delta-\sigma}\right)^{1/2} \left(\xi + \frac{\sigma-1}{\beta}\right)\right] d\sigma$$

In both cases  $C_1(\eta)$  represents the leakage contribution from grain boundary into the grain while  $C_2(\xi, \eta, \beta)$  represents in-diffusion into the grains from the external source<sup>28</sup>.

Diffusion kinetics

Due to the complicated process that involves a grain boundary diffusion Harrison<sup>35</sup> introduced a classification for the diffusion kinetics which is shown in Figure 18.

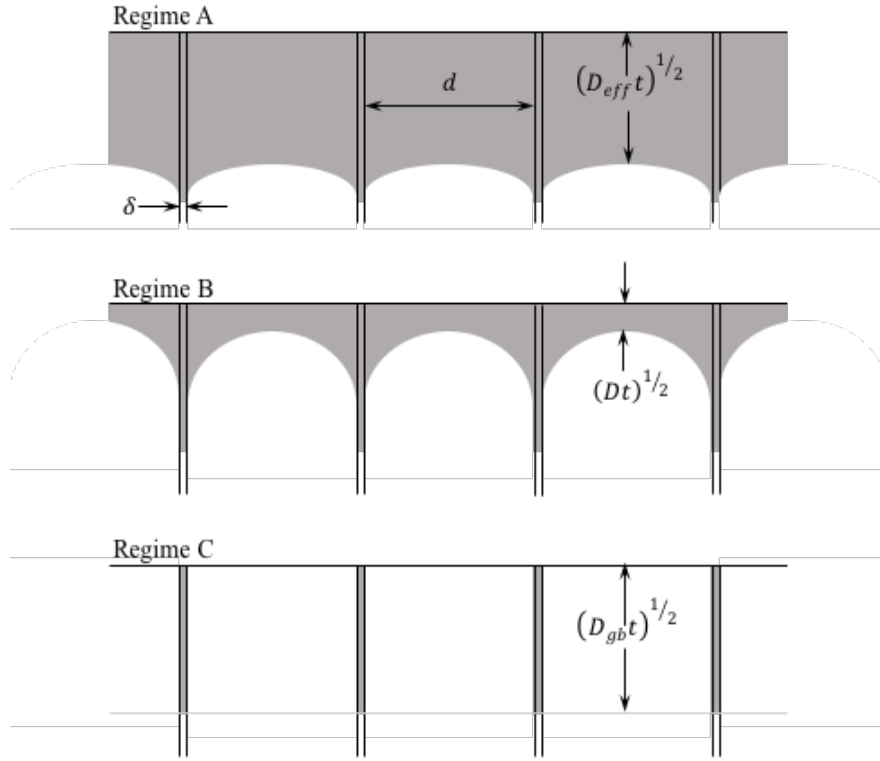


Figure 18: Diffusion regimes in a polycrystal according to Harrison classification<sup>28</sup>

- Regime A: it is found only at high temperatures and/or long annealing times and/or small grain sizes. Under these conditions lattice diffusion characteristic length is larger than the spacing between grain boundaries:  $\sqrt{Dt} \gg d$ <sup>28, 33</sup>. For this regime Hart proposed an effective diffusivity given by<sup>33</sup>:

$$D_{eff} = gD_{gb} + (1 - g)D$$

where:  $g$  = fraction of atomic sites in the grain boundary of the polycrystal and is defined by:

$$g = \frac{q\delta}{d}$$

Table 8: Numerical factor  $q$

Grain shape	$q$
Parallel grain boundaries	1
Cubic grains	3

- Regime B: it is encountered when temperatures are low and/or the annealing times are short and/or the grain size is larger than the one found in regime A, with these conditions the spacing between grain boundaries becomes larger than the lattice diffusion characteristic length which is considerably larger than the grain boundary width:  $d \gg \sqrt{Dt} \gg \delta$ <sup>28, 33</sup>.
- Regime C: this regime considers lower temperature conditions and/or annealing times than the ones observed in regime B giving as result diffusion only along grain boundaries, consequently the characteristic length is much smaller than the grain boundary width:  $\sqrt{Dt} \ll \delta$ <sup>28, 33</sup>.

### 2.2.2.3 Dislocation pipe diffusion

Basically, all crystals contain dislocations, however, their contribution to the diffusion process depends on the high or low dislocation densities contained in such crystal as well as the temperature; its contribution is negligible at high temperatures and/or in materials containing low dislocation densities, but it becomes significant at low temperatures because of the low activation energy found for dislocation diffusion when compared to the one observed in lattice diffusion. A characteristic parameter of the dislocation pipe diffusion is the average distance between dislocations which is a function of the dislocation arrangement and is given by:

$$\Lambda = \frac{K}{\sqrt{\rho_d}}$$

where  $K$  is of the order of unity

$$\rho_d = \text{number of dislocations that penetrate the unit area}$$
<sup>28</sup>

As in the grain boundary diffusion, it can also be classified in three regimes depending on  $\Lambda$  and the lattice diffusion characteristic length.

- Regime A:  $\sqrt{Dt} > \Lambda$
- Regime B:  $a \ll \sqrt{Dt} \ll \Lambda$
- Regime C:  $a > \sqrt{Dt}$

where  $a$  is the dislocation pipe radius.

*Dislocation pipe model:*

As mentioned before, most materials contain a certain number of defects and it is one of these defects, dislocations, that can increase the diffusivity of solute atoms by offering regions where the solute concentration is higher and the activation energy for diffusion through them is lower than the diffusion through the lattice.

Smoluchowski proposed a model analogous to the one proposed by Fisher for grain boundary diffusion. In this model, dislocations are treated as cylindrical pipes of radius  $a$  (Figure 19).

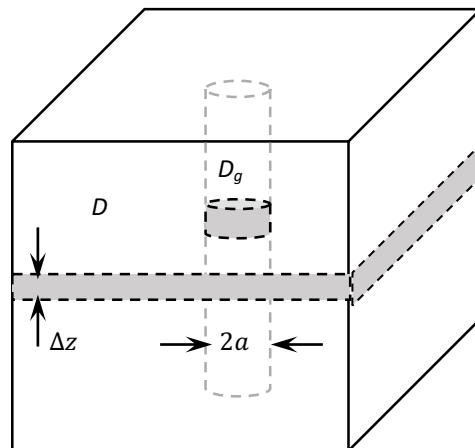


Figure 19: Smoluchowski model of a dislocation pipe<sup>28</sup>

It is assumed that the dislocation pipe diffusivity  $D_d$  is larger than the lattice diffusivity  $D$  outside the pipe. Consequently, two equations are developed in a cylindrical coordinate system based on the assumptions:

$$\frac{\partial C}{\partial t} = D \left[ \frac{1}{r} \frac{\partial}{\partial r} \left( r \frac{\partial C}{\partial r} \right) + \frac{\partial^2 C}{\partial z^2} \right] \quad \text{for } r \geq a$$

$$\frac{\partial C_d}{\partial t} = D_d \left[ \frac{1}{r} \frac{\partial}{\partial r} \left( r \frac{\partial C_d}{\partial r} \right) + \frac{\partial^2 C_d}{\partial z^2} \right] \quad \text{for } r < a$$

In order to solve these equations, it is necessary to have boundary conditions:

$$\left( D \frac{\partial C}{\partial r} \right)_{r=a^+} = \left( D_d \frac{\partial C_d}{\partial r} \right)_{r=a^-}$$

$$C(r = a^+) = C_d(r = a^-)$$

The solution is given for two cases and their respectively initial conditions at the surface  $z = 0$ <sup>36</sup>:

- Constant source:  $C(r, z, t) = C_0; \quad z = 0$
- Instantaneous source:  $C(r, z, t) = 2M\delta(y); \quad t = 0$

where  $\delta(y)$  is the delta Dirac function and  $2M$  is the solute atoms per unit area. The solution is given in the form of:

$$C(r, z, t) = C_1(y, t) + C_2(r, z, t); \quad a \leq r \leq R$$

### 2.2.2.4 Surface diffusion

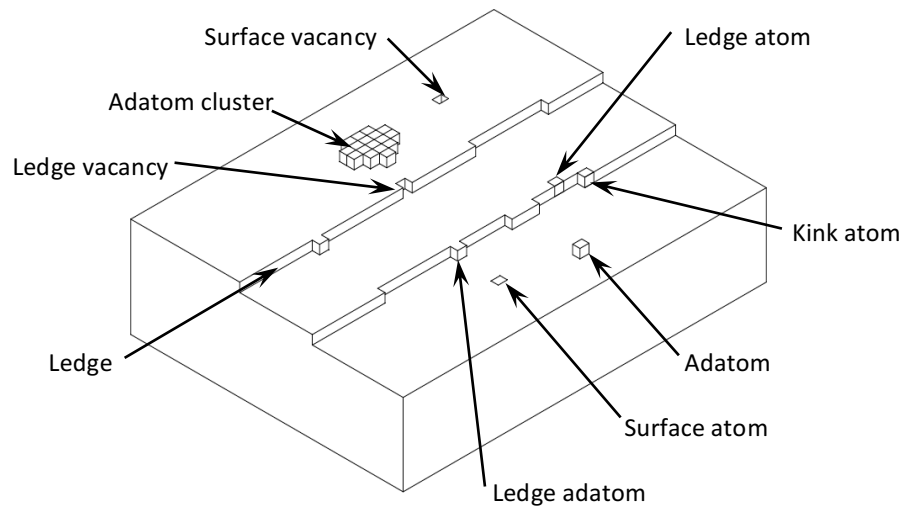


Figure 20: Various points and line defects on a vicinal crystal/vapor surface <sup>30</sup>

In a metallurgical process, surface diffusion is very important because real surfaces contain defects (Figure 20). Surface diffusion shares similar characteristics with grain boundary diffusion because the diffusion path is defined as a slab of high diffusivity where the solute moves through the slab surface and crystal <sup>30</sup>. In metallurgical processes, surface diffusion plays an important role. However, if the surface area is compared to the average grain boundary area, the last one is the most important <sup>32</sup>.

If the separation between defects is smaller than the lattice diffusion characteristic length the number of mobile particles and consequently diffusion becomes strongly temperature dependent. It has been found through experimentation that surface diffusion can also be expressed by an Arrhenius equation:

$$D_S = D_S^0 \exp\left(-\frac{Q_S}{RT}\right)$$

where  $D_S^0$  = frequency factor

$Q_S$  = activation energy, experimentally determined for surface diffusion <sup>32</sup>

As temperature increases the surface roughness increases which adds complexity to this diffusion mechanism.

### 2.3 Intermetallic compounds

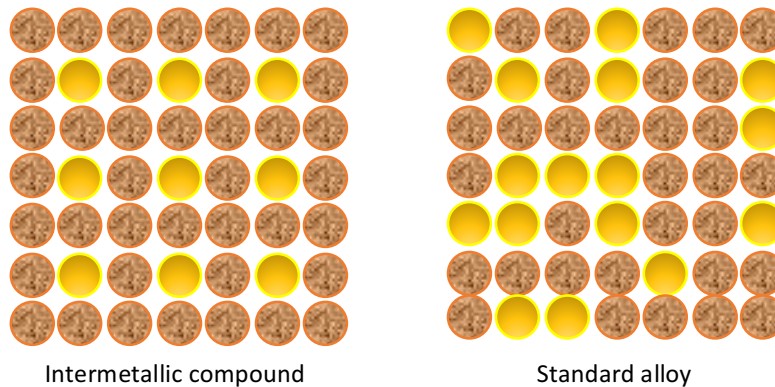


Figure 21. Schematic comparison between IMCs and standard alloys

Contrasting standard metal alloys, where certain percentages of elements are added to a host material, IMCs are compounds of metals or of metals and semimetals<sup>37</sup> that have particular chemical formulae with a fixed or narrow range of a well-defined chemical composition. The atoms in the IMCs are not linked by the relatively weak metallic bond, but may be linked by a partial ionic or covalent bond, a reason by which their crystal lattice structure is frequently ordered and different from the crystal structure of any of the primary elements. Commonly, the IMC formation is associated with the electronegativity difference of the primary elements, larger the electronegativity difference higher the predisposition to form IMCs. The main properties of IMCs are<sup>6, 38</sup> : high melting points, high thermal conductivity, low densities, high strength, mainly at high temperatures, good oxidation resistance at high temperatures (because of the formation of oxide films), low ductility, brittle fracture at room temperature and processing problems.

### 2.3.1 Mechanisms of diffusion in intermetallic compounds

IMCs are generally highly ordered crystal structures, where the atoms “are preferentially surrounded by unlike atoms”<sup>39</sup>. Consequently, their diffusion process usually does not take place through the random vacancy motion because otherwise the process would disturb the ordered arrangement of the atoms in the crystalline structure. Several models have been proposed to explain the diffusion process in such materials. These models “allow atom-vacancy exchanges to take place without concomitant long range disordering”<sup>40</sup>, maintaining the thermodynamic equilibrium between the jumps in the crystal structure.

In many cases, diffusion involves multiple IMC phases, which takes place across phase boundaries that constantly move during the process. Usually, Boltzmann-Matano analysis is applied, in order to find the layer growth of an IMC as a function of time. In general, a process governed by volume diffusion would follow a parabolic growth law, but, in IMC formation and growth it is not clear if the thermal equilibrium is kept through the process because at the beginning there is an incubation time that deviates the process of the parabolic growth, it is a usual case that grain boundary diffusion plays a dominant role in IMC formation and growth because, unlike ordered matrix, the disordered structure at grain boundaries allow faster diffusion kinetics<sup>40</sup>. IMCs are classified according to several crystal structures, and depending on this classification the proposed diffusion model is different from each other. Table 9 lists the most common IMC crystal structures and the proposed diffusion mechanism.



Table 9: Diffusion in intermetallic compounds<sup>28, 39, 40, 40</sup>

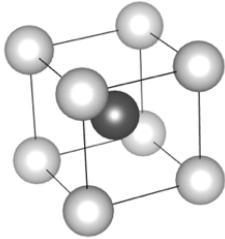
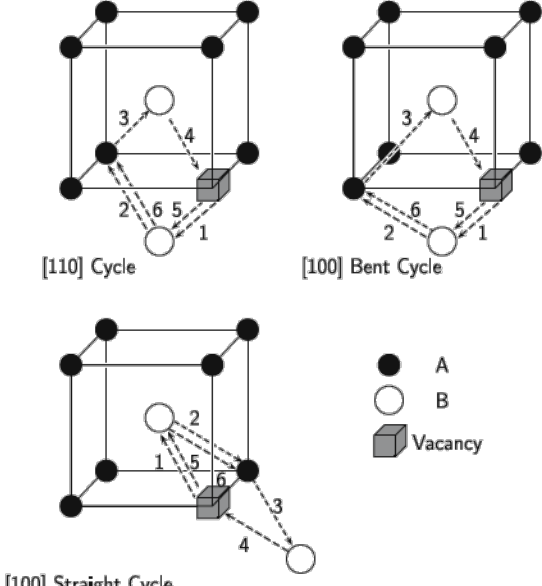
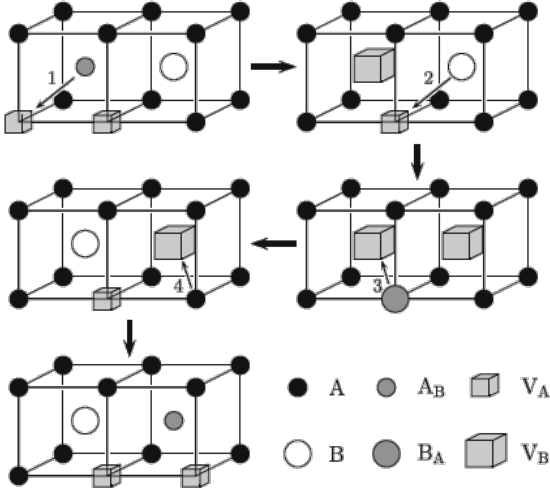
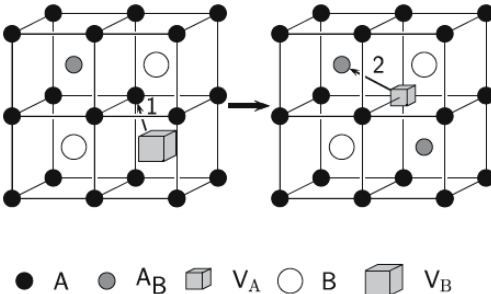
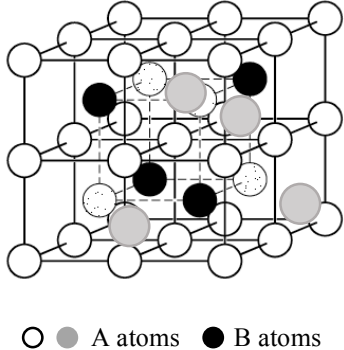
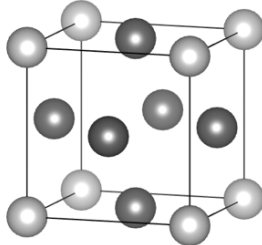
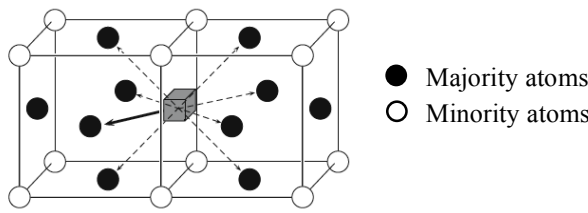
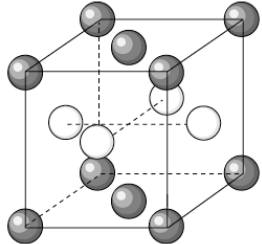
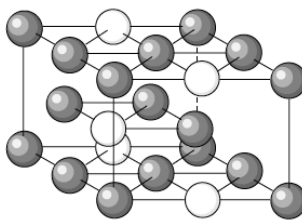
Crystal structure	Diffusion mechanism
<p style="text-align: center;">B2</p> 	 <p style="text-align: center;">Six jump cycle mechanism</p>
	 <p style="text-align: center;">Triple defect diffusion mechanism</p>
	 <p style="text-align: center;">Antistructural bridge mechanism</p>

Table 9. Continued

<p style="text-align: center;"><math>D0_2</math></p>  <p style="text-align: center;">○ ● A atoms   ● B atoms</p>	<p>A atoms diffuse through their own sublattice via nearest-neighbour jumps, while B atoms can move either through their own sublattice using a third nearest neighbor jump or to the nearest neighbor which create B antisite defects. In any case, a high activation enthalpy is needed for B atoms to diffuse.</p>
<p style="text-align: center;"><math>L1_2</math></p> 	<p style="text-align: center;">Sublattice vacancy mechanism</p>  <p style="text-align: right;">● Majority atoms ○ Minority atoms</p> <p>In this crystal structure the majority atoms are interconnected by nearest neighbor bond while the minority atoms are not. Therefore, the motion is restricted to the majority sublattice promoting the diffusion of its atoms. The minority atoms migration requires larger jumps than the nearest neighbor or to form antisite defects, both cases are energetically unfavorable.</p>
<p style="text-align: center;"><math>L1_0</math></p> 	<p>This tetragonal crystal structure has an ordered atomic arrangement similar to an FCC crystal structure where A and B atoms occupy sequential planes. In this structure, the diffusion mechanism is usually faster in the direction perpendicular to the tetragonal axis rather than in the parallel direction to it.</p>
<p style="text-align: center;"><math>DO_{19}</math></p> 	<p>This hexagonal crystal structure is equivalent to the <math>L1_2</math> structure where the majority atoms tend to diffuse faster than the minority atoms.</p>

### 2.3.2 Intermetallic formation in binary systems

It has been mentioned previously that there exist several factors that could and would affect the formation and growth of IMCs between dissimilar materials, factors that have to be controlled during the bonding process in order to minimize the negative effects of the growth of brittle IMCs at the interface of the bond.

Researchers have proven that there exist several stages in the formation and growth of IMCs: “the first stage comprises the interdiffusion of the materials at different diffusion rates until a supersaturated solid solution is formed to later form a crystal nuclei of the IMC phase which are usually produced at defects where concentration of diffusing element is high. These crystal nuclei grow along the interface connecting longitudinally; the sequence is repeated when crystal nuclei of a second IMC are formed at the interface and grows up”<sup>41</sup>.

Diffusion theory establishes that a new phase will not form instantaneously when the diffusion couple comes into contact but rather there will be an incubation period where under optimal temperature conditions and diffusion time, the reaction will take place. Then the IMC will be stable as long as the conditions are favorable.

On the other hand, the formation of the IMC phases is in direct relation to the atomic diffusion capability of the materials at the bonding interface<sup>41</sup>. Once the layer of the first IMC is formed, it will start growing as function of the diffusion time until the diffusion flux at one or both sides of the IMC is progressively altered and then as product of this alteration there would exist a condition of simultaneous consumption of the components favoring the growth of the first phase until it reaches a thickness where the stoichiometric conditions are ideal for the formation and growth of a second IMC; thus the process will repeat favoring the formation of new IMCs.

The individual properties of the base materials at the interface of the diffusion couple define the kinetic driving force while the ratio in which each material is present at the diffusion couple will restrict or favor the flux rate of one or another of the elements in the diffusion couple at the contact interface.

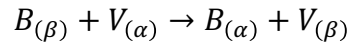
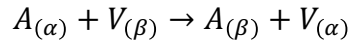
According to Paul et.al., “For a diffusion couple, which (a) has end members that are pure elements with negligible solubility or IMCs with negligible solubility range and (b) forms only intermetallic phases with narrow homogeneity range”<sup>42</sup>. The interdiffusivity can be estimated by using Wagner’s model. Wagner has shown that the integrated interdiffusion coefficient of each phase can be calculated using the expression:

$$\begin{aligned} \bar{D}_{int}^{\beta} = & \frac{\Delta x_{\beta}^2 (N_i^{\beta} - N_i^{-}) (N_i^{+} - N_i^{\beta})}{2t (N_i^{+} - N_i^{-})} \\ & + \left[ \frac{(N_i^{+} - N_i^{\beta})}{(N_i^{+} - N_i^{-})} \sum_{v=2}^{v=\beta-1} \left( \frac{V_m^{\beta}}{V_m^v} (N_i^v - N_i^{-}) \Delta x_v \right) \right. \\ & \left. + \frac{(N_i^{\beta} - N_i^{-})}{(N_i^{+} - N_i^{-})} \sum_{v=\beta+1}^{v=n-1} \left( \frac{V_m^{\beta}}{V_m^v} (N_i^{+} - N_i^v) \Delta x_v \right) \right] \frac{\Delta x_{\beta}}{2t} \end{aligned}$$

where  $\beta$  is the phase of interest;  $N_i^{\pm}$  is the mole fraction of element  $i$ , with “-” and “+” indicating the left and right-hand side end members, respectively;  $V_m^v$  and  $\Delta x_v$  are the molar volume and layer thickness of the  $v$ th phase and  $t$  is the annealing time”<sup>42, 43</sup>. This expression can aid to determine the integrated interdiffusion coefficient of an IMC phase in a defined infinite binary system where two or more intermetallic phases can be formed.

However, this is not the only approach that has been used to predict the formation and growth of the IMCs in binary systems, and Van Loo et.al.<sup>44</sup> have proposed a system of equations

based on a physicochemical approach, “where the interface reaction can be described by an exchange of A and B species between  $\alpha$  and  $\beta$  phases such as:



where  $V_{(\alpha)}$  and  $V_{(\beta)}$  indicate vacancies in the  $\alpha$  and  $\beta$  phases”<sup>44</sup>.

Though, it must be noticed that while there exist several approaches to describe the formation and growth of IMCs in binary systems, in most of the cases they do not necessarily yield a consistent result due to the characteristics of the systems under study, conditions of analysis and compositions among other factors.

### 2.3.3 Intermetallic compounds in Au-Al systems

Due to the widespread use of the Au-Al system for wire bonding the system has been well studied<sup>45</sup>. In the Au-Al wire bonding process, IMCs form at the interface between the Au wire and the Al pad. The usual way to study the interface IMCs in this kind of systems is to create thin-film diffusion couples<sup>46</sup>. In spite of numerous studies on Au-Al system, there have been conflicting reports according to different researchers about the number of IMCs, as well as their kinetics of formation and how they affect the strength of the diffusion couple. It is suggested that these differences are the result of variation in IMC conditions that depends highly on the manufacturing conditions.

The Au–Al phase diagram (Figure 3) reveals five IMCs which are stable at low temperatures<sup>47</sup> as listed in Table 10; however, it should be noted that in wire bonding, Au and Al are rapidly bonded and therefore equilibrium may never be reached<sup>48</sup>. Consequently, it is possible that some of these IMCs could not appear<sup>48</sup>. It seems that interdiffusion in Au-Al is rapid even at

low temperatures. Multiple studies found a growth of IMC phases at temperatures as low as 100°C. Further, it is reported that the growth of IMC phases can occur with a rate of 0.3 nm/h<sup>49</sup> even at room temperature, which should increase the electrical resistance as well as internal stress at the bonding interface.

Table 10: Structural information for the IMC formed in the Al-Au system

Phase	at. %Au	Space group	Crystal structure	Lattice parameter
(Al) <sup>47</sup>	0 – 0.06	Fm3m	FCC	$a = 4.2906\text{Å}$
$Al_2Au$ <sup>50</sup>	32.92 – 33.92	Fm3m	Cubic	$a = b = c = 4.2407\text{Å}$
$AlAu$ <sup>51</sup>	50	$P2_1/m$	Monoclinic	$a = 6.415\text{Å}, b = 3.331\text{Å}, c = 6.339\text{Å}$ $\alpha = \gamma = 90^\circ, \beta = 93.04^\circ$
$\gamma - AlAu_2$ <sup>52</sup>	65 – 66.8	14/mmm	Tetragonal	$a = 3.349\text{Å}, c = 8.893\text{Å}$
$\beta - AlAu_2$ <sup>52</sup>	65.1 – 66.1	Pnmm	Orthorhombic	$a = 16.772\text{Å}, b = 3.219\text{Å}, c = 8.801\text{Å}$ $\alpha = \beta = \gamma = 90^\circ$
$\alpha - AlAu_2$ <sup>52</sup>	66.3 – 66.7	Pnma	Orthorhombic	$a = 6.715\text{Å}, b = 3.219\text{Å}, c = 8.815\text{Å}$ $\alpha = \beta = \gamma = 90^\circ$
$Al_3Au_8$ <sup>53*</sup>	71.43	R-3c	Rhombohedral	$a = b = c = 14.78\text{Å}$ $\alpha = \beta = \gamma = 90^\circ$
$\beta$ <sup>49</sup>	80 – 81.2	Im3m	Cubic	$a = 3.236\text{Å}$
$AlAu_4$ <sup>54</sup>	80	---	Cubic	$a = b = c = 6.9227\text{Å}$ $\alpha = \beta = \gamma = 90^\circ$
(Au) <sup>49</sup>	84 - 100	Fm3m	FCC	$a = 4.0784\text{Å}$

\* There is not an agreement about the formula of this intermetallic, some studies consider it as  $Al_2Au_5$

Even though the existence of several studies, they have shown different IMC formation and growth sequence and none of them can be solely adopted in order to explain and fully understand the diffusion mechanisms acting in a binary system having a limited solubility.

Table 11: List of interface transformations determined by Xu et.al. <sup>46</sup>

$1\mu\text{m Al} + 1\mu\text{m Au}$			
Time	125°C	150°C	175°C
0 min	$Au + Al$	$Au + Al$	$Au + Al$
0.25 h	$Au + Al_2Au_5 + Al$	$Au + Al_2Au_5 + Al$	$Au + Al_2Au_5 + Al$
0.50 h	$Au + Al_2Au_5 + Al$	$Au + Al_2Au_5 + Al$	$Au + Al_2Au_5 + AlAu_4 + Al$
1.00 h	$Au + Al_2Au_5 + Al$	$Au + Al_2Au_5 + AlAu_4 + Al$	$Au + Al_2Au_5 + AlAu_4 + Al$
2.00 h	$Au + Al_2Au_5 + Al$	$Au + Al_2Au_5 + AlAu_4 + Al$	$AlAu_2 + Al_2Au_5 + Al$
4.00 h	$Au + Al_2Au_5 + Al$	$AlAu_2 + Al_2Au_5 + AlAu_4 + Al$	$AlAu_2 + Al_2Au_5 + Al$
8.00 h	$Au + Al_2Au_5 + AlAu_4 + Al$	$AlAu_2 + Al_2Au_5 + Al$	$AlAu_2 + Al_2Au_5 + Al$
16.0 h	$AlAu_2 + Al_2Au_5 + AlAu_4 + Al$	$AlAu_2 + Al_2Au_5 + Al$	$AlAu_2 + Al_2Au_5 + Al$
24.0 h	$AlAu_2 + Al_2Au_5 + Al$	$AlAu_2 + Al_2Au_5 + Al$	$AlAu_2 + Al_2Au_5 + Al$

Table 11 lists the formation sequence of IMCs as a function of annealing time and temperature in a study performed by Xu et.al. <sup>46</sup> using Au-Al diffusion couple made of thin films. According to these results, the sequence of formation at all temperatures is very similar.

However, in a similar study published by Majni et.al. <sup>55</sup>, the sequence of IMC formation is different, even though the study has been performed also in Au-Al thin films. The main difference is the ratio of Au and Al, and consequently, the results deviate from the study performed by Xu et.al. <sup>46</sup>. The results published by Majni et.al. <sup>55</sup> are displayed in Figure 22.

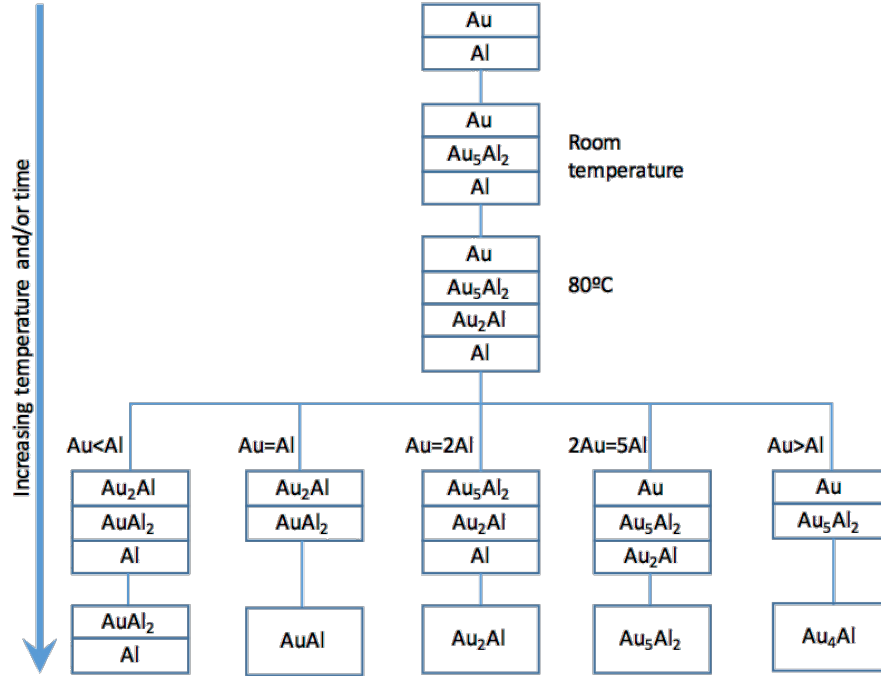


Figure 22. Schematic diagram showing the sequence in phase formation in the Au-Al thin film according to Majni et.al.<sup>55</sup>

In order to resolve inconsistencies among studies and also to better understand how different sequence or IMC formation can occur with varying amount of available materials for interdiffusion, a new approach has been developed. The computational simulation of IMC growth can be done but it requires fundamental data such as diffusion coefficient and IMC formation energies. These data are not available in a consistent manner, and therefore attempts are made by computational modeling. Ulrich et.al.<sup>56</sup> calculated the formation enthalpies  $\Delta H_F$  of the  $Al_aAu_b$  IMCs using the quantum-mechanical density functional theory (DFT) based on the following equation:

$$\Delta H_F = \frac{1}{a+b} (E[Al_aAu_b] - a\mu_{Al}^{FCC} - b\mu_{Au}^{FCC})$$

where  $a$  and  $b$  = Al and Au atoms in the stoichiometric formula

$$E[Al_aAu_b] = \text{energy of the cell}$$



$a\mu_{Al}^{FCC}; b\mu_{Au}^{FCC}$  = bulk chemical potentials of Al and Au respectively

Ulrich et.al.<sup>56</sup> do not consider any temperature or pressure contribution in this calculation however their results are in good agreement with experimental values. The results obtained are listed in Table 12:

Table 12: Formation enthalpies of the low-temperature Al-Au phases<sup>56</sup>

Compound	$\Delta H_F$ [kJ/mol]
Al <sub>2</sub> Au	-46.6
AlAu	-43.4
$\beta$ -AlAu <sub>2</sub>	-36.3
$\alpha$ -AlAu <sub>2</sub>	-35.7
Al <sub>3</sub> Au <sub>8</sub>	-31.0
AlAu <sub>4</sub>	-23.3

In the Au-Al wire bonding, there are two common forms of IMCs responsible for the interconnection failure, and they are known as white plague ( $Al_2Au_5$ ) and purple plague ( $Al_2Au$ ). According to the data listed in Table 12, the  $Al_2Au$  phase has a low formation enthalpy. This result may explain the reason why  $Al_2Au$  phase is commonly seen in Au-Al wire bond interface. The presence of  $Al_2Au$  produces a reduction in volume, which creates cavities in the metal surrounding this compound (Kirkendall effect). As temperature increases, the diffusion of Au favors the formation of  $Al_2Au_5$ . This compound has a low electrical conductivity combined with the void induced during  $Al_2Au$  formation leads to the increase in electrical resistance, affecting the physical integrity of the interconnection and ultimately to the total failure of the component.

#### 2.3.4 Intermetallic formation in Cu-Al systems

The study on the sequence of formation and growth of IMCs and associated diffusion mechanisms in Cu-Al systems is as difficult to determine as it is in the Au-Al system or any other

binary system where multiple stoichiometric phases are likely to form. However, if the focus of the comparison is about the wire bonding, there is a considerable difference between Cu-Al and Au-Al systems in reliability terms. Several studies have shown that the reaction rate between Cu and Al is approximately  $1/10$  *th* of that one between Au and Al at temperatures from 150°C to 300°C<sup>18, 57</sup>. These results suggest that Cu wire bonding is likely to provide much better reliability against failure induced IMC growth at the bond interface.

However, it is precisely in this range of temperature that the studies of several Cu-Al systems do not agree “with each other” in terms of type and number of IMC forming at interface. For instance, Pfeifer et.al.<sup>19</sup> reported that  $CuAl_2$  is the main IMC phase forming at temperatures between 100°C – 200°C in Cu-Al diffusion couple made of PVD (physical vapor deposition) thin films, while  $CuAl$  is the main IMC at temperatures between 200°C – 250°C. The  $\gamma - Cu_9Al_4$  phase is seen to be forming at temperatures higher than 300°C. These results suggest that  $Cu_9Al_4$  would not be present at device operating temperatures, around 90°C – 140°C. However, when the electrochemical deposition process is used instead of PVD process the sequence of formation is found to be different. On the other hand, a study conducted by Yu et.al.<sup>58</sup> showed the formation of  $CuAl_2$  at the Cu-Al interface, but later reports found either  $Cu_9Al_4$  or  $CuAl$  being the main phase.

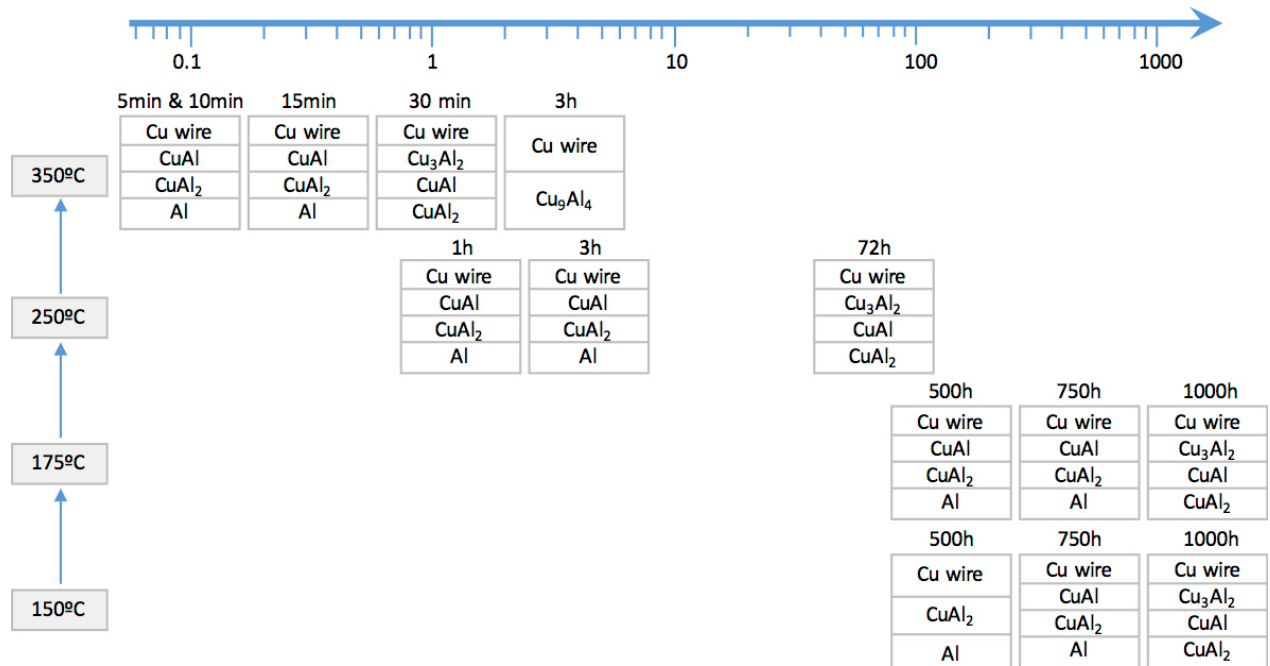


Figure 23. Schematic illustration showing the IMC evolution during aging at 150°C, 175°C, 250°C and 350°C. The time axis is in log scale<sup>58</sup>

Figure 23 shows the summary of IMC formation sequence as a function of temperature found in various studies. It can be seen that there is a wide range of the IMC formation in wire bond interface seen in those studies. One possible reason for such scattering may be related to the variation in wire bonding condition that may result in different stress condition along the interface and initial IMC phase present at interface<sup>58</sup>. However, according to the phase diagram of Cu-Al system shown in Figure 6, there are a lot more phases that is supposed form by interdiffusion at a temperature range between 150°C to 300°C<sup>59</sup>. In this range, the phase diagram predicts the formation of five stable IMC phases:  $\theta - CuAl_2$ ,  $\eta - CuAl$ ,  $\xi - Cu_4Al_3$ ,  $\gamma - Cu_9Al_4$  and  $\alpha_2 - Cu_3Al_2$ . It is clear that not all of the stable phases possible to form at interface have been identified in the studies so far, but most studies agree that  $\theta - CuAl_2$ ,  $\eta - CuAl$  and  $\gamma - Cu_9Al_4$  are the ones that prevail in the concerned temperature ranges<sup>18,57</sup>.

## 2.4 Electromigration

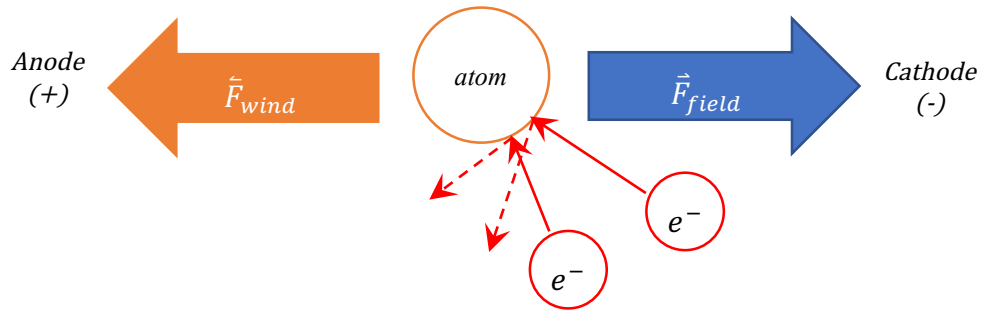


Figure 24. Electromigration representation

EM is a phenomenon by which mass transport in a metal is produced due to the momentum transfer from conduction electrons colliding with metal atoms resulting in the atomic migration in the opposite direction to an applied electric field (Figure 24). In EM, there are two opposite driving forces acting on the metal ion <sup>60, 61, 62</sup>:

- The action exerted by the external field on the migrating ion (direct or field force) in the opposite direction to the electron flow.
- The scattering produced by the ions on the conduction electrons (wind force) in the same direction to the electron flow.

The EM force is consequently the addition of these driving forces, being dominated by the wind force that is much higher than field force when the applied current increases.

This EM makes atoms to migrate even if there is no chemical potential gradient. In fact, EM force is becoming of the chemical potential gradient that constitutes the driving force for the migration. Therefore, EM can be viewed as a diffusion induced by the wind force. It then follows that the flux created by EM is represented by the following equation where the first term governs the kinetics and the second is the driving force.

$$J = \frac{D \cdot C}{k \cdot T} z^* \cdot e \cdot \rho \cdot j$$

where:  $D$  = diffusion coefficient

$k$  = Boltzmann constant

$C$  = concentration

$T$  = temperature

$z^*$  = effective valence

$e$  = electron charge

$j$  = current density

#### 2.4.1 Failure by electromigration

It is a fact that in a perfect crystal lattice, the activation energy for diffusion that dictates  $D$  is high so that EM occurs in a slow manner. Also, the flux is uniform. However, real materials contain defects such as grain boundaries with lower activation energy for diffusion, such microstructural defect provides easy diffusion path. This makes EM to occur predominantly along the microstructural defect in device operation conditions. More important, EM through such defects makes the EM flux to be non-uniform because they are not uniformly distributed. The resulting flux divergence makes two type of failure to occur in interconnects: voids or mass depletion (gradient  $>0$ ,  $\vec{J}_{in} < \vec{J}_{out}$ ) and hillocks or mass accumulation (gradient  $<0$ ,  $\vec{J}_{in} > \vec{J}_{out}$ ). In materials where diffusion occurs by substitutional mechanism, EM of atomic species is equivalent to the flow of vacancies at opposite direction. At place where flux divergence exists, those vacancies are accumulated to nucleate void. At opposite case, vacancies are destroyed by accumulation of excess vacancies so that hillocks (deposition of atoms) occur. In an interconnect, such mechanisms lead to the circuit failure by a form of open failure (voiding) or short circuit (hillock formation). Since

EM is accelerated at higher temperature and higher current density, any void formed by EM in interconnects makes EM failure to proceed with exponentially increasing rate primarily because the voided area is with smaller cross section. Further acceleration can occur because of Joule heating the voided area is with higher electrical resistance. Since Joule heating is determined by the equation as follows, it is likely that the area is heated up more so than the others.

$$J_H = I^2 \cdot R$$

In an interconnection, these mechanisms will provoke the failure by either open circuit (voids) or a by short-circuit (hillocks). In either case, the failure will decrease the interconnection performance and reliability. EM tends to be accelerated by thermal stress due to the local increase of temperature, which leads to void nucleation and coalition causing a localized current density increment directly related to the reduction of the cross section of the interconnection area.

Therefore, the EM failure by voiding is seen to develop almost as soon as stale void forms. This occurs because a local Joule heating and higher current density at voided area makes EM flux to increase. This increases the flux divergence leading to growth of void. The growth of void then makes the current density and temperature to increase further leading to higher EM flux<sup>63</sup>. This process will continue until the void is large enough for complete failure. Figure 25 shows cycle of such events leading to the failure:

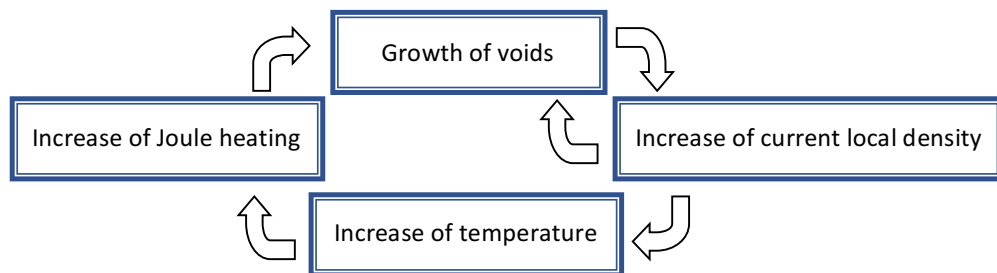


Figure 25: Thermal acceleration loop during electromigration<sup>64</sup>

Understanding EM failure often becomes complex because EM is not only force acting on the atomic flux. It has been found that there exists a force acting against EM, and this force is often referred as a stress driven backflow. The backflow effect plays a significant role when EM occurs in a short length segment. Deposition of vacancies in one end and their depletion in the other produces gradient mechanical stress. The area of mass accumulation becomes subjected to a compressive stress, while tensile stress develops at the area where vacancies are accumulating. Then stress gradient can develop across the interconnect segment and such chemical potential produces force that act against EM force. Physical dimension is not only contributing factor for the backflow. It can be produced by any local inhomogeneities in interconnect microstructure, temperature and current. This makes the control of EM failure rate to be one of major challenges in microelectronics and many numerical models are developed for the purpose of addressing them<sup>65</sup>.

#### 2.4.2 Electromigration and current density: Black's equation

Failure prediction in interconnections by EM is difficult due to the interaction of several factors that even today have not been properly identified. However, there is an empirical kinetics model based on experimental data, where the mean time to failure (MTTF) is a function of the temperature of the system, current density  $j$ , and material properties<sup>60, 62</sup>:

$$MTTF = \frac{A}{j^n} \exp\left(\frac{Q}{k \cdot T}\right)$$

where  $A$  = constant that involves material properties and geometry of interconnect

$n$  = current exponent

$Q$  = activation energy [eV]

$k$  = Boltzmann constant

$T$  = absolute temperature [K].

The values of  $A$ ,  $n$ , and  $Q$  can be determined for experimental data using accelerated tests. When the tests are performed at a constant current but with varying temperatures the activation energy can be found. In order to find the exponent  $n$ , the tests are performed at a constant temperature, but with variation of the current density.

According to the results of several theoretical studies performed in thin-film samples, an exponent  $n$  close to 1 is suggested to be dominated by void growth mechanism where the time that the void takes to grow and produce failure dominates a major portion of the lifetime<sup>66, 67</sup> although a value close to 2 is related to the mechanism where failure time is governed by the time the void takes to nucleate<sup>68, 69, 70</sup>. However, studies such as the one done by Lloyd<sup>71</sup> have concluded that Black's equation could mislead the lifetime results if consideration on pre-existing conditions such as thermal and mechanical stresses in the interconnection is not properly taken into consideration.



## CHAPTER 3

### 3. EXPERIMENTAL METHODS

#### 3.1 Test chip

In assessing EM failure mechanism, there are several considerations to be taken into account in order to clearly elucidate its role, especially when significant amount of Joule heating is expected<sup>72</sup>. EM testing typically involves the use of high temperature and high current density to accelerate the failure. The use of high current density becomes problematic because it inevitably generates significant amount of Joule heat that may alter temperature and thus failure rate of sample. This temperature increased by Joule heat is especially problematic for testing the wire bond EM failure. The electrical resistance of the wire itself is substantial and is suspended in the air without heatsink. In this situation, temperature can vary significantly from sample to sample, making it impossible to extract the true impact of EM on the failure rate.

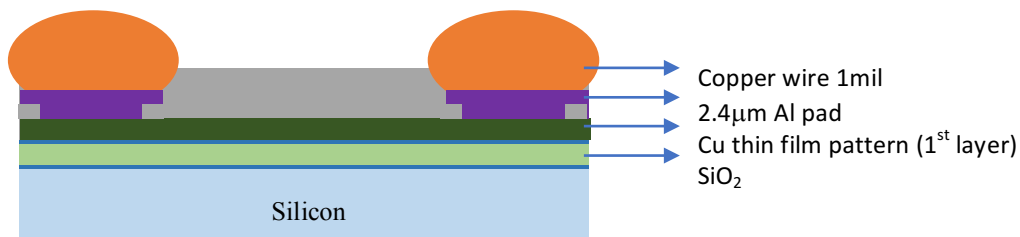


Figure 26. Schematic representation of the two-level test structure

Figure 26 shows the schematics of the sample structure used for EM test; as it is shown, the wire bond is formed on a two-level interconnect structure. The sample consists of two Al pads that are connected by underlying Cu interconnections patterned on the Si substrate. This structure

is advantageous in carrying out EM testing for two reasons. The first is the guaranteed uniformity of temperature in the Cu-Al wire interface. The Si substrate is a material with an excellent heat conductivity and thus it allows effective heat dissipation as well as heat transfer between the two pads. This enforces the interface to be immune to temperature difference as well as temperature rise from the ambient in a significant level. The second is the fact that the sample allows direct comparison of EM direction. Since EM is a directional diffusion, the resulting failure rate must show difference depending the direction of EM flow at the failure site. With the given configuration, where test current enter to one end of Al pad and exits at other end of Al pad, the two interfaces are subjected to EM condition with an opposite polarity. If the failure rate of these two pads is remarkably different, then only leading source of such difference should be attributed to EM.

### 3.2 Sample package

For EM testing, the Si chips with two Al pad patterns are first packaged into the chip carrier (Figure 27). Two types of wire bonding are made and tested in our study. The first is long-wire (L), meaning that the wire length between Al pad and pad on chip carrier is about 4 mm long. The second is the short-wire (S) which uses shorter length of wire for bond between Al pad and pad on the chip carrier, about 0.5 mm long. The four long wires shown in Figure 28 are for connection to the thermistor, which is placed in a Si chip for temperature monitoring during EM testing. For both cases of configuration, there are total of 6 wires connected to the test pattern. Two wires are for feeding currents to the test pattern while the other four wires are for measuring resistance of test pattern. Since our aim to characterize the interface failure. Four wires are needed to measure the interface resistance of each pad. The pad labeled as V1 and V4 is the tab connected to Al pads (on top of), while V2 and V3 pads are connected Cu pattern underneath the Al pads. In this

configuration, the voltage drop between V1 and V2 then measures the interface resistance of one Al pad, and the drop between V3 and V4 measures the resistance of the other Al pad. The wires used for our testing are 1 mil diameter for Cu and 1.3 mil diameter for Au.

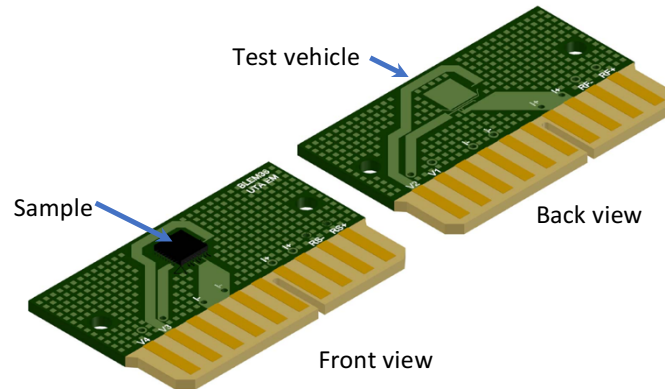


Figure 27. Cu(Au)-wire/Al-pad wire bonded sample

The internal configuration of long and short wire Cu(Au)-Al samples is shown in Figure 28, L-Cu and S-Cu samples use 1 mil diameter Cu-wire, while the S-Au samples use 1.3 mil diameter Au-wire. In both cases, Cu-Al and Au-Al, the length for S-Cu and S-Au is around 0.5mm while for L-Cu samples is about 4mm. Each sample contains only one of the configurations.

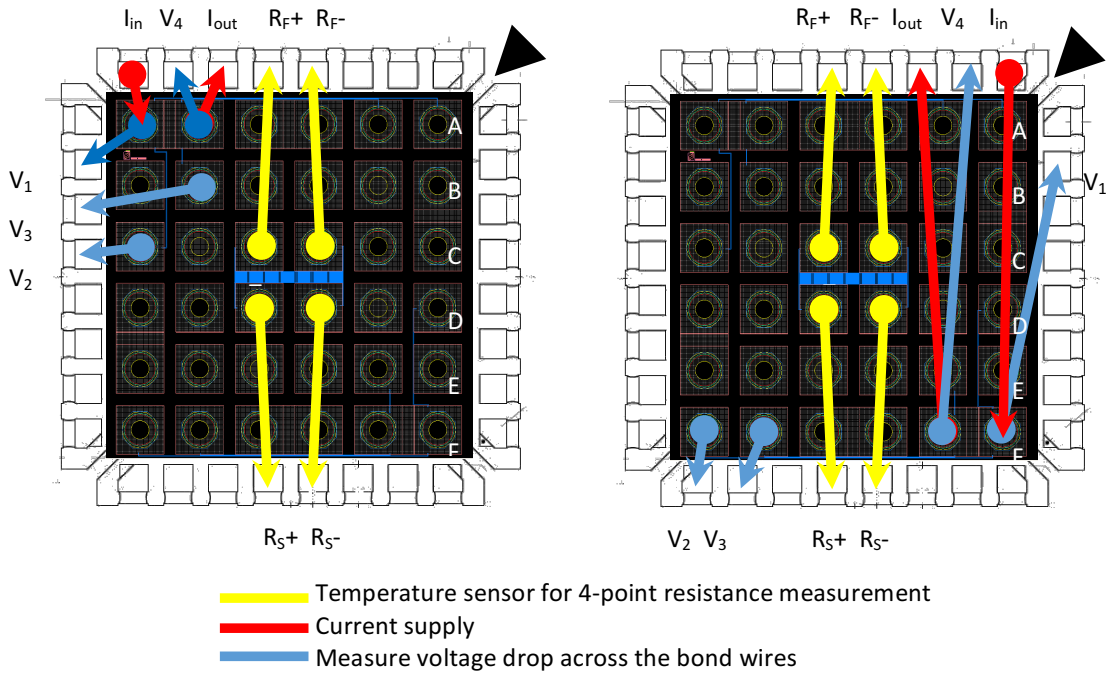


Figure 28. Short wire (left) and long wire (right) internal configuration

### 3.3 Electromigration testing

In order to perform the high-temperature EM test, it is necessary to build testing boards where a number of test vehicles shown in Figure 27 are placed and serially connected for EM testing because the  $T_g$  (glass transition temperature) of the epoxy used in available commercial boards (around 140°C) is too low to withstand the thermal load of EM testing. For this reason, we make our own board based on high temperature polyimide.

The samples are connected in series on the testing board, and therefore each of them is subjected to the same testing current and temperature conditions. This design has to be supported by the inclusion of the current by-pass boards, that by-pass current from the failed sample so that there is no interruption of test current. The by-pass board contains a temporary junction where current is routed until current to the failed sample is replaced with a more permanent connector.

A number of samples, typically 16 per test condition, are placed in a convection oven for EM testing. The convection oven is used in order to achieve temperature uniformity as well as drainage of Joule heat as much as possible. With the use of the convection oven, the difference between the oven temperature and the interface temperature (measured by the thermistor) is kept within 5°C at maximum and the temperature variation among samples is kept less than 2°C.

During EM testing, the voltage signals from samples are collected through computer controlled data acquisition (DAQ) system. This DAQ is equipped with a number of channels so that voltage signals from different samples are sequentially collected. The voltage measured in our system has a resolution of 1  $\mu\text{V}$ .

### 3.4 Test conditions

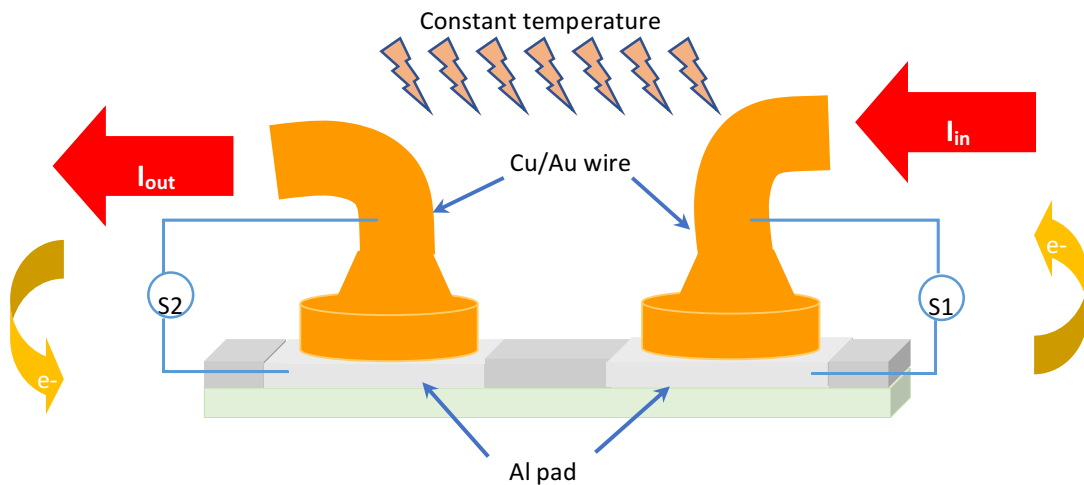


Figure 29. Test schematics

Figure 29 shows the schematic representation of wire bond connection to the test chip used in this study. As is shown, the test current is routed through the Cu-wire towards the one end of Al-pad (S1), and leaves the test chip through the Al-pad that is connected through the underlying Cu pattern (S2). This means that the EM flux is directed to the opposite direction, that is that, the

EM is directed toward Al pad in S2 while it is away from Al pad in S1. In this way, dependence of EM failure kinetics of interface between Al pad and Cu wire bond on the direction can be compared with improved consistency.

Prior to EM testing, the level of Joule heating is estimated by conducting current vs. temperature calibration. Also, the test chip is equipped with a thermistor. The thermistor is a material that shows significant change in resistance with temperature. Therefore, the temperature of the test chip can be accurately tracked during EM testing by monitoring the resistance of the thermistor. This thermistor is a stack of *TiN* thin films with 4-point Kelvin type configuration. In our testing, the resistance of thermistor is tracked by applying 1mA current. The resistance is calculated by measuring the voltage drop, and temperature is estimated by using the following equation:

$$R = R_0 \cdot [1 + \alpha \cdot (T - T_0)]$$

where:  $R$  = resistance at time  $t$

$R_0$  = resistance at  $t_0$

$\alpha$  = temperature coefficient

$T$  = temperature at time  $t$

$T_0$  = temperature at time  $t_0$

## CHAPTER 4

### 4. ELECTROMIGRATION FAILURE KINETICS AND MECHANISM

The results presented in this work are based on two type of tests performed in Cu-wire/Al-pad and Au-wire/Al-pad wire bonded samples. The first set of results are the outcome of an accelerated test based on the combination of different current densities and temperatures (conditions listed in Table 13) in order study the failure kinetics (EM test), while the second set of results are result of aging test (condition listed in Table 13) performed in S-Cu samples. The aging test is conducted to characterized the growth kinetics of IMC phases in Cu-wire/Al-pad. The result of aging test can serve as reference because it represents the growth of IMC without EM force.

Table 13. Electromigration conditions for different samples

Sample	150°C	160°C		
S-Au	2.15A	1.55A	1.75A	2.15A
L-Cu	2.10A	2.10A	2.25A	1.75A
S-Cu	2.10A	2.10A	2.30A	1.75A

Table 14. Aging test conditions for S-Cu samples

Test temperature [°C]	Aging time [h]
160	100
	250
	500
	750
	1000
180	100
	250
	500
	750
	1000
190	100
	250
	500
	750
	1000

Table 14. Continued

200	105
	250
	500
	750
	1000

The conditions listed in Table 14 have been established by taking into account the temperatures at which the EM test has been conducted. A current of 0.2A, low enough to avoid the EM and/or Joule heating affecting the interface reaction is applied to the samples in order to monitor the resistance variation at S1 and S2.

#### 4.1 Characteristics of electromigration failure in wire bond

The EM test is carried out in two types of samples: Cu-wire/Al-pad wire bond samples with wire diameter 1 mil (25.4 $\mu$ m) and Au-wire/Al-pad wire bond samples with wire diameter 1.3 mils (33 $\mu$ m). The reason for testing the two types of samples is to compare the EM failure behavior of two different systems and to extract a commonality for understanding how EM failure proceeds at interface in general. In this test, both Cu-Al and Au-Al samples are subjected to EM testing at various conditions (listed in Table 13) until at least one of the two interfaces shows resistance increase exceeding the failure criteria. For both Au-Al and Cu-Al wire bonds, the failure criteria are set to 20% increase. As indicated previously, our testing tracks the interface resistance of two pads with difference in EM polarity. Here, S1 is designated as the pad where the direction of EM is from Al pad to wire, while S2 is for the case where EM is directed from the wire to the Al pad.



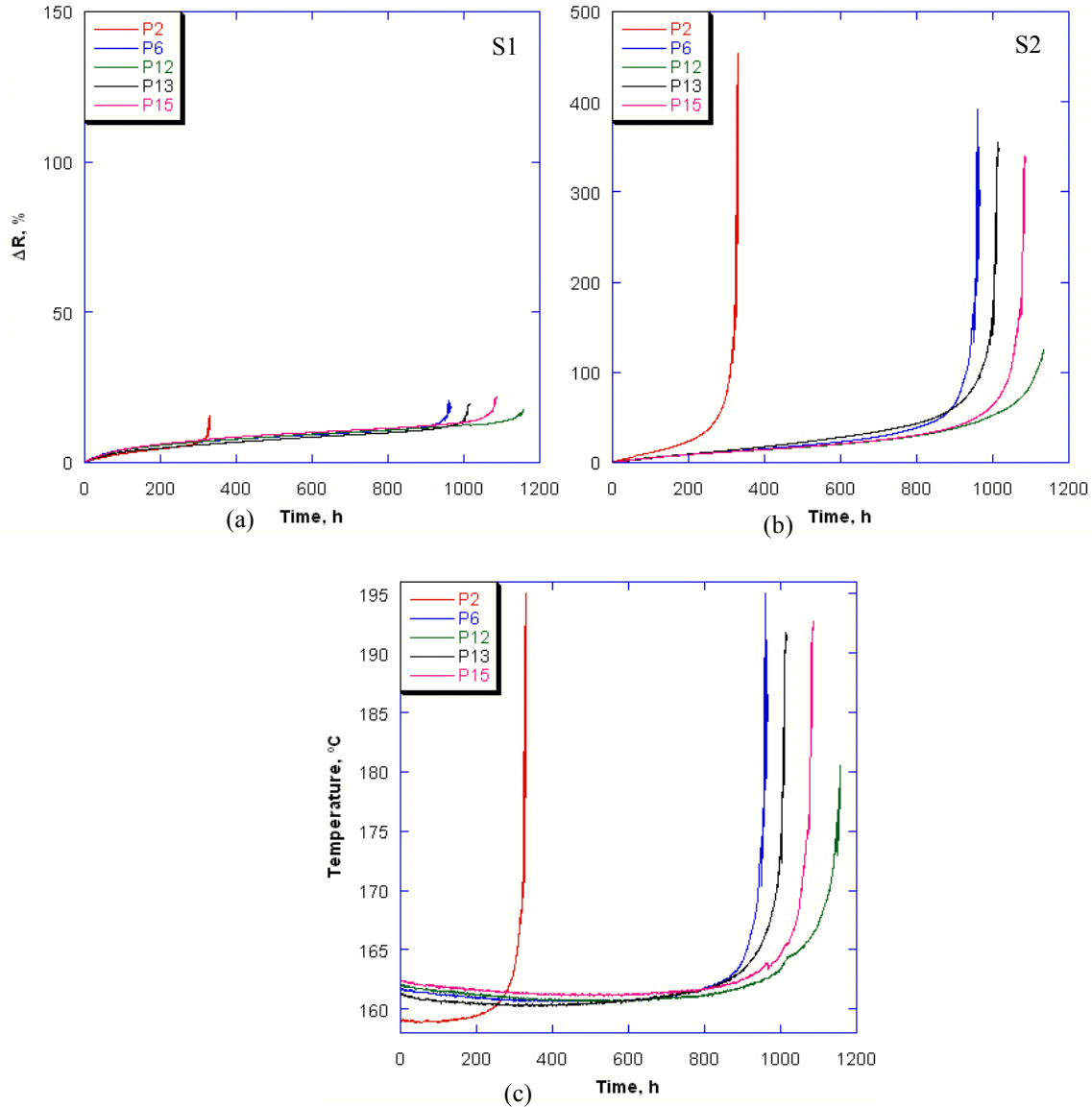


Figure 30. Failure signal from S-Au samples: (a) S1 failure signal, (b) S2 failure signal and (c) Sample temperature

The tracking of S1 and S2 resistance during EM testing shows S1 and S2 have remarkably different failure rate. An example data is shown in Figure 30 where S1 and S2 resistance tested at 160 $^{\circ}\text{C}$  and current of 1.75A. This data is obtained from samples with short-Au wire (S-Au). The failure signal clearly shows a considerable difference when signals from S1 and S2 are compared in the same samples. Note that the resistance of S2 (Figure 30 (b)) increases significantly while S1 is showing small initial increase until reaching some type of saturation. This behavior is the same

for all samples tested in our study, which provides decisive evidence that EM is acting as primary factor for driving failure in wire bonded interface. If the failure proceeds by thermal aging, then there should not be any difference in S1 and S2 failure kinetics. The fact that S2 fails much faster than S1 indicates that EM condition at S2 makes the interface failure to be accelerated. For reference, the level of Joule heating (indicated by temperature increase) is shown in Figure 30 (c). It can be seen that the sample temperature parallels with the increase in S2 resistance. Since sample temperature increases significantly with failure in S2, S1 is also likely to be subjected to accelerated EM condition. The fact that S1 resistance is not altered much even with temperature rise indicates that EM in S1 is directed in a manner to suppress the damage development (Figure 30 (b)).

The EM testing conducted on Cu-Al wire bonded samples shows essentially the same behavior to the case of S-Au sample shown in Figure 30. The result shows that S2 increases much faster than S1. Figure 31 and Figure 32 show example of EM testing data showing such behaviors. The data shown in these figures are connected from samples with long-Cu wire bond (L-Cu) and short-Cu wire bond (S-Cu) tested at 170°C and current of 2.10A. Notice that S2 resistance increases far faster than S1, and the sample temperature follow the locus of S2. Also, it can be seen that the rate of S2 resistance increase becomes exponential when the increase in S2 reaches ~5 – 10%. We believe it is a result of failure acceleration due to increase in the sample temperature that occurs with the failure at interface.

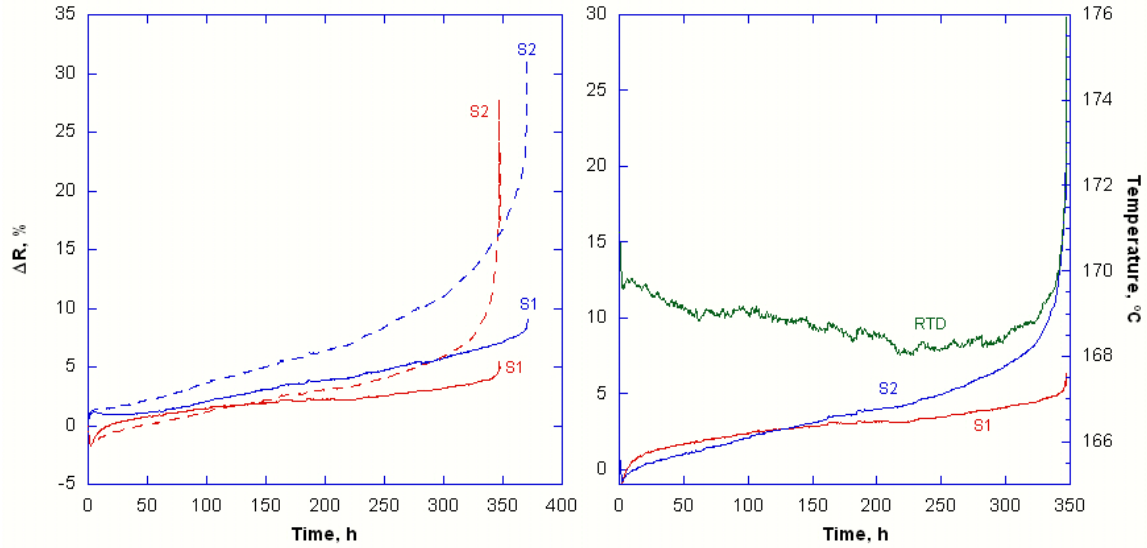


Figure 31. Failure signal for L-Cu samples

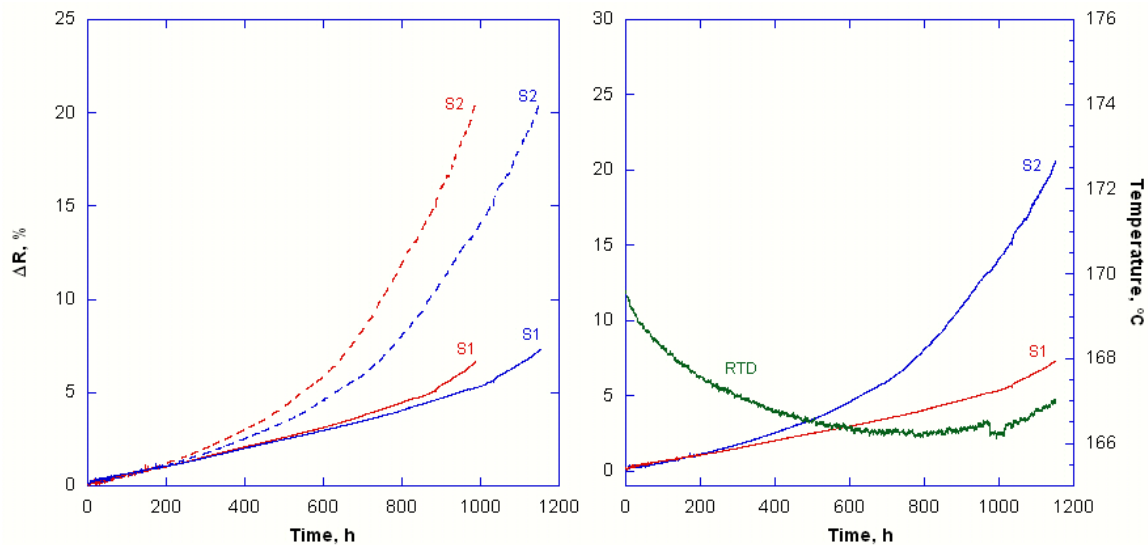


Figure 32. Failure signal for S-Cu samples

In all three cases of EM samples, S-Au, S-Cu, and L-Cu, there is a consistency that S2 fails far faster than S1. This means that the damage process at interface is fundamentally the same for both Cu and Au wire bond, and that the process occurs much more rapidly when EM is directed from the wire to the pad. Also, the failure measured by the resistance increase develop slowly at initial stage but gets accelerated as its damage develops. The increase in the resistance is near exponential with time. This type of failure behavior is commonly seen in EM testing of other types

of interconnects such as Al interconnects. The exponentially accelerated failure rate is usually considered to be the result of an increase in the current density (due to void growth) and the local temperature (due to Joule heat). We believe that the same mechanism is active in our case.

While there is a similarity in EM failure behavior between Au and Cu wire bond samples, there is also a noticeable difference. A close inspection of failure behavior indicates that Cu-Al wire bond samples show an abnormal failure rate at the early failure stage. Figures shown in Figure 33 compare the S1 and S2 resistance with EM testing. In the case of Au wire bond, S2 resistance is always higher than S1. This is no longer the case in the case of Cu wire bond. At the initial stage, S1 resistance shows a faster rate of increase until time reaches a critical point where the rate difference becomes the opposite. It can be seen that S2 resistance becomes higher than S1 after the critical point (cross-over point). This result indicates the damage process or the metallurgical process responsible for the increase in the interface resistance is initially faster at S1 than at S2 interface. The mechanism behind such behavior is not very well determined; however, as is discussed in the later sections, we believe that it is the result of EM affecting the growth of IMC phases with different specific resistivities. While the mechanism needs further elaboration, this result at least indicates that the interface resistance well represents the failure as well as IMC phase formation ongoing at the interface under EM.

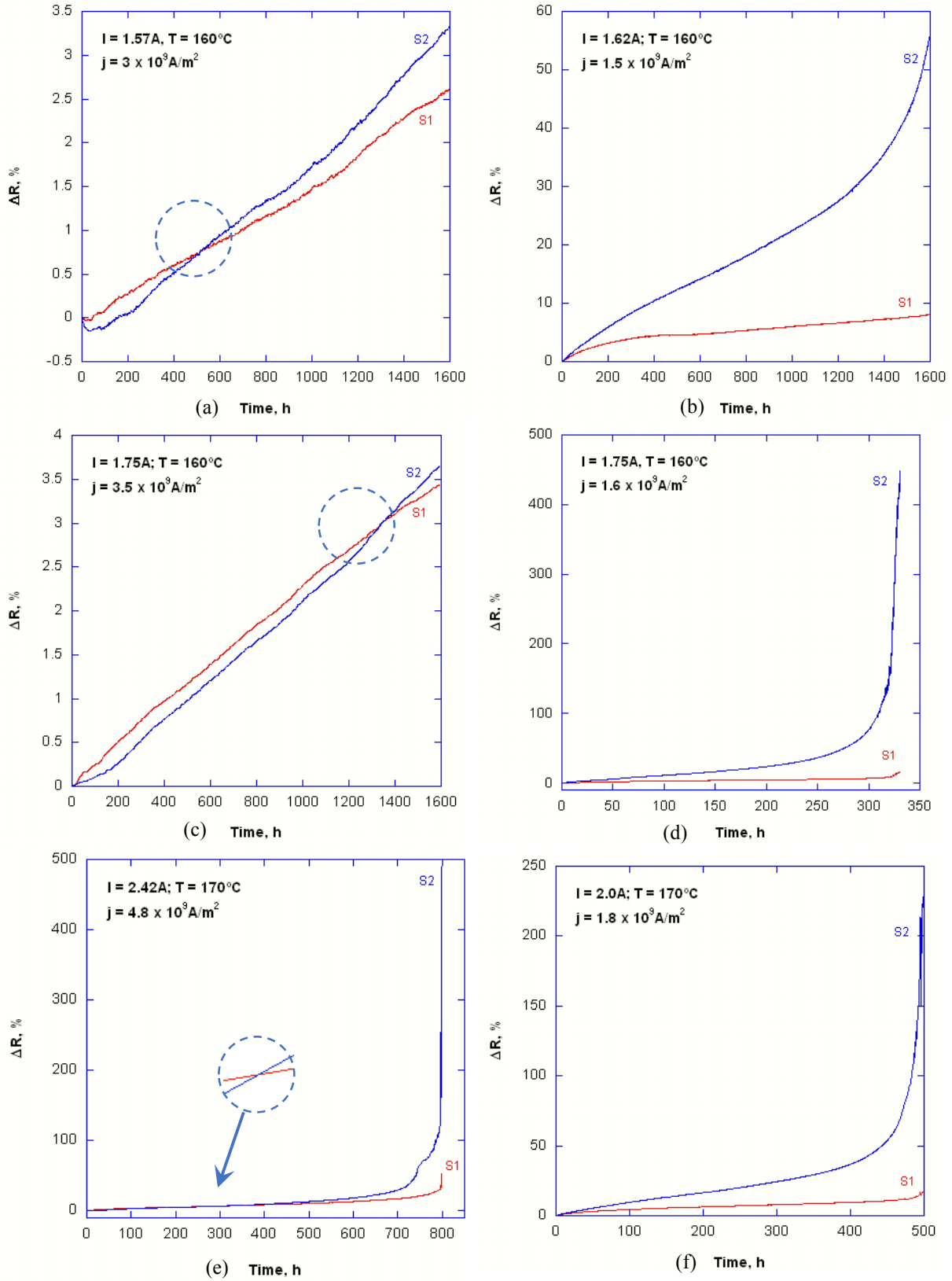


Figure 33. Failure signal for wire bonded samples (a), (c), (e) Cu-Al system, (b), (d), (f) Au-Al system

## 4.2 Electromigration failure kinetics

In order to evaluate the kinetic mechanism of EM failure, total of 16 sample per test condition is tested and time to reach 20% failure criteria is collected. The test result is shown in Figure 34 where the time to failure is plotted as a function of the cumulative probability. The failure time shown in Figure 34 represents the time for S2 resistance to reach 20% increase.

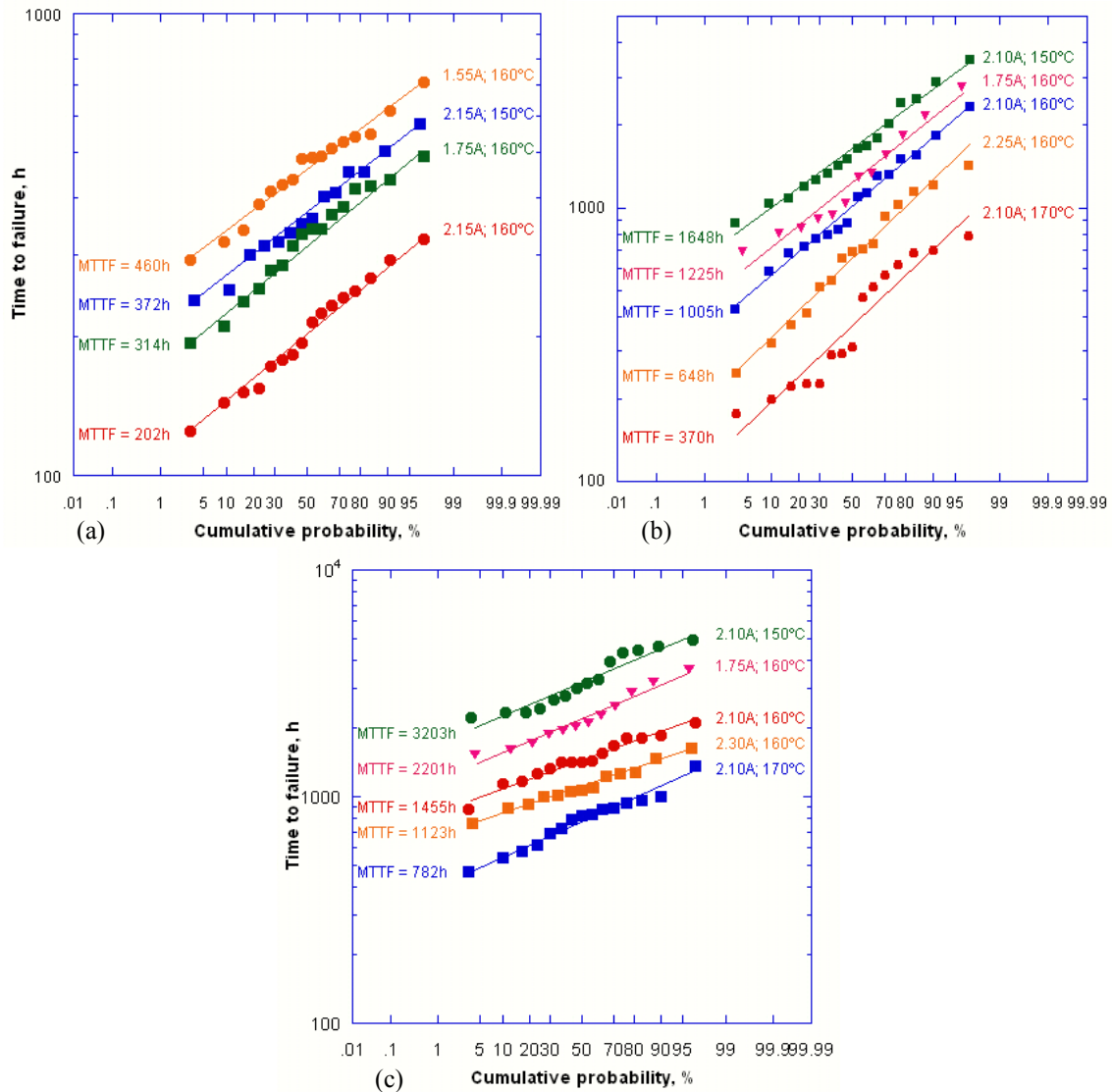


Figure 34. Cumulative probability: (a) S-Au, (b) L-Cu and (c) S-Cu

It can be seen that the time to failure fits reasonably well to the classic log-normal distribution. The mean time to failure (MTTF) and the deviation parameter fitted from the log-normal distribution is also included in the figure.

The fact that the time to failure fits well to the log-normal distribution at all conditions and also there exists a consistent change in MTTF with variation in testing conditions permits further analysis on EM failure kinetics using:

$$MTTF = \frac{A}{j^n} \exp\left(\frac{Q}{k \cdot T}\right)$$

where:  $A$  = constant that involves material properties and geometry of interconnect

$n$  = current exponent

$Q$  = activation energy [eV]

$k$  = Boltzmann constant ( $8.65 \times 10^{-5} \text{ eV/K}$ )

$T$  = absolute temperature [K]

The MTTF data collected from EM testing can be fitted to this Black's kinetic equation, through which  $n$  and  $Q$  can be determined.

Figure 35 shows the MTTF plotted as a function of temperature. According to Black's equation, the MTTF is expected to show an exponential increase with decrease in temperature if EM test is conducted under an identical current. The plot shows that it indeed shows the Arrhenius behavior and permits determination of the activation energy  $Q$ . One the other, MTTF should scale inversely with the test current,  $j$  with an exponent  $n$ . Figure 36, where MTTF of samples tested at 160°C is plotted as a function of test current, verifies the MTTF determined in our test follows Black's equation.

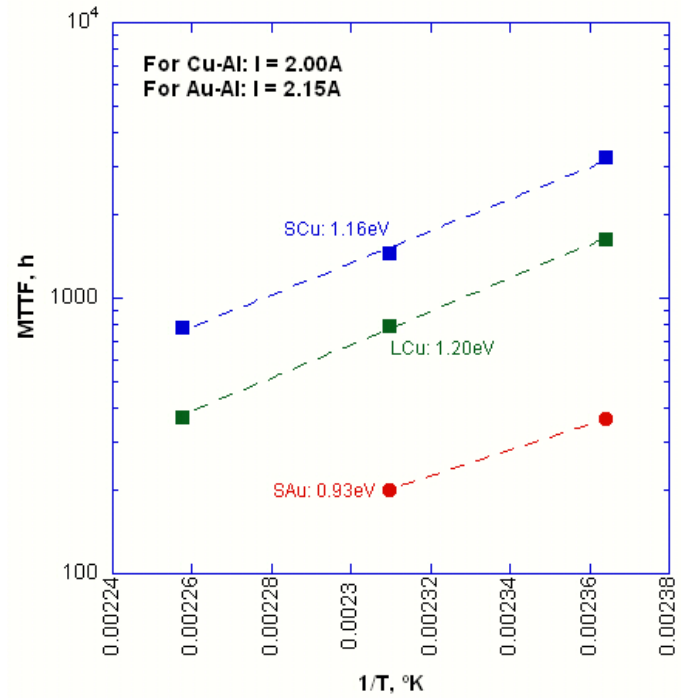


Figure 35. Activation energy based on MTTF

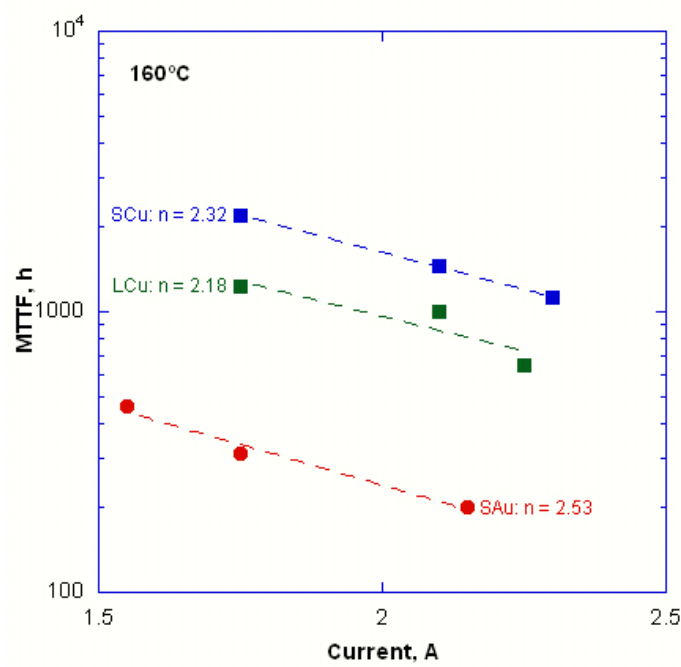


Figure 36. Current exponent based on MTTF



The activation energy for EM failure determined from Figure 35 is found to be 1.16 – 1.20 eV for Cu-Al interface failure while it is 0.93 eV for Au-Al interface. The higher activation energy for Cu-Al interface is somewhat expected because studies on interdiffusion indicates that interdiffusion in Cu and Al requires higher activation energy than that of Au and Al interdiffusion. However, the level of activation energy, which is close or greater to 1 eV, is somewhat unexpected. Since Al-pad is a thin film and EM is conducted at condition where short-circuit diffusion such as a grain boundary diffusion is more active, the activation energy for EM failure is expected to be related to activation energy for grain boundary diffusion in Al. However, it should be noted that the activation energy determined in our study is the activation energy for failure not for interdiffusion. The activation energy for EM failure is closely related not only to interdiffusion but also to the microstructure that determines the specific process of the failure<sup>73</sup>. In this regard, an analysis made by Lloyd et al.<sup>74</sup> is informative. They assert a low activation energy for failure is an indication of a poorly formed interface. For well-made interface where interface is completely formed to prevent diffusion along interface or surface, the activation energy for wire bond EM failure is at level of 1.2 eV or higher. This is consistent with what is observed in our study. On the other hand, the current exponent  $n$  is determined to be close to 2 for all cases. Classic EM failure kinetic theories established for EM failure of thin film interconnects attribute  $n = 2$  to the failure limited by the void nucleation while  $n = 1$  to the void growth. Therefore, it is tempting to use the same mechanism for our data, that is that EM failure in wire bond interface proceeds by a process of void nucleation. However, it is too premature to make such a conclusion. In case of thin film interconnects, the failure occurs almost immediately after void nucleation. Therefore, the time to failure is solely determined by the time to nucleate the stable void. A number of analytical analysis of the void nucleation kinetics indicates  $n = 2$  in that case. On the other hand, the wire bond

interface is excessively long compared to the size of embryonic void, meaning that the failure will not occur immediately after voiding. Rather, the growth of voids would take long time before the structure reaches to the point of failure. It is therefore reasonable to conclude that the meaning of  $n$  in wire bond EM case is not as simple as in the case of thin film interconnects.

Figure 37, where SEM micrographs of S1 and S2 are compared for the case of non-failed and failed interface, present evidences in supportive of our view, that is that the interface failure is not limited by the void nucleation. It can be seen that the interface shows voids or cracks developed during EM testing. There is a clear distinction between the size of the crack in the failed interface and the non-failed, suggesting that the interface EM failure proceeds by a slow growth of voids or cracks. It is our belief that the void nucleation and growth plays an equally important role for failure development. If each process take  $n = 1$ , then  $n = 2$  may become possible for the failure of interface under EM.

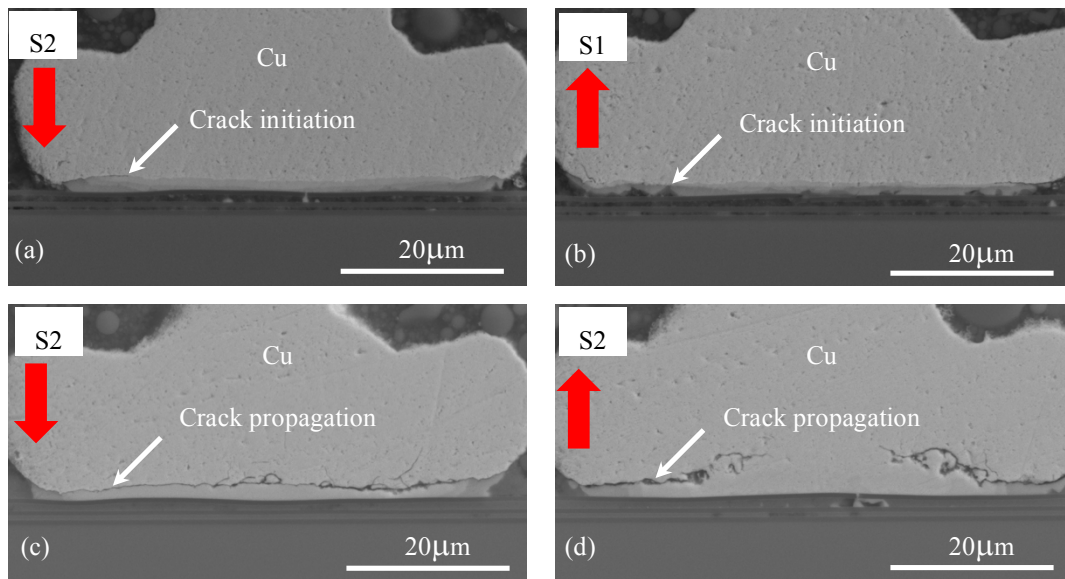


Figure 37. SEM micrographs that according to failure criteria: (a) and (b) not failed sample, (c) and (d) failed sample

### 4.3 Intermetallic phase growth by aging

In order to understand the mechanism of EM failure seen in our study, it is necessary to characterize the formation and growth mechanism of IMC phases under EM as well as without EM. For this, we first carry out the microscopic characterization of IMC phase growth of Cu-Al wire bond samples aged at various conditions. the results of this study are collectively presented in Figure 38, Figure 39, Figure 40, and Figure 41.

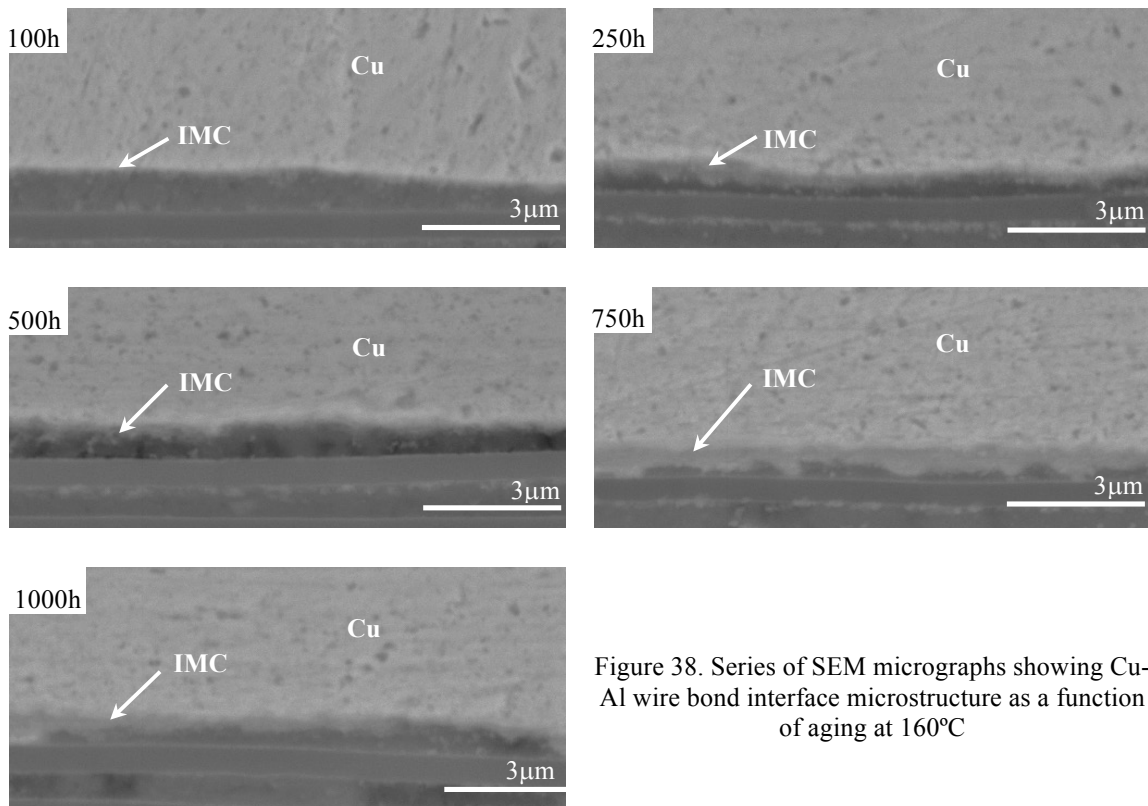


Figure 38. Series of SEM micrographs showing Cu-Al wire bond interface microstructure as a function of aging at 160°C

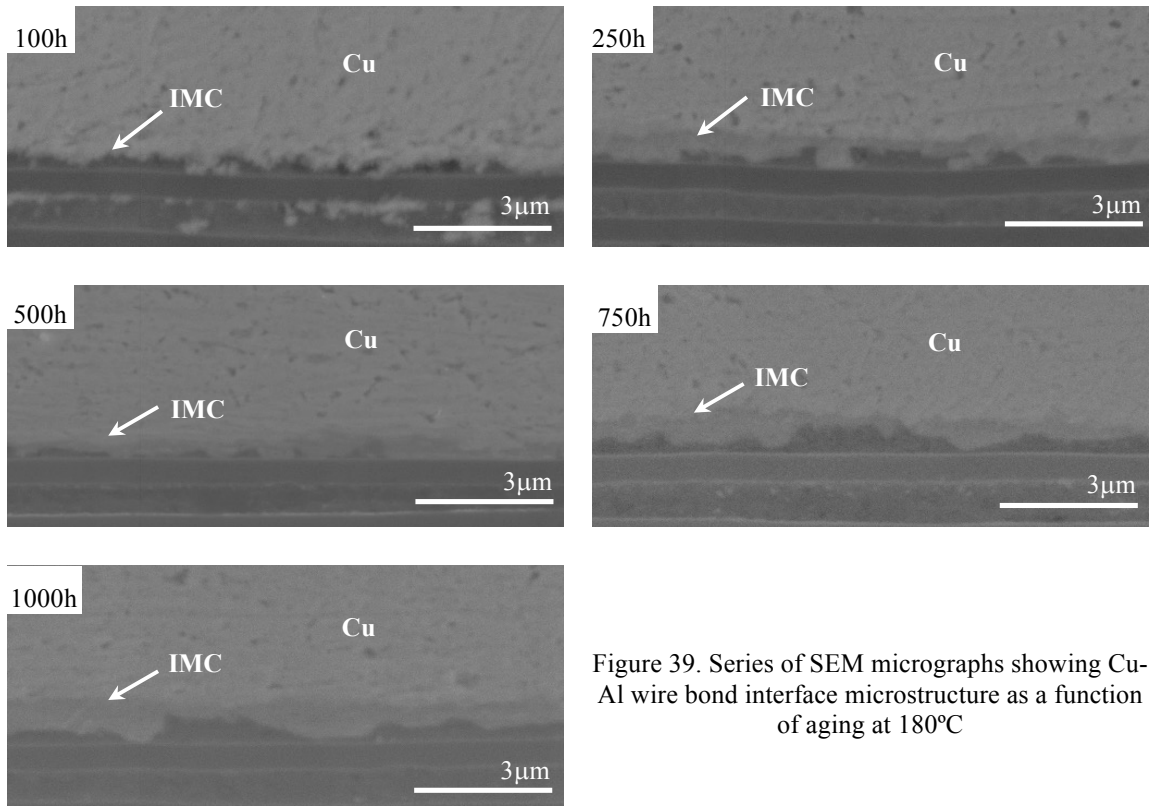


Figure 39. Series of SEM micrographs showing Cu-Al wire bond interface microstructure as a function of aging at 180°C

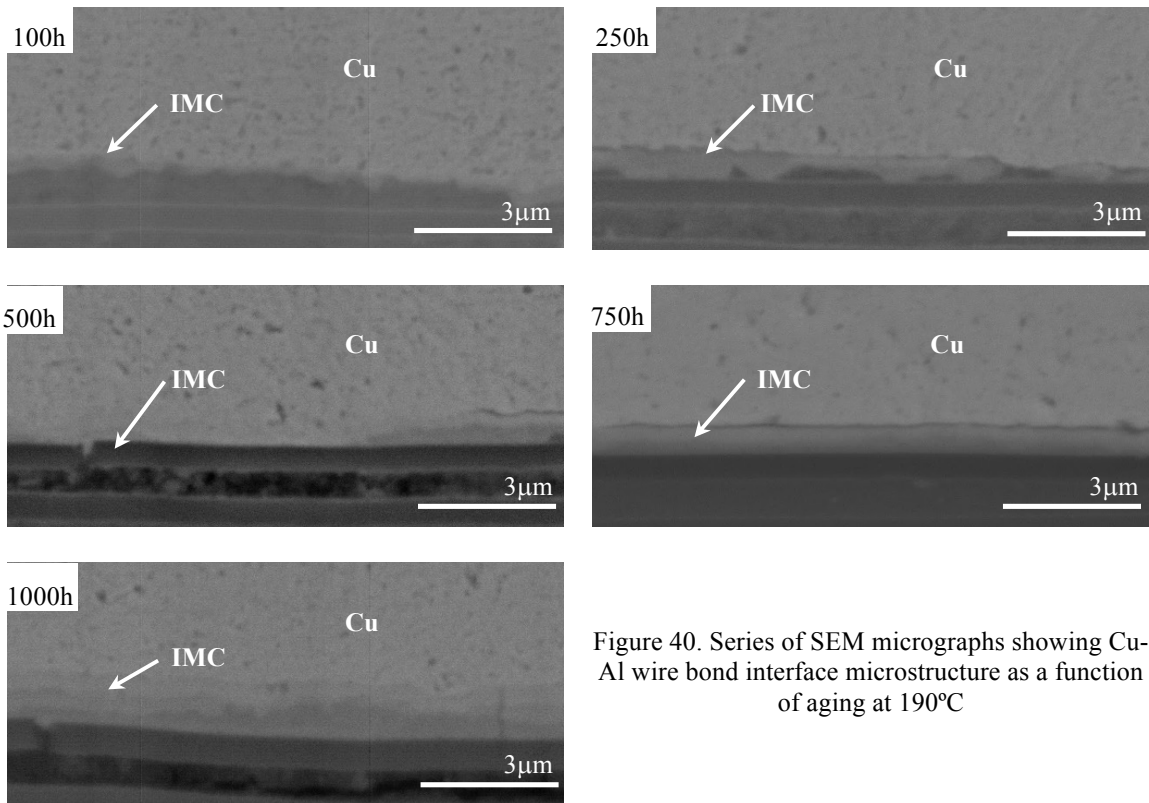


Figure 40. Series of SEM micrographs showing Cu-Al wire bond interface microstructure as a function of aging at 190°C

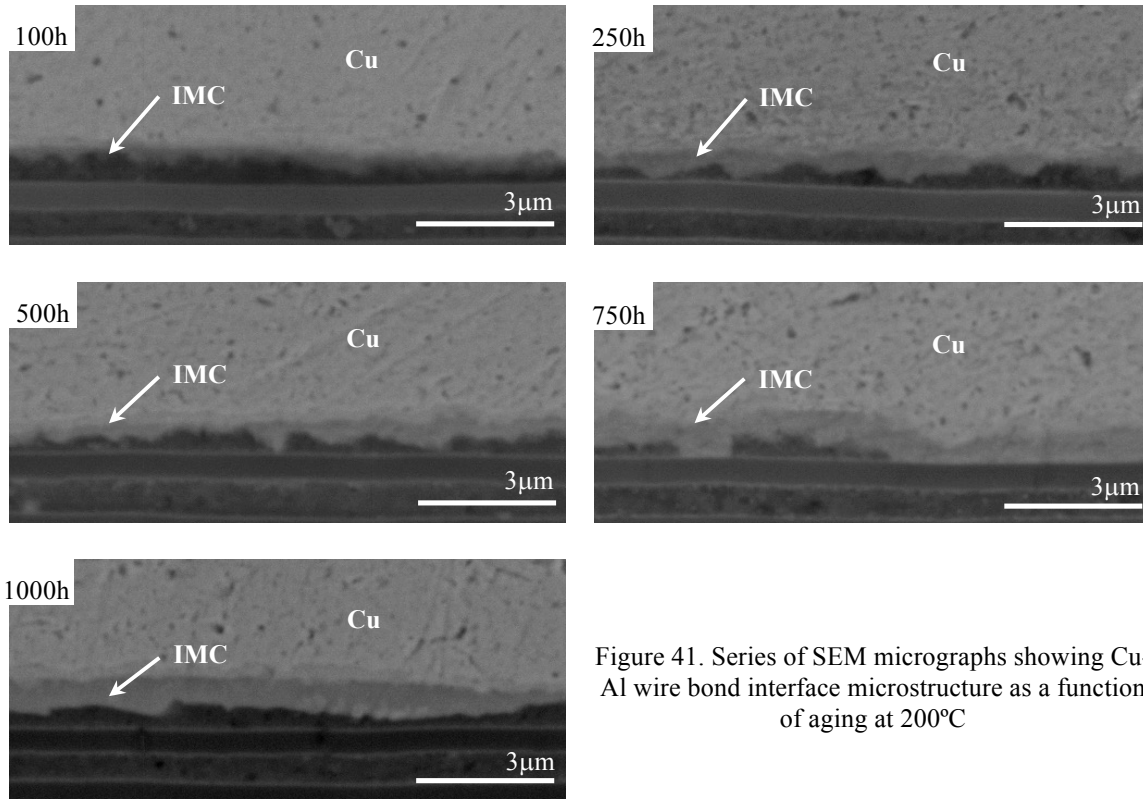


Figure 41. Series of SEM micrographs showing Cu-Al wire bond interface microstructure as a function of aging at 200°C

As shown in SEM micrographs, the interface show a growth of multiple IMC phases at the interface with aging, and its growth rate seems faster at higher aging temperature. Prior to the characterization of each IMC phase present at the interface, the SEM micrographs permits the kinetic analysis of IMC phase growth. By the use of graphic analysis software, it is possible to determine the average phase thickness at the interface, such analysis is done in our study.

The Al pad and Cu or Au wire bond configuration is assumed to be the case of the interdiffusion in semi-infinite system with a limited amount of source at surface. Then, the total IMC thickness presents the diffusion depth of Al into Cu (or Cu into Al). In such a case, the total thickness is found to follow the kinetic relation given by:

$$X = k (t)^n$$

where  $X$  = thickness of the IMC layer

$k$  = growth constant at a specific temperature

$t = \text{time}$

$n = \text{time exponent}$

Figure 42, where the total Cu-Al IMC thickness is plotted as a function of aging time is displayed, presents our attempts to fit the thickness data to the kinetic equation. It can be seen that the IMC thickness growth rate follows reasonably well the given kinetic equation.

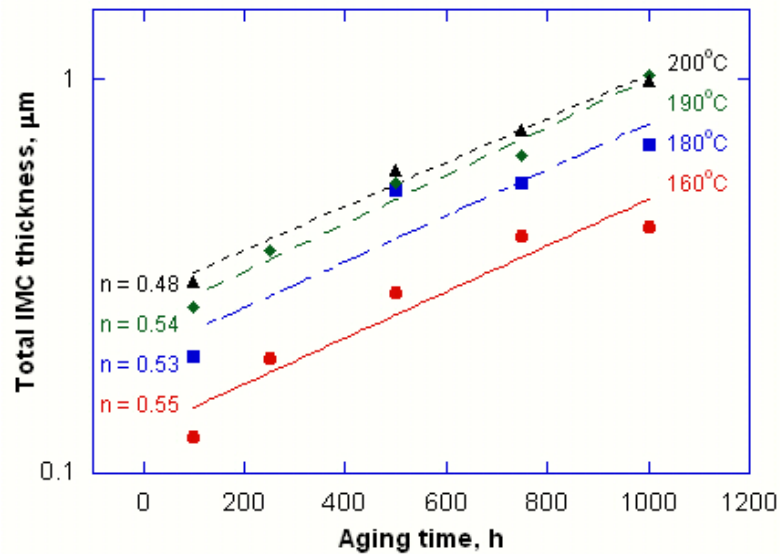


Figure 42. Time exponent based on aging time

Our analysis on data shown in Figure 42 indicates that the time exponent is consistently  $\sim 1/2$ , which is an expected exponent value from the diffusion analysis<sup>75</sup> (refer to chapter 2). What this result indicates is that the growth of IMC phase in Cu-Al wire bond interface is limited by the interdiffusion rate.

The growth kinetic equation can also enable the determination of the IMC growth activation energy, and our analysis is shown in Figure 43, where the kinetic constant  $k$  is plotted as a function of temperature. Notice the fact that the kinetic constant follows the Arrhenius behavior yielding an activation energy of 0.52 eV.

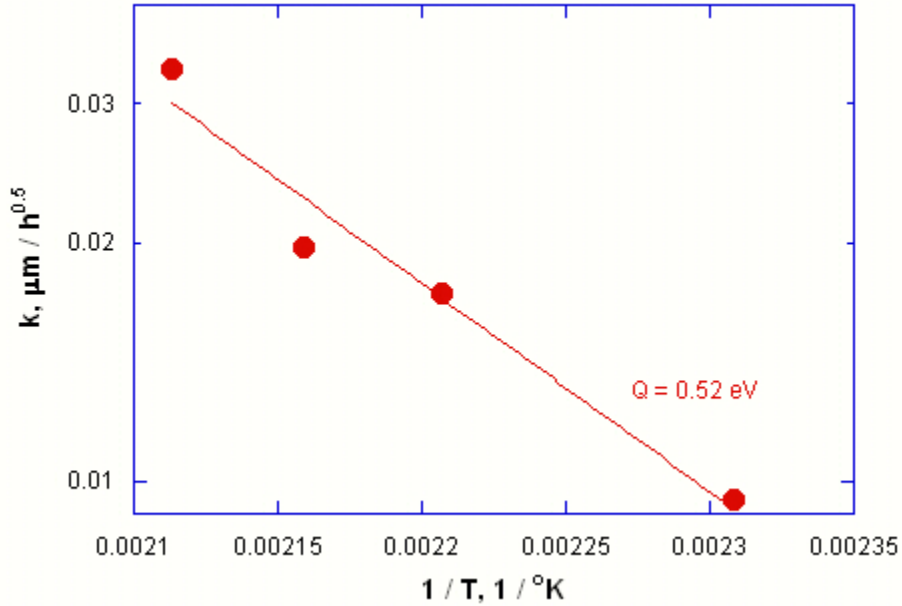


Figure 43. Plot showing the kinetic constant  $k$  of IMC phase growth as a function of aging temperature

Although there exists an ambiguity in the physical meaning of 0.52 eV activation energy seen in our study, it is not much different from what is seen by Xu et.al.<sup>76</sup>. They measure the growth kinetics of two predominant IMC phase at Cu-Al wire bond interface, and the resulting activation obtained in their study is shown in Table 15.

Table 15. Activation energy ( $Q$ ) for IMC growth in Cu/Al bonds<sup>76</sup>

IMC	$Q$	
	$[kJ/mol]$	$[eV]$
$\theta-CuAl_2$	60.66	0.63
$\gamma-Cu_9Al_4$	75.61	0.79

The activation energies listed in Table 15 are for the independent formation of the two major IMCs phases at interface:  $\theta - CuAl_2$  and  $\gamma - Cu_9Al_4$ . This table shows that the activation energy is somewhat higher than what is measured in our study but the difference is not very significant. Considering the fact that wire bond process produces significant influence on the

interface microstructure and also that the activation energy measured in our study is a combined growth of these phases, the difference in activation energy can be considered to be minor.

Xu et.al.<sup>77</sup> explains that a lower activation energy corresponds to a short-circuit diffusion process by which IMC grow by means of structural defects in the lattice. Consequently, since the diffusion rate is a direct function of crystal defects, it may be possible to conclude that the sample teste in our study may be subjected to large deformation and high stresses applied during the wire bonding formation, leading to somehow lower its activation energy.

This view is also consistent with the analysis presented by Kim et.al.<sup>12</sup> studies, where it is found that at early aging stages of annealing the growth of IMCs tend to be faster than expected from a simple interdiffusion, probably due to the enhanced diffusion rate by the presence of short-circuit diffusion path or an internal stress.

#### 4.4 Intermetallic compound formation in Cu-Al diffusion couple

The main difference between the aged samples and EM tested samples is the presence or absence of the driving force for the directional atomic movement. In the case of aging, the driving force is pure chemical potential gradient, but EM force is added to the potential gradient when the sample is subjected to current<sup>78</sup>. It is for these reasons that the results obtained in the aging test of Cu-wire/Al-pad wire bonded samples gave a helpful insight on the growth of the IMC layers founded in the wire interface. When EM force is added to the interdiffusion process, it should assist or suppress diffusion of either Cu or Al and thus formation of a particular IMC. What this means is that EM force may assist the growth of IMC in one direction, while it can retard its growth at the opposite direction. Knowing the direction of IMC growth enhancement or suppression and the type of IMC that is affected by an EM directionality can be helpful in understanding the mechanism responsible for EM failure behaviors seen in our study. However, the phases formed



at interface are usually too thin to identify their nature even with high resolution microscopic analysis tools. It is therefore necessary to investigate first the IMC formation using a simulate sample where phase identification can be done with easiness using X-ray diffraction as well as other microscopic analysis technique. A series of SEM micrographs shown in Figure 44 exemplifies the influence of EM on the interface reaction and IMC formation. As noted in the micrographs, there are multiple phases visible under the microscope, and their number and thickness is clearly different depending on the interdiffusion treatments that the samples are subjected to. Notice that there are three phases distinctive phases formed at EM tested samples, while only two is visible when such EM force is absent.

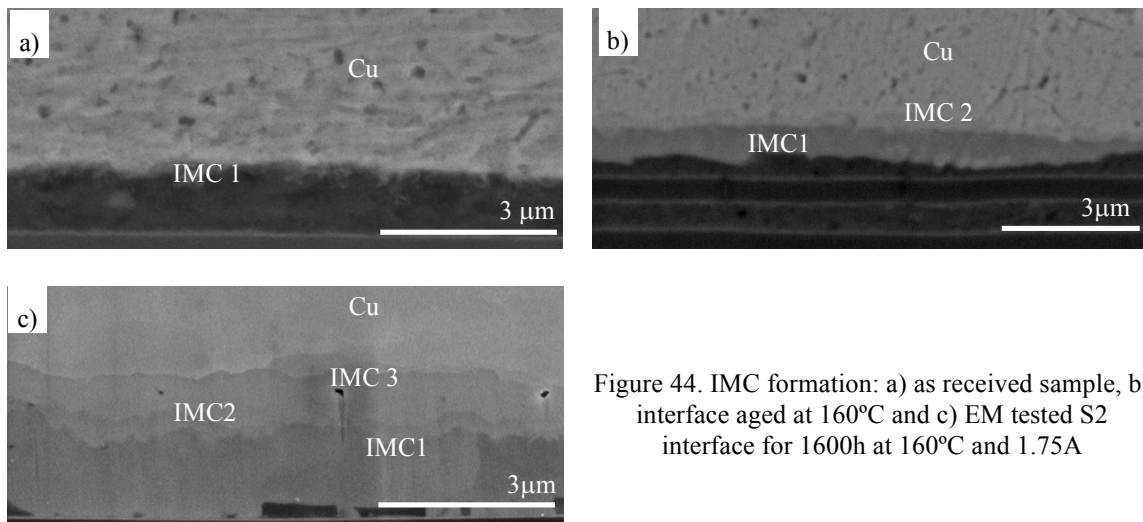


Figure 44. IMC formation: a) as received sample, b) interface aged at 160°C and c) EM tested S2 interface for 1600h at 160°C and 1.75A

In this regard, the work conducted by Mishler et.al.<sup>79</sup> can provide a useful insight because their work is motivated by the same reason. They used pure Cu plates (purity exceeding 99.95%) of approximately 1mm thickness, where an Al layer of 2μm thickness is deposited using sputter deposition process. Figure 45 shows a cross-sectional SEM micrograph of the sample produced for the purpose. As it is shown, a thin layer of Al film is deposited on Cu plate. In this configuration, Al thin film represents the Al pad, and the Cu plate represent the Cu wire. These

samples are then aged at elevated temperatures to induce formation and growth of IMC at the interface.

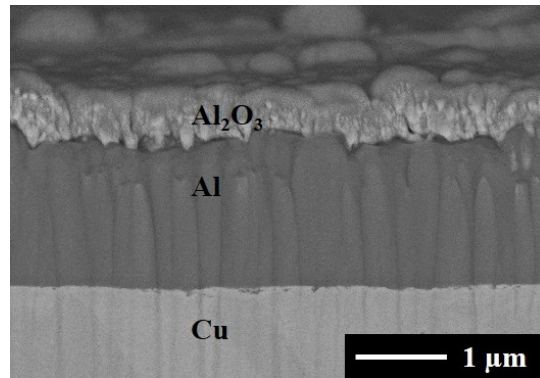


Figure 45. Cross-sectional microstructure of Cu/Al interface <sup>79</sup>

The aging treatment is conducted at temperature ranging from 350°C to 450°C, and such study find three main IMC phases:  $\theta - CuAl_2$ ,  $\gamma - Cu_9Al_4$ , and  $\alpha_2 - Cu_3Al$ . Other phases in the phase diagram (Figure 6) such as  $\eta - CuAl$ ,  $\xi - Cu_4Al_3$ , and  $\delta - Cu_3Al_2$  are not found in this study. The absence of such phases is attributed to the fact that they have high formation energy so that they may not be existing as stable phases during interdiffusion process. The evidence for three phase formation is found from X-ray diffraction study and the result is shown in Figure 46, where X-ray diffraction intensity is plotted as a function of  $2\theta$  angle for samples aged for various hours at 400°C and 450°C. Note the formation and growth of three IMC. It is found that  $\theta - CuAl_2$  phase forms at Al thin film, while  $\gamma - Cu_9Al_4$  forms at Cu plate side. This appears to suggest that there are only two phases. However, a close inspection of X-ray diffraction data, as shown in Figure 47, reveals that there are peaks belonging to one more phase. The crystal structure of this phase is similar to that of Cu, which is the face centered cubic (FCC) so that its diffraction peak appears close to diffraction peaks from Cu. According to existing literature on Cu-Al alloys, this phase is known as  $\alpha_2 - Cu_3Al$ .

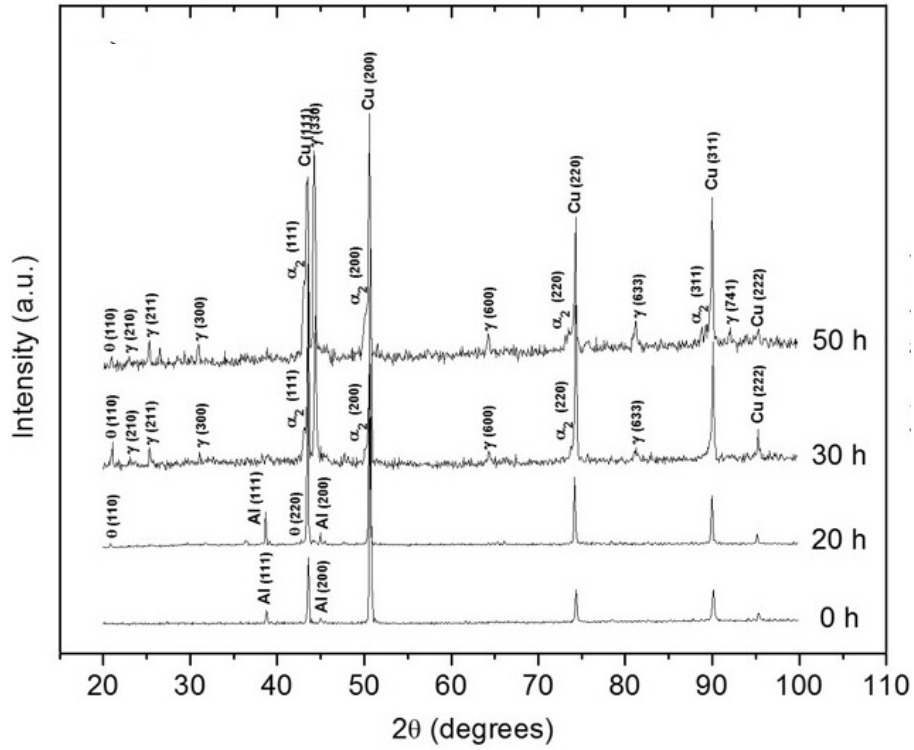


Figure 46. X-ray diffraction for a sample aged at 400°C<sup>79</sup>

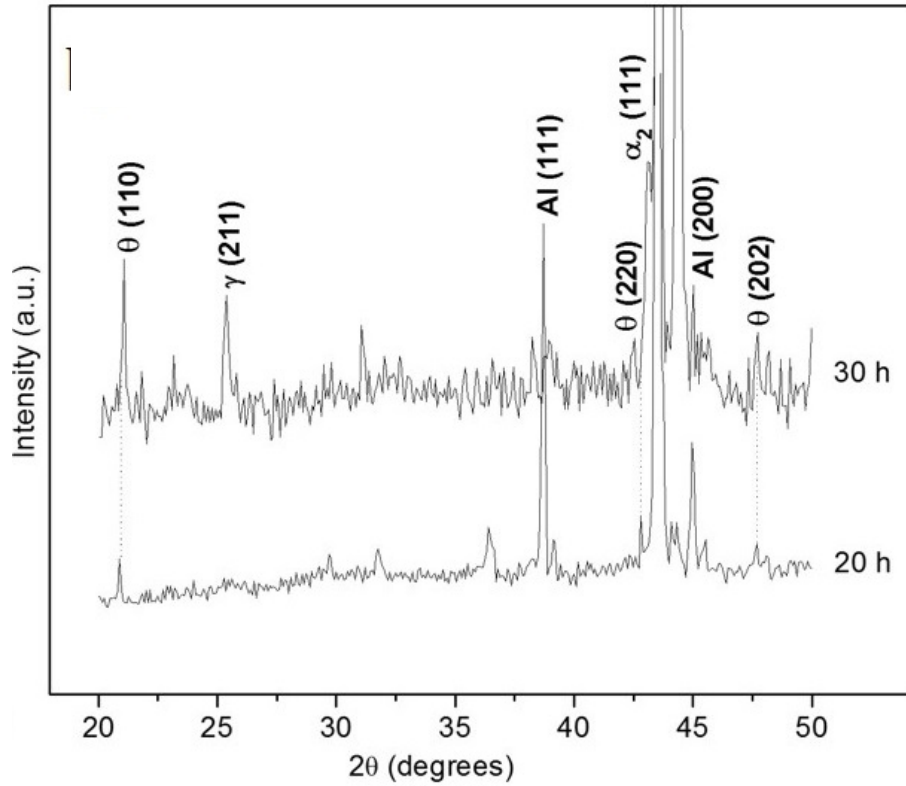


Figure 47. Enlarged view of Figure 46 near θ-CuAl<sub>2</sub><sup>79</sup>

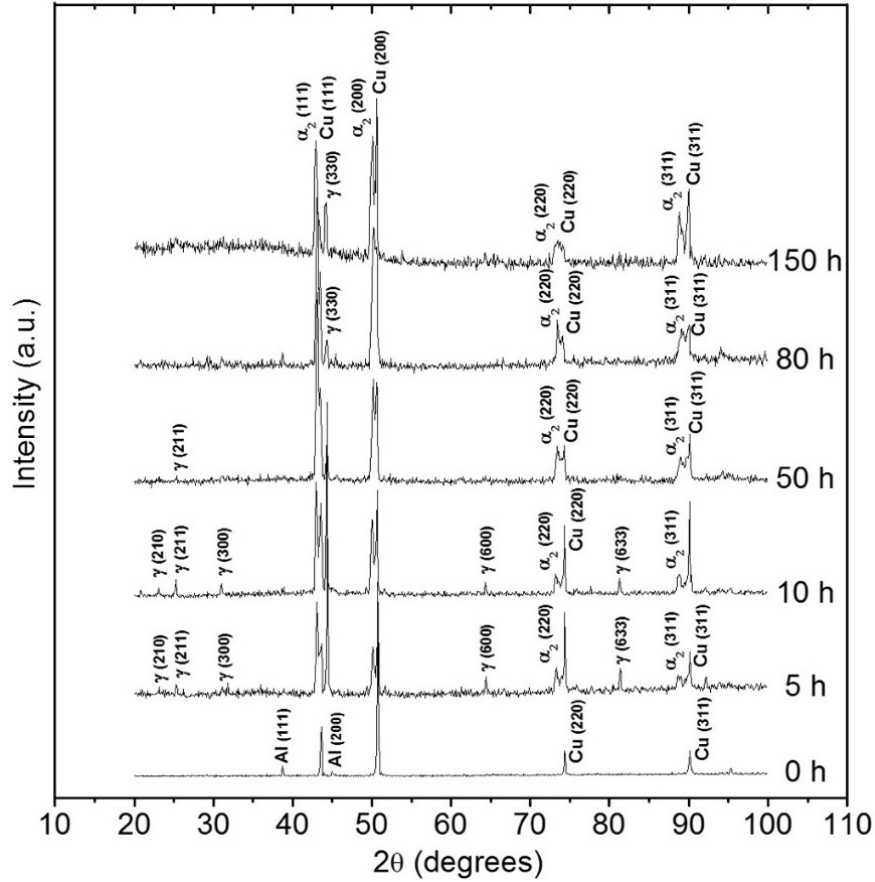


Figure 48. X-ray diffraction of a sample aged at 450°C <sup>79</sup>

The formation and growth of IMC phases found in X-ray diffraction data is confirmed by the microstructural characterization shown in Figure 49, where a series of cross-sectional SEM micrographs are displayed in samples aged at 450°C. It can be seen that there exist layers with distinctive contrast under back-scattered electron image (BEI) and they correspond to  $\theta - CuAl_2$ ,  $\gamma - Cu_9Al_4$ , and  $\alpha_2 - Cu_3Al$  phases. These micrographs also present two important features that may be helpful in understanding the phases and failures developing at Al pad-Cu plate interface shown in Figure 45. The first is the fact that there are three IMC phases forming at Cu-Al interface. As shown in Figure 48, EM tested interface shows three layers with differing contrast. The  $\theta - CuAl_2$  forms at Al, and the  $\alpha_2 - Cu_3Al$  phase forms at the Cu side. From this observation, it can be concluded that the IMC phase interfaced with Cu wire is  $\alpha_2 - Cu_3Al$  and

the one with Al pad is  $\theta - CuAl_2$ . The phase in between these phases must be  $\gamma - Cu_9Al_4$ . It is further concluded that the interdiffusion under EM does not change the fundamental stability of IMC phases. Secondly, SEM micrographs shown in Figure 49 indicate that the growth of IMC phases can trigger formation of interface crack. This crack develops at interface between  $\alpha_2 - Cu_3Al$  and  $Cu$  substrate. Interestingly, the failure seen in EM tested sample resembles the crack found in Figure 49. This result suggests that EM failure may develop as a form of crack induced by IMC growth. The exact reason why crack develops at the interface is currently unknown; however, it is believed to be related to the stress resulted by the lattice mismatch between  $\alpha_2 - Cu_3Al$  and  $Cu$  phase.

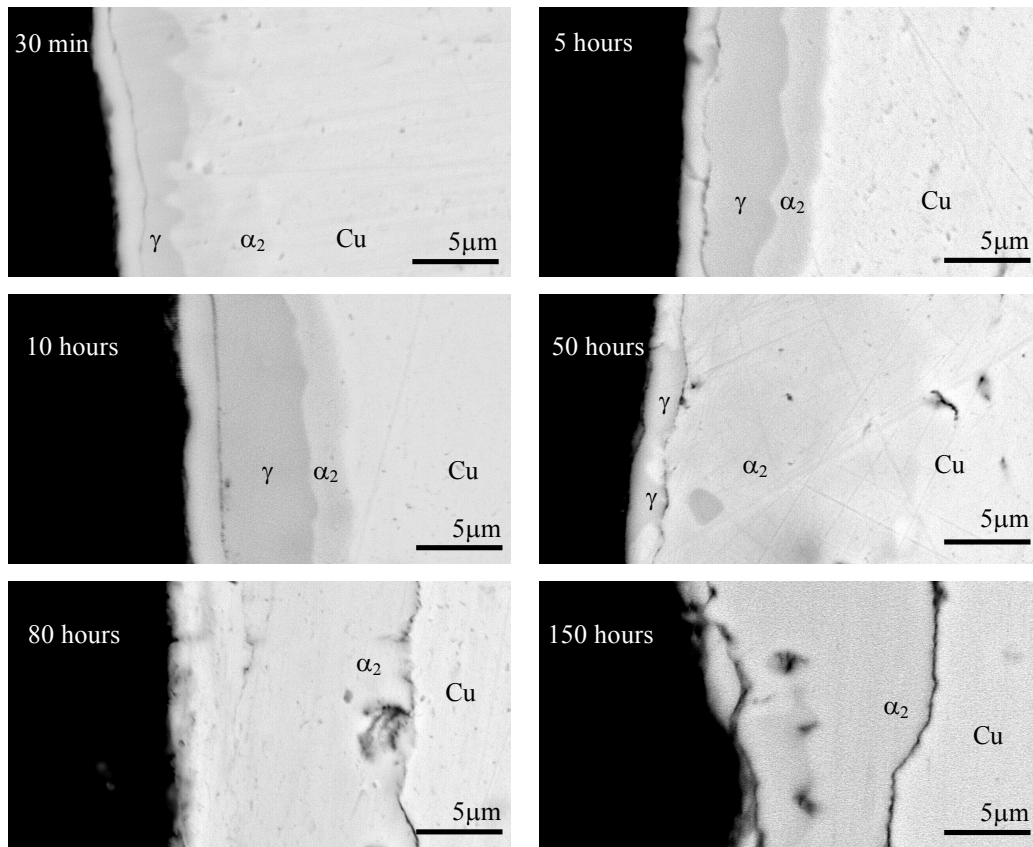


Figure 49. IMC phases in a sample aged at 450°C <sup>79</sup>

From the interdiffusion analysis conducted by Mishler et.al., multiple conclusions can be made, and EM failure mechanism can be understood by using such mechanism. Firstly, it can be concluded that IMC phase found at as-wire bonded condition is likely to be  $\theta - CuAl_2$ . This phase forms because the diffusion time during wire bond is short that interface reaction occurs in a limited scale. Since Al is a thin film filled with diffusion short-circuit, it allows easy diffusion of Cu into Al and thus formation of  $\theta - CuAl_2$  phase. Secondly, subsequent reaction makes the other two phases grow along with  $\theta - CuAl_2$ . Depending on the direction of EM, however, their growth occurs with a different rate. This mechanism is further detailed in the following section. Finally, when the IMC thickness, especially the thickness of  $\alpha_2 - Cu_3Al$ , reaches a critical thickness, interface crack develops probably as a result of lattice distortion. The presence of EM makes this process to occur in much more pronounced rate.

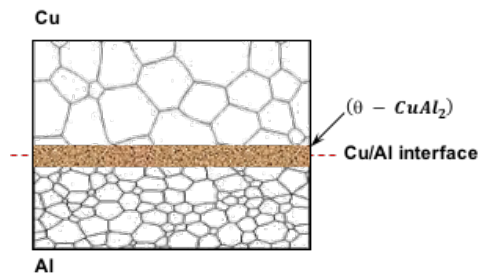


Figure 50: Schematics of S1 and S2 after wire bonded process

## 4.5 Failure mechanism analysis

### 4.5.1 Effect of electromigration on the intermetallic compound growth mechanism

The main objective of our study is to understand the wire bond failure mechanism by EM. Failure kinetics analysis as well as microstructural analysis indicate that EM effect needs to be analyzed with consideration on the growth of IMC phases. The question as to how EM affects the IMC growth needs to be answered. This requires to consider the biased interdiffusion (by EM) and

its contribution to IMC growth because EM creates two different situations of the biased interdiffusion. Our observations suggest that EM promotes the growth of IMC layers when EM flow is directed from the wire to Al pad.

Figure 51 present the schematic representation of the interdiffusion mechanism that may explain the reason why such result is possible. The basis of our mechanism lies on the fact that diffusion of Al into Cu is sluggish compared to the diffusion of Cu into Al pad. This is a reasonable assumption to make because the microstructure of Cu (or Au) wire is such that diffusion should occur predominantly through the bulk diffusion. Consisting of large grains, the Cu wire has very low grain boundary density. Furthermore, being a high melting temperature material, diffusion in Cu wire requires high diffusion activation energy. On the other hand, diffusion into Al pad must be relatively easier. Firstly, it is a material with low melting temperature, requiring lower activation energy for diffusion of any species. Further, the high grain boundary density makes the grain boundary diffusion to be dominant. These factors make diffusion of Cu into Al pad to proceed easier than the opposite.

Then, the EM effect will be most pronounced when it is directed from the wire to Al pad direction because it is the direction of easy diffusion. The opposite direction will make IMC growth to be retarded. A schematic representation this mechanism is displayed in Figure 51. As is shown, the IMC growth at S2 is enhanced by EM, while it is suppressed at S1. Note also that the failure is assumed to occur at the interface between Cu or Au wire and IMC. This assertion is made because it is likely the place of maximum flux divergence. Since flux toward Cu or Au wire is suppressed in S2, while it is accelerated by EM in Al and IMC side, the interface between IMC and the wire will be subjected to the maximum flux divergence. Combined with possible stress

created by lattice mismatch between IMC and the wire, this flux divergence can lead to the formation of either void or crack. Subsequently, the failure proceeds faster at S2 than at S1.

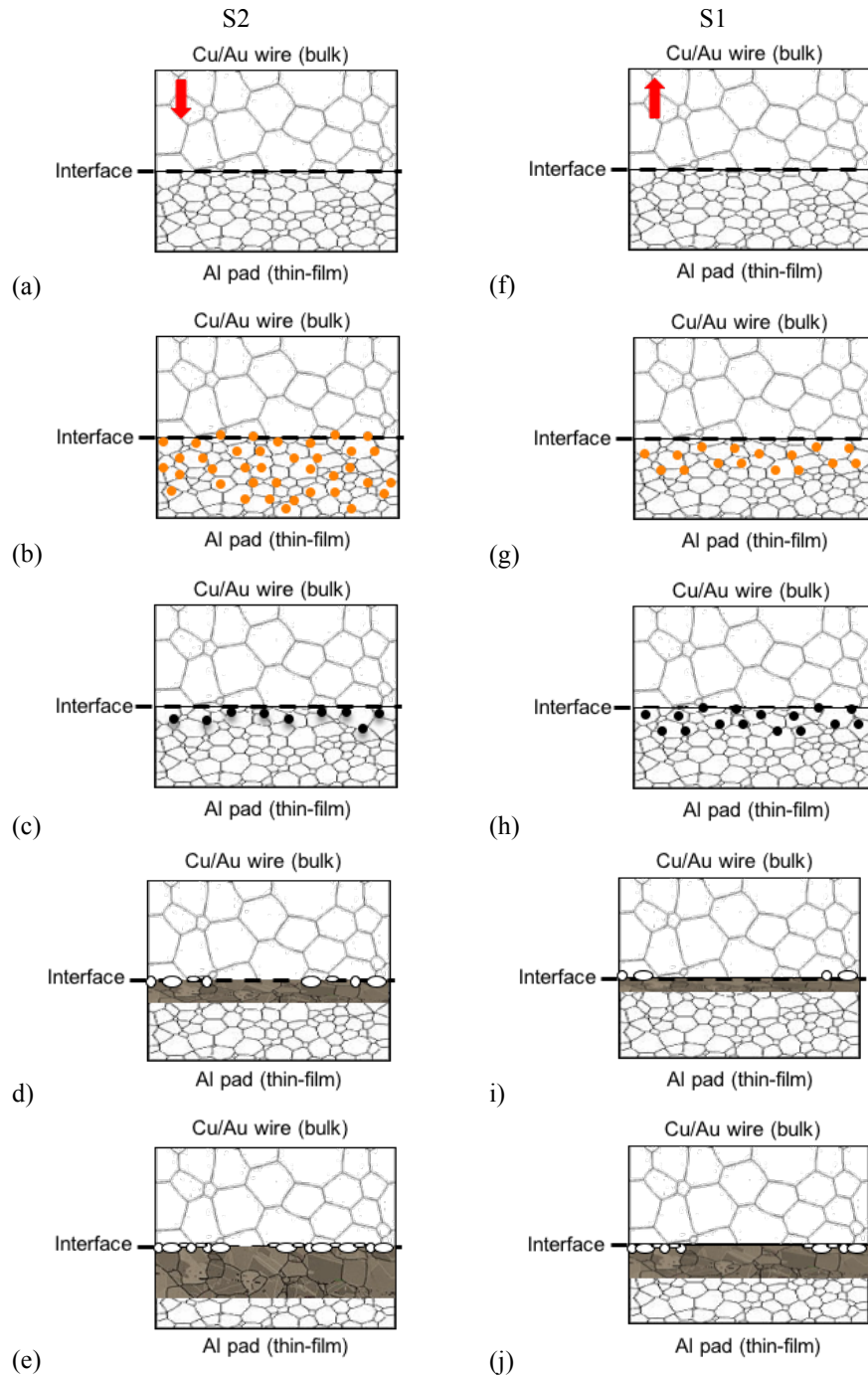


Figure 51. Schematic representation of intermetallic compound growth under electromigration



#### 4.5.2 Mechanism of failure rate change in Cu-Al wire bond interface

One of the most interesting and peculiar features found in Cu-Al wire bond EM is the fact that S2 shows slow failure rate at the beginning of EM testing but later overwhelm the rate of S1. It is consistently found that there exists a cross-over time where the amount of resistance increase in S1 is the same as the S2 interface. Before this cross-over time, the resistance is higher at S1, but the order becomes reversed after the critical time. There is no metallurgical difference between S1 and S2, and therefore the only possible mechanism behind such behavior must be found from EM affecting the IMC growth rate.

At an initial stage of EM testing when EM effect should play a minor role, it is likely that IMC formation at S1 and S2 is not much different. However, as is shown in Figure 52 where S1 and S2 resistance is compared, S1 shows a higher increase rate of resistance almost immediately.

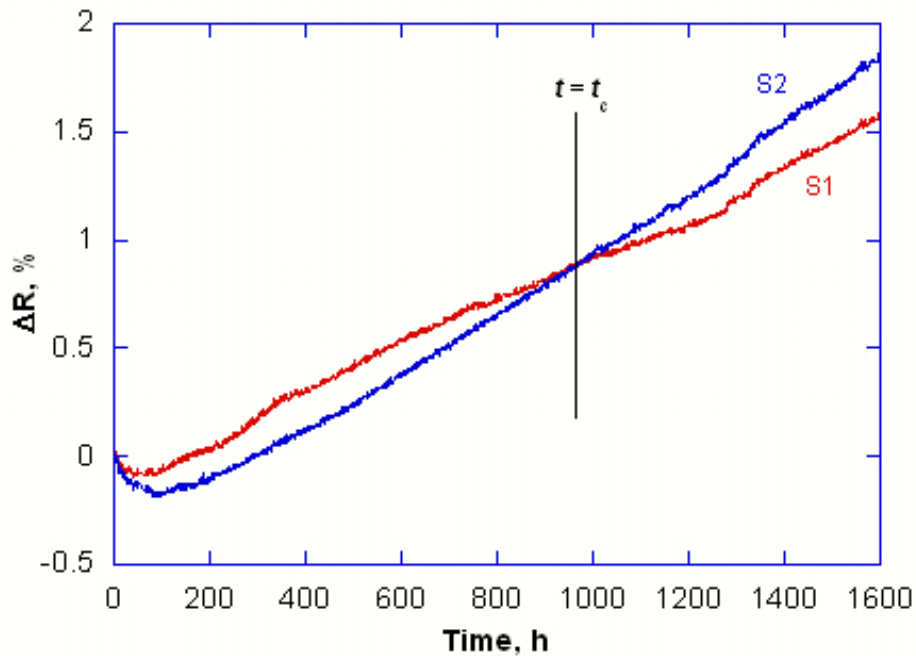


Figure 52: Signal obtained from S1 and S2 under EM conditions

Therefore, it is reasonable to assume that the reason for S1 resistance increasing faster than S2 is related to a particular IMC that is favorably growing under S1 EM condition. As shown in Figure 44.a and also in Figure 53, the starting interface structure is not IMC free but contains a thin layer of  $\theta - CuAl_2$ .

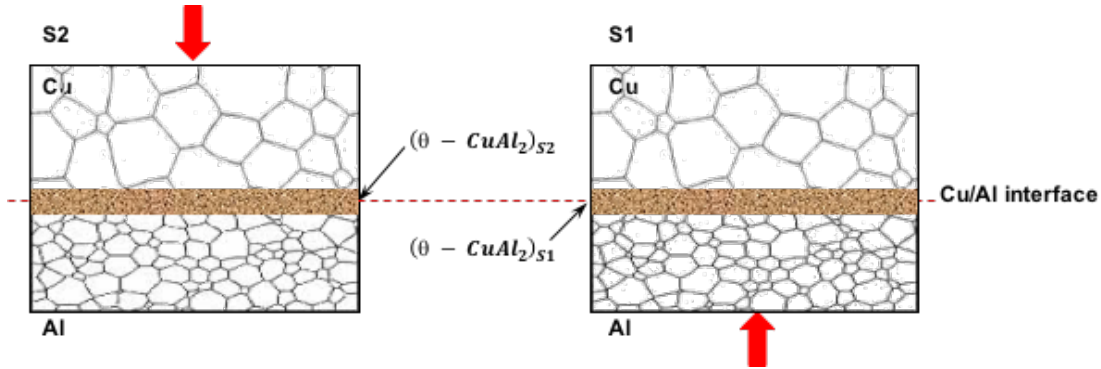


Figure 53: Wire bonded interfaces at  $t = 0$

Consequently, the resistance of S1 and S2 interface should be equal at start and contains resistance contribution from the pre-existing  $\theta - CuAl_2$  phase. Assuming that the interface area is the same for S1 and S2, then the identical interface resistance of S1 and S2 at  $t = 0$  lead to:

$$\rho_{\theta} \cdot l_{\theta S1} = \rho_{\theta} \cdot l_{\theta S2}$$

When EM commences, the first phase that will grow should be the  $\theta - CuAl_2$  phase. The interface then develops  $\theta - CuAl_2$  at interface followed by  $\alpha_2 - Cu_3Al$  at Cu wire end. The interface resistance starts to contain the contribution from the IMC phases forming at interface. Their contribution to the total interface resistance depends on the specific resistivity and thickness of each phase. The specific resistivity of Cu-Al IMC phases at 300K is shown in Table 16.

Table 16. Cu-Al intermetallics characteristics <sup>21</sup>

Phase	Resistivity, [ $\mu\Omega \cdot cm$ ]	Coefficient of thermal expansion, [ $ppm/^{\circ}C$ ]
CuAl <sub>2</sub>	7 – 8	23.5
CuAl	11.4	11.9
Cu <sub>4</sub> Al <sub>3</sub>	12.2	16.1
Cu <sub>3</sub> Al <sub>2</sub>	13.4	15.1
Cu <sub>9</sub> Al <sub>4</sub>	14.2 – 17.3	17.6

The specific resistivity of  $\alpha_2 - Cu_3Al$  phase is currently unknown but is expected to be higher than other phases. The reason for this belief is based on the fact that the resistivity of IMC phase tends to increase with increase in Cu content. Since  $\alpha_2 - Cu_3Al$  phase is the IMC phase with most Cu, it is likely that  $\alpha_2 - Cu_3Al$  phase is the phase with highest resistivity. Under this assumption, then the most influential phase among the three possible IMC phases at interface on the interface resistance is the  $\alpha_2 - Cu_3Al$  phase and the next is  $\gamma - Cu_9Al_4$ . Note that the growth of  $\gamma - Cu_9Al_4$  or  $\alpha_2 - Cu_3Al$  phase can make twice greater impact to the interface resistance than the  $\theta - CuAl_2$ . This analysis leads to the belief that the cross-over phenomena occurs because high resistivity IMC formation is preferred at S1 interface in the beginning of EM. The growth rate of this phase becomes slow as time continues, then S2 resistance can catch up with S1 resistance. This sequence is presented in Figure 51 where schematic representation of IMC formation in S1 and S2 is compared.

As it is shown in Figure 54, Figure 55 and Figure 56, when  $t < t_c$ , the main IMC forming at S2 is  $\theta - CuAl_2$  while it may be either  $\alpha_2 - Cu_3Al$  or  $\gamma - Cu_9Al_4$  at S1 interface. In S2 interface, EM of Cu in Al is in parallel with diffusion. This makes  $\theta - CuAl_2$  phase to grow by consuming Al pad. In S1 interface however, the EM direction is in parallel with Al diffusion into Cu wire. The EM direction for Cu in Al pad is opposite to the diffusion direction. This suppresses the growth of  $\theta - CuAl_2$  phase and promotes the growth of either  $\gamma - Cu_9Al_4$  or  $\alpha_2 - Cu_3Al$  phase. Since  $\gamma - Cu_9Al_4$  or  $\alpha_2 - Cu_3Al$  phase is high resistivity phase, their growth makes S1 interface to be with higher resistance. However, the requirement of the bulk diffusion in Cu wire results in slow growth of those phases. Therefore, the S1 resistance increases rapidly upon commencement of EM but quickly slows down overtime.

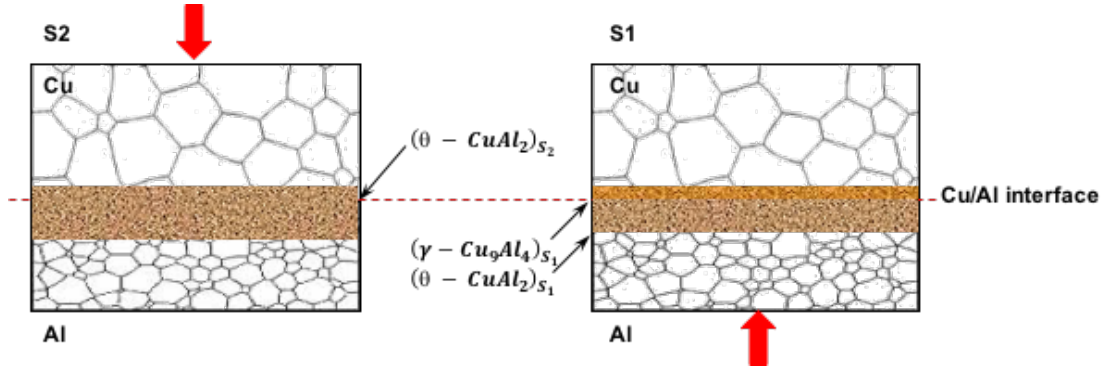


Figure 54: Wire bonded interfaces at a time  $t_1$  between  $0 < t < t_c$

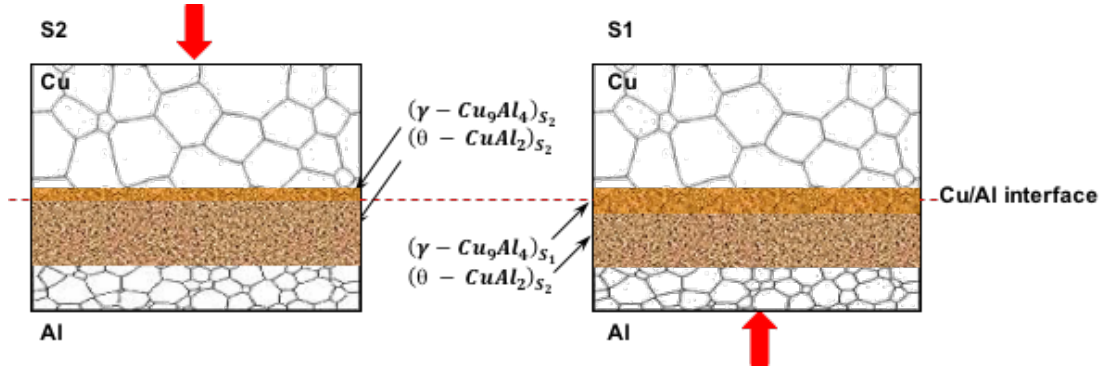


Figure 55: Wire bonded interfaces at a time  $t_2$  between  $0 < t < t_c$

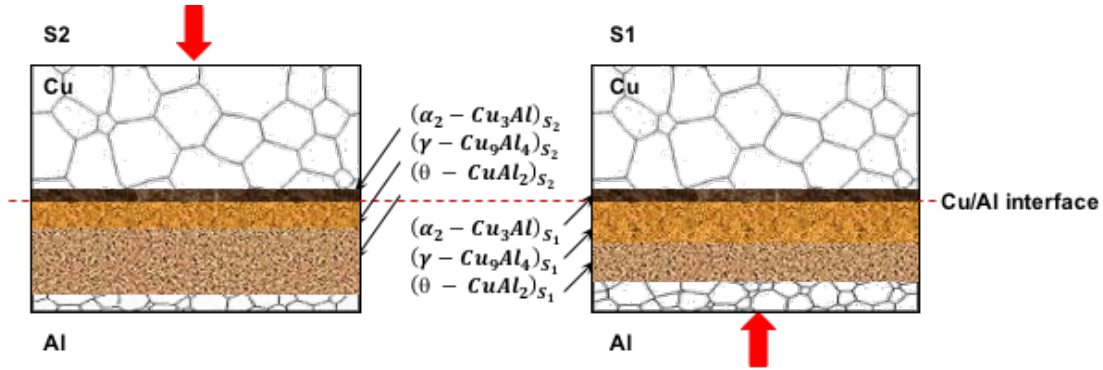


Figure 56: Wire bonded interfaces at a time  $t_3$  between  $0 < t < t_c$

In the meantime, the growth of  $\theta - CuAl_2$  continues at S2 with an accelerated manner so that S2 resistance can finally catch up with the S1 resistance. Therefore, at  $t = t_c$ , the condition of equal resistance occurs:

$$\rho_{\theta} \cdot l_{\theta S2} + \rho_{\gamma} \cdot l_{\gamma S2} + \rho_{\alpha_2} \cdot l_{\alpha_2 S2} = \rho_{\theta} \cdot l_{\theta S1} + \rho_{\gamma} \cdot l_{\gamma S1} + \rho_{\alpha_2} \cdot l_{\alpha_2 S1}$$

In summary, following analysis can be made as to the S1 and S2 resistance change. When  $0 < t < t_c$ , the S1 resistance is higher because the interface is filled with high resistivity IMC:

$$\rho_{\theta} \cdot l_{\theta S_2} + \rho_{\gamma} \cdot l_{\gamma S_2} + \rho_{\alpha_2} \cdot l_{\alpha_2 S_2} < \rho_{\theta} \cdot l_{\theta S_1} + \rho_{\gamma} \cdot l_{\gamma S_1} + \rho_{\alpha_2} \cdot l_{\alpha_2 S_1}$$

On the other hand, when  $t > t_c$ , the S2 interface resistance is higher because of extended growth of IMCs, including  $\theta - CuAl_2$  and  $\gamma - Cu_9Al_4$ , and also consumption of low resistivity Al pad (Figure 57).

$$\rho_{\theta} \cdot l_{\theta S_2} + \rho_{\gamma} \cdot l_{\gamma S_2} + \rho_{\alpha_2} \cdot l_{\alpha_2 S_2} > \rho_{\theta} \cdot l_{\theta S_1} + \rho_{\gamma} \cdot l_{\gamma S_1} + \rho_{\alpha_2} \cdot l_{\alpha_2 S_1}$$

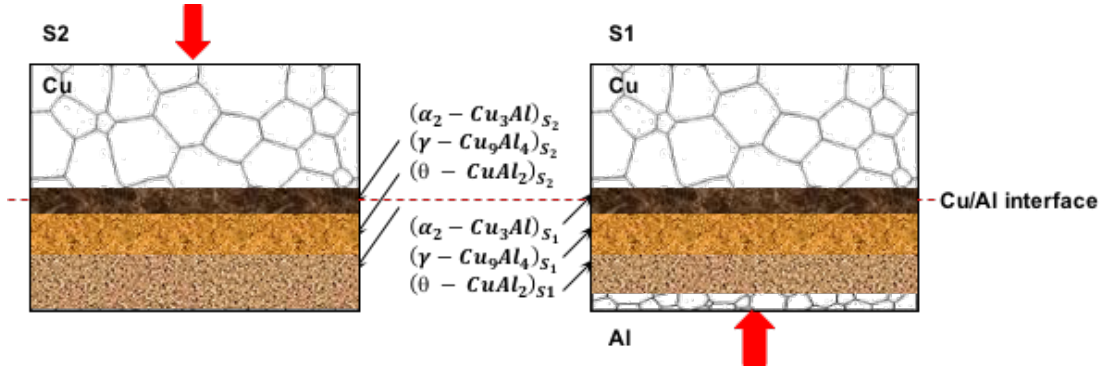


Figure 57: Wire bonded interfaces at a time  $t > t_c$

These three stages of IMC formation sequence in relation to the interface resistance dependence on EM polarity are indeed seen in our experiment. Figure 58 and Figure 59, where cross-sectional SEM microstructure of S1 and S2 is compared, shows an example.

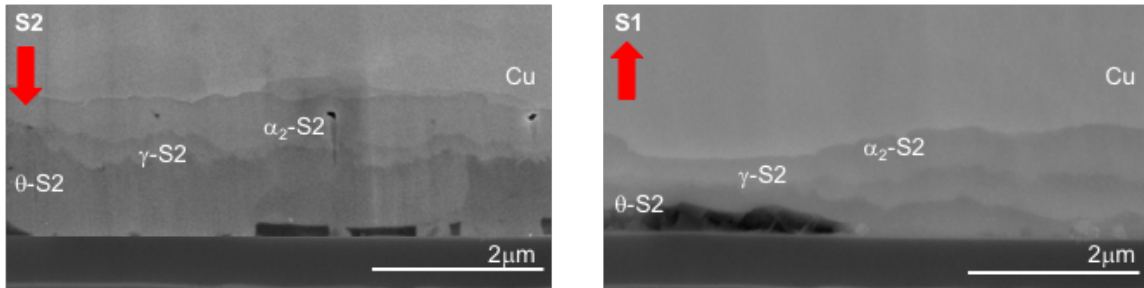


Figure 58. Magnified image of intermetallic formation in S1 and S2. EM testing conditions: 160°C and 1.75A

Note the fact that S2 shows an extensive growth of  $\theta - CuAl_2$  while the other two phases are similar in thickness to S1 interface. More quantitative measurement of interface IMC thickness after EM testing at 160°C under 1.75A for 1600 hours is summarized in Table 17. Note that overall IMC thickness is thicker in S2 due to an extended growth of the  $\theta - CuAl_2$ .

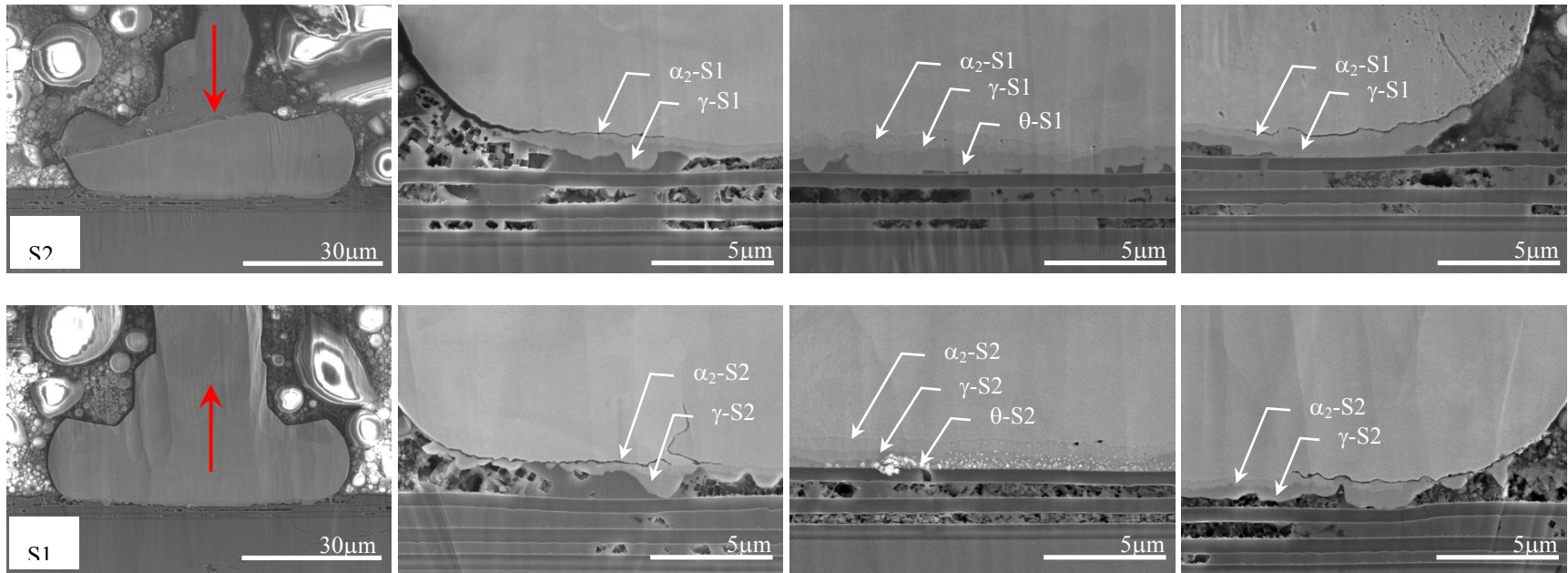


Figure 59: SEM micrographs, the arrow shows the direction of the electron flow. EM testing conditions: 160°C and 1.75A

Table 17: Average thickness measured in an electromigration tested sample

IMC	S1			S2		
	Left	Center	Right	Left	Center	Right
$\alpha_2$	0.31 $\mu\text{m}$	0.46 $\mu\text{m}$	0.37 $\mu\text{m}$	0.29 $\mu\text{m}$	0.48 $\mu\text{m}$	0.38 $\mu\text{m}$
$\gamma$	0.37 $\mu\text{m}$	0.18 $\mu\text{m}$	0.53 $\mu\text{m}$	0.47 $\mu\text{m}$	0.19 $\mu\text{m}$	0.69 $\mu\text{m}$
$\theta$	---	0.49 $\mu\text{m}$	---	---	0.74 $\mu\text{m}$	---
total	0.68 $\mu\text{m}$	1.13 $\mu\text{m}$	0.90 $\mu\text{m}$	0.76 $\mu\text{m}$	1.41 $\mu\text{m}$	1.07 $\mu\text{m}$

Finally, attempts are made to extract the interdiffusivity of Cu and Al under the influence of EM using the data given in Table 17. A kinetic model proposed by Wagner is used for this analysis and the result is shown in Table 18. Note that Al diffusivity shows a significant enhancement under S2 EM condition in all phases. This is more or less consistent with the mechanism developed in our study.

Table 18. Interdiffusion coefficients based on Wagner's equation

$\beta$	Cu		Al	
	$\bar{D}_{int}^{\beta} (S1), \mu\text{m}^2/h$	$\bar{D}_{int}^{\beta} (S2), \mu\text{m}^2/h$	$\bar{D}_{int}^{\beta} (S1), \mu\text{m}^2/h$	$\bar{D}_{int}^{\beta} (S2), \mu\text{m}^2/h$
$\alpha_2 - \text{Cu}_3\text{Al}$	0.000027	0.000035	0.000096	0.000143
$\gamma - \text{Cu}_9\text{Al}_4$	0.000039	0.000053	0.000120	0.000180
$\theta - \text{CuAl}_2$	0.000025	0.000051	0.000022	0.000047

## 4.6 Summary and discussion

### 4.6.1 IMC formation in Cu-Al system

IMC formation during the wire bonding process is known to increase the bonding strength between Cu wires and Al pads. However, their excessive growth can make the bonding interface brittle and act as a major cause for bonding failure<sup>12, 13, 80, 81, 82</sup>. While there exists no disagreement on the formation and growth of IMC and their possible contribution failure process, there still exists numerous ambiguities as to the exact nature of IMC forming at the interface and contributing factors to their growth. Such ambiguities exist because wire bonding process results in

metallurgically complex microstructure involving multiple IMCs, residual stress and other types of defects. Although our study is conducted using the actual wire bonding samples, our analysis method is highly idealized. It is therefore necessary to discuss the complexity of IMC formation in our bonding situation here so that connection of our result can be made to the process happening in actual wire bonds.

Early results reporting extremely thin Cu-Al IMC formed in the interface, which could not have been observed using an optical microscope or conventional SEM, led to speculate that there may be no IMC formation after wire bonding. However, later analysis revealed the presence of intermetallic in the “as bonded interfaces”<sup>83, 84, 85</sup>; these latest findings are confirmed when “as received” sample provided by TI is analyzed in our study (Figure 60).

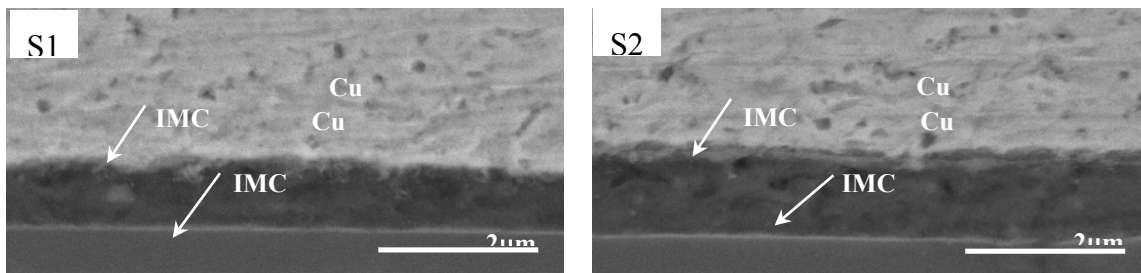


Figure 60. As received Cu-Al wire bonding sample

When the wire bonding is performed, the pressure required to form the metallurgical bond between the Cu-wire and the Al-pad is applied through the capillary. This pressure can be high enough to induce severe deformation at the ball bond. However, the particular geometry of the capillary (Figure 61) creates a stress distribution that is not homogeneous along the interface, thus resulting in uneven formation and growth of the IMC<sup>86</sup>.



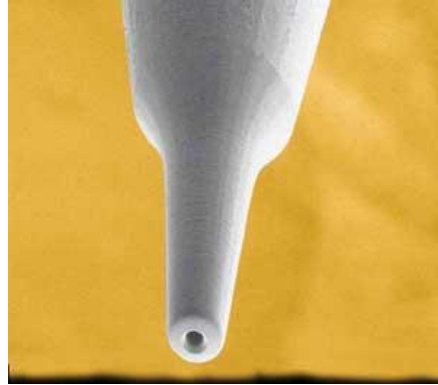


Figure 61. Capillary

According to Murali et.al.<sup>87</sup> the Cu-Al IMC distribution at the wire bond periphery is related to the shape of the clamping tool. Consequently, the larger deformation is expected to occur at the interface boundary resulting in the appearance of features such as dislocations and slip bands that could have a similar effect as vacancies on the interdiffusion process. On the other hand, the non-uniform deformation will also produce a non-uniform residual stress distribution in the bond. Thus, IMC found at the bond center, after the wire bonding is done, is more uniform and continuous, while the IMC found at the joint boundary is discontinuous and less uniform<sup>88</sup>. Lum et.al.<sup>89</sup> suggested that during the wire bonding process the “contact between the ball and pad is produced by the elastic or elastoplastic deformation, where the tensile stress occurs at the edge of the contact area”. Drosdov et.al.<sup>88</sup> speculated that IMC will primarily grow in regions where IMC has formed during the wire bonding process. Simulation performed by Chen et.al.<sup>90</sup> confirmed that the maximum residual stress gradient under pad occurs at the bond periphery. The representation of Chen et.al.<sup>90</sup> results is given by the schematic provided by Hang et.al.<sup>13</sup> (Figure 62).

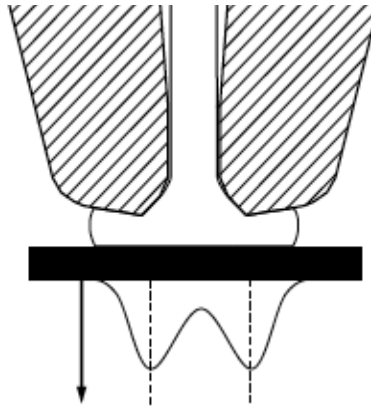


Figure 62. Schematic of residual stress distribution <sup>13</sup>

The presence of all these factors at wire bonded interface is presumed to assist the Cu-Al IMC to growth from the outer surface of the interface as they lower the activation energy of the metal atoms <sup>13</sup>. Additionally, several studies suggest that the store energy (plastic deformation energy) may influence the IMC phase growth. They found such effects by investigating the IMC formation kinetics at high temperature where the release of stored energy can be very rapid. This is a reasonable assumption to make considering the fact that the plastic deformation in wire can produce high density dislocation. Dislocation can serve as a diffusion short-circuit that can enhance the IMC growth. However, since dislocation can also be annealed out, such kinetic enhancement effect cannot last long so that its impact will be limited only to early growth of IMCs.

A number of studies have attempted to characterize the mechanism of IMC formation in Cu-Al system and some of them have concluded that the IMC formation is the result of several diffusion mechanisms taking place at the bimetallic interface <sup>19</sup>, while others insists that Cu-Al IMC growth is more sensitive to annealing temperature than annealing time <sup>91</sup>. Xu et.al. <sup>77</sup> has made two clear observations in this respect:

- IMC phases with melting temperatures higher than 1000°C will be stable at interfaces and should not significantly affect the reliability of the bond.

- IMC phases with melting temperatures below 500°C will be less stable and affect the bond reliability.

According to the binary phase diagram of the Cu-Al system (Figure 6), it is expected to have the following IMCs when working with temperatures below 300°C:  $\theta - CuAl_2$ ,  $\eta_2 - CuAl$ ,  $\xi_2 - Cu_4Al_3$ ,  $\delta - Cu_3Al_2$ ,  $\gamma - Cu_9Al_4$ . However, not all of them would appear or appear in that specific sequence because IMC formation depends on various factors. For instance, in case of welded bulk, it has been reported to have most of the possible IMC phases,  $\theta - CuAl_2$ ,  $\eta_2 - CuAl$ ,  $\xi_2 - Cu_4Al_3$ ,  $\delta - Cu_3Al_2$ ,  $\gamma - Cu_9Al_4$ , formed layer by layer and assisted by volume diffusion<sup>18</sup>. On the other hand, a thin film interdiffusion couple is known to produce only:  $\theta - CuAl_2$ ,  $\eta_2 - CuAl$ , and  $\gamma - Cu_9Al_4$  phases<sup>92</sup>. Moreover, the result variation is such that even similar studies have reported contradictory findings, such is the case of early thin film studies of Cu-Al diffusion couple where  $\theta - CuAl_2$ <sup>93</sup> was reported as the first compound nucleating at the bonded interface, but later reports found either  $\gamma - Cu_9Al_4$  or  $\eta_2 - CuAl$  being the main phase<sup>86</sup>.

Even though there exist several discrepancies about the IMC formation sequence in the Cu-Al system, it does not mean they are mistaken because there are factors that may result in such a variation of defects (e.g., vacancies, dislocations, and grain boundaries) in the crystal lattice<sup>77</sup>. Further, the wire bonding process can create large amount of localized plastic deformation at the bonded interface, that can alter the type and sequence of IMC formation at Cu-Al interface<sup>77</sup>.

Considering the possibility of having wide variety of IMC formation mechanism depending on the specifics of the wire bonding conditions, it is not so unusual that considerable variation in voiding behavior is also observed. Drozdov et.al.<sup>88</sup> suggest that there may be two type of voids at wire interface. The first type is the formed during the wire bonding process and it is largely located along the periphery of the bond. The second is the void formed by subsequent

exposure to high temperature condition. On other hand, Hang et.al.<sup>13</sup> suggest that there is no void or crack at the “as bonded interface”. They further conclude that all voids or cracks found existing at interface should be attributed to the growth of IMC phases by post wire bond heat exposure.

Similarly, some studies suggest that the failure proceeds along the boundary as a form of crack under the influence of internal stress.

All these different findings clearly suggest that IMC formation and interface failure is far more complex to be simplified. However, based on the findings made in our study, it is not so unreasonable to conclude the nature of IMC formation and failure process as follows. It is our belief that the IMC formed at Al pad/Cu wire interface is dictated by the temperature and pressure used during wire bonding. However, considering the fact that the simulative diffusion couple finds the same type of IMC phases found in the wire bond interface, it is very likely that the IMC phase forming at interface is  $\theta - CuAl_2$ . Exposure of interface to high temperature may induce the formation other phases like  $\gamma - Cu_9Al_4$  and  $\alpha_2 - Cu_3Al$ , but the most probable phase formed at interface during wire bonding is  $\theta - CuAl_2$ . Also possible is that fact that the wire bonding process leaves a considerable amount of residual stress as well as plastically deformed area, not in a uniform manner across the interface but highly localized pattern. The residual stress combined with stress generated by lattice mismatch may trigger failure by cracking. This process, however, can be dominant at lower temperature because stress can be better persisting. On the other hand, the stress and effect of localized deformation may play a small role at high temperature because such features can be quickly annealed out. At such condition, failure may be closely linked with void formation and their growth, more so that crack nucleation and growth. In either case, the failure rate must be controlled by the growth of the interface IMC because it is the source of the additional stress or the vacancies needed for voiding.

#### 4.6.2 Failure mechanism by electromigration

Our study finds the evidence supporting that EM can induce interface failure of Cu-Al wire bond. The most decisive evidence is the result showing that S2 interface shows faster failure rate than the S1 interface. This result cannot be explained without the inclusion of EM effect. The consistency of failure kinetics changing with temperature and current makes our conclusion to be firm. Microscopic analysis conducted on the EM failed samples also produces supporting evidences. The results suggest that the EM makes the interface to be much more prone to failure because it accelerates the growth of IMC phases.

While the EM failure mechanism is reasonably well understood in our study, there are two features that remain unanswered. The first has to do with the failure morphology. It is found that the interface failure appears to initiate at the outer surface of the interface and develop toward inner interface with the shape of crack. At first glance, the cracking does not seem to be a reasonable mechanism because there is no obvious source. However, considering the fact that the interface is with high residual stress, especially along the periphery of the bond, and also that lattice mismatch can generate internal stress, the failure by cracking may not be impossible. In particular, the fact that the failure starts at the outer surface of the interface strengthens our view because it is the place of high residual stress.

The failure by crack growth may also explain the EM activation energy, which is far higher than the activation energy for IMC phase growth. If EM failure proceeds in proportion to IMC phase growth, then the activation energy for EM and IMC growth should be close to each other. However, if the failure involves more than IMC growth, having two different activation energies is a possibility. Among various possibilities, we believe that the differing activation energy is related to the process of stress relaxation. The interface stress, whether residual or

developed during IMC growth, is an elastic by nature and can be released in various ways. At high temperature, the relaxation is rapid such that more time is required for interface to reach a critical point for cracking. This makes the failure rate to be slower than expected at high temperature. The end result of this effect is the higher activation energy for EM failure than that of IMC growth. Undoubtedly, this mechanism requires further analysis for confirmation; however, results obtained in our studies so far provide supportive evidence of it.

## CHAPTER 5

### 5. SUMMARY AND CONCLUSIONS

This study investigates the mechanism of EM failure in interface formed by wire bond on Al thin film pad. Using two types of samples, Cu-Al and Au-Al, the characteristic behaviors of IMC formation with and without EM are investigated.

The study find that there are at least three factors that make the IMC growth within Al pad to be favored:

- Cu faster diffusion in the Cu-Al diffusion couple ( $D_{Cu} > D_{Al}$ ).
- EM force affecting the interface movement: towards the Cu-rich region (in the case of S1) or toward the Al-rich region (in the case of S2).
- Preferential growth of IMC phase in Al pad ( $D_{gb}^{Cu} < D_{gb}^{Al}$ ).

The combination of these factors result in:

- EM failure rate of Cu/Al is far slower than Au/Al wire bonded interface. This occurs because the general interdiffusion rate is low in Cu-Al than in Au-Al system.
- S2 interface is more susceptible to failure than S1 for both Cu/Al and Au/Al wire bonded systems. This occurs because S2 is the direction where EM force makes Cu diffusion to be enhanced into Al pad (where diffusion is easier than that of Al in Cu).

Finally, it needs to be mentioned that our result provides only a fraction of mechanism under pursuit even with our best efforts. There are multiple aspects of IMC formation mechanism as well as its connection to EM failure. Among various possible studies that can be suggested as a future study, the most pressing appears to be the study of interface with high resolution microscopy. It has been our speculation that the stress is involved in EM failure and part of such

stress is related to the lattice mismatch between Cu and  $\alpha_2 - Cu_3Al$  phase. It is a possibility but remains as a speculation. An analysis by a high-resolution microscopy such as HRTEM can reveal the nature of  $\alpha_2 - Cu_3Al$  phase and the presence/absence of stress associated with it.



## 6. REFERENCES

- <sup>1</sup> Renesas, 2014: [http://www.renesas.eu/company\\_info/fab/line/line3.html](http://www.renesas.eu/company_info/fab/line/line3.html)
- <sup>2</sup> O'Connor P.: "Future Trends in Microelectronics: Impact on Detector Readout", SNIC Symposium, Stanford, California, 3 – 6 April 2006.
- <sup>3</sup> Laherrere J., 2010: <http://europe.theoil drum.com>
- <sup>4</sup> Dayah M., 1997: <http://www.p table.com/>
- <sup>5</sup> Standard Atomic Weights, 2013: <http://www.ciaaw.org/atomic-weights.htm>
- <sup>6</sup> Wolfram Research, 2016: <http://www.periodictable.com/Elements/029/data.html>
- <sup>7</sup> ASM International: "ASM Handbook, Volume 4C: Induction, Heating, and Heat Treatment", 2010.
- <sup>8</sup> Lenntech BV, 2016: <http://www.lenntech.com/>
- <sup>9</sup> ASM International: "ASM handbook, Volume 2: Properties and Selection: Nonferrous Alloy and Special Purpose Materials", 2010.
- <sup>10</sup> Automated Technology (Phil.) Inc., 2011: <http://www.atecphil.com/technologies-and-capabilities/capabilities/copper-wire-bonding.aspx>
- <sup>11</sup> Hu G., "Comparison of Copper, Silver, and Gold Wire Bonding on Interconnect Metallization", International Conference on Electronic Packaging Technology & High Density Packaging, 2012, pp. 529 – 533.
- <sup>12</sup> Kim H.J., Lee J.Y., Paik K.W., Ko K.W., Won J., Choe S., Lee J., Moon J.T., and Park Y.J.: "Effects of Cu/Al IMC (IMC) on Copper Wire and Aluminum Pad Bondability", IEEE Transactions on Components and Packaging Technologies, Vol. 26, No. 2, June – 2003, pp. 367 – 374.

- <sup>13</sup> Hang C.J., Wang C.Q., Mayer M., Tian Y.H., Zhou Y., and Wang H.H.: “Growth Behavior of Cu/Al IMCs and Cracks in Copper Ball Bonds During Isothermal Aging”, *Microelectronics Reliability*, Vol. 48, 2008, pp. 416 – 424.
- <sup>14</sup> LTPMN, 2012: <http://www.conductivity-app.org/single-article/cu-overview>
- <sup>15</sup> Altek-MHD, 2016: <http://altek-mhd.com/en/articles/overview2k>
- <sup>16</sup> Ponweiser N., Lengauer C., and Richter K.: “Re-investigation of Phase Equilibria in the System Al-Cu and Structural Analysis of the High-Temperature Phase  $\eta_1$ -Al<sub>1- $\delta$</sub> Cu”, *Intermetallics*, Vol. 19, 2011, pp. 1737 – 1746.
- <sup>17</sup> Wikipedia, 2016: [https://en.wikipedia.org/wiki/List\\_of\\_space\\_groups](https://en.wikipedia.org/wiki/List_of_space_groups)
- <sup>18</sup> Funamizu Y. and Watanabe K.: “Interdiffusion in the Al-Cu system”, *Trans. Japan Institute of Metals*, 1971, Vol. 12, pp. 147 – 152.
- <sup>19</sup> Pfeifer S., Großmann S., Freudenberger R., Willing H., and Kappl H.: “Characterization of IMCs in Cu-Al Bimetallic Interfaces”, *IEEE*, 2012.
- <sup>20</sup> Mishler Codie Michael: “Interface Reaction Induced Stress Development in an Aluminum Thin Film Copper Bulk Plate Diffusion Couple”, The University of Texas at Arlington, 2015.
- <sup>21</sup> Wulff F.W., Breach C.D., Stephan D., Saraswasti, and Dittmer K.J.: “Characterization of Intermetallic Growth in Copper and Gold Ball Bonds on Aluminum Metallization”, *IEEE Electronics Packaging Technology Conference*, 2004, pp. 348 – 353.
- <sup>22</sup> Kouters M.H.M., Gubbels G.H.M., O’Halloran O., and Rongen R.: “Characterization of IMCs in Cu-Al Ball Bonds: Layer Growth, Mechanical Properties and Oxidation”, *13<sup>th</sup> International Conference on Thermal, Mechanical and Multi-Physics Simulation and Experiments in Microelectronics and Microsystems*, 2012.

- <sup>23</sup> Ivy Wei Qin: “Wire bonding tutorial”, Solid State Technology: Inside for Electronics Manufacturing, Advances in Bonding Technology, July 2005.
- <sup>24</sup> Harman G.G.: “Wire Bonding in Microelectronics: Materials, Processes, Reliability and Yield”, McGraw Hill, New York – U.S.A., Second Edition, 1997.
- <sup>25</sup> Pan J. and Fraud P.: “Wire Bonding Challenges in Optoelectronics Packaging”, Society of Manufacturing Engineers, 2004.
- <sup>26</sup> Yu S., Wan M., and Hon M.: “Formation of IMCs at Eutectic Sn-Zn-Al Solder/Cu Interface”, Journal of Materials Research, Vol. 16, No.1, January 2001, pp. 76 – 82.
- <sup>27</sup> Lee, Y.G. and Duh J.G.: “Characterizing the Formation and Growth of IMC in the Solder Joint”, Journal of Materials Science, 33, 1998, pp. 5569 – 5572.
- <sup>28</sup> Mehrer, H.: “Diffusion in Solids: Fundamentals, Methods, Materials, Diffusion-Controlled Processes”, Springer, 2007.
- <sup>29</sup> Dohmen R. and Milke R.: “Diffusion in Polycrystalline Materials: Grain Boundaries, Mathematical Models and Experimental Data”, Reviews in Mineralogy & Geochemistry, Vol. 72, 2010, pp. 921 – 970.
- <sup>30</sup> Balluffi R.W., Allen Samuel M. and Carter W. Craig: “Kinetic of Materials”, Jon Wiley & Sons Inc., 2005.
- <sup>31</sup> Flewitt P.E.J. and Wild R.K.: “Grain Boundaries: Their Microstructure and Chemistry”, Jon Wiley & Sons Ltd., 2001.
- <sup>32</sup> Porter D.A. and Easterling K.E.: “Phase Transformations in Metals and Alloys”, Florida – U.S.A., Third Edition, 2004.
- <sup>33</sup> Mishin Y. and Herzig C.: “Grain Boundary Diffusion: Recent Progress and Future Research”, Materials Science and Engineering A260, 1999, pp. 55 – 71.

- <sup>34</sup> Suzuoka T.: “Lattice and Grain Boundary Diffusion in Polycrystals”, *Trans. Japan Institute of Metals*, Vol. 2, 1961, pp. 25 – 33.
- <sup>35</sup> Belova I.V., Fiedler T., and Murch G.E.: “The Harrison Diffusion Kinetics Regimes in Solute Grain Boundary Diffusion”, *Philosophical Magazine*, Vol. 92, No. 14, May 2012, pp. 1748 – 1763.
- <sup>36</sup> Murch Graeme and Nowick Arthur: “Diffusion in Crystalline Solids”, Academic Press Inc., 1984.
- <sup>37</sup> Kozubski, R.: “Recent Progress in Diffusion Thermodynamics and Kinetics in IMCs”, Switzerland, *Trans. Tech. Publications Ltd.*, 2014.
- <sup>38</sup> Fields R.J., Low S.R., and Lucey G.K.: “Physical and Mechanical Properties of IMCs Commonly Found in Solder Joints”, *Metal Science of Joining*, 1991.
- <sup>39</sup> Mehrer H.: “Diffusion in Intermetallics”, *Material Transactions*, Japan Institute of Metals, Vol. 37, No. 6, 1996, pp. 1259 – 1280.
- <sup>40</sup> Nakajima H., Spregel W., and Nonaka K.: “Diffusion in IMCs”, *Intermetallics* 4, 1996, S17 – S28.
- <sup>41</sup> He P. and Liu D.: “Mechanism of Forming Interfacial IMCs at Interface for Solid State Diffusion Bonding of Dissimilar Materials”, *Materials Science & Engineering A* 437, 2006, pp. 430 – 435.
- <sup>42</sup> Paul A., Ghosh C., and Boettinger W.: “Diffusion Parameters and Growth Mechanism of Phases in the Cu-Sn System”, *Metallurgical and Material Transactions Volume* 42A, April 2011, pp. 952 – 963.
- <sup>43</sup> Wagner C.: “The Evaluation of Data Obtained with Diffusion Couples of Binary Single-Phase and Multiphase Systems”, *Acta Metallurgica*, Vol. 17, February 1969, pp. 99 – 107.

- <sup>44</sup> Van Loo F.J.J., Pieraggi B., and Rapp R.A.: “Interface Migration and the Kirkendall Effect in Diffusion-Driven Phase Transformations”, *Acta Metallurgica of Materials*, Vol. 38, No. 9, 1990, pp. 1769 – 1779.
- <sup>45</sup> ITRS Reports, 2009: “International Technology Roadmap for Semiconductors, 2009 edition Assembly and Packaging”.
- <sup>46</sup> Xu C., Sritharan T., and Mhaisalkar S.G.: “Interface Transformations in Thin Film Aluminum-Gold Diffusion Couple”, *Thin Film Solids* 515, 2007, pp. 5454 – 5461.
- <sup>47</sup> Murray J.L., Okamoto H., and Massalski T.B.: “The Au-Al (Gold-Aluminum) System”, *Bulletin of Alloy Phase Diagrams*, Vol 8, No. 1, 1987, pp. 20 – 30.
- <sup>48</sup> Philofsky E.: “Intermetallic Formation of Gold-Aluminum Systems”, *Solid State Electronics*, Vol. 13, 1970, pp. 1391 – 1399.
- <sup>49</sup> Markwitz N., Vandesteene M., Waldschmidt M., and Demortier G.: “Characterization of the Interdiffusion in Au-Al Layers by RBS”, *Fresenius’ Journal of Analytical Chemistry*, 1997, pp. 59 – 63.
- <sup>50</sup> Straumanis M.E. and Chopra K.S.: “Lattice Parameters, Expansion Coefficients and Extent of the Al<sub>2</sub>Au Phase”, *Zeitschrift für Physikalische Chemie Neue Folge*, Bd. 42, 1964, pp. 344 – 350.
- <sup>51</sup> Frank K. and Schubert K.: “Kristallstruktur von AuAl”, *Journal of Less Common Metals*, Volume 22, Issue 3, 1970, pp. 349-354.
- <sup>52</sup> Puselj, M. and Schubert K.: “Kristallstrukturen der Phasen Au<sub>2</sub>Al (h), Au<sub>2</sub>Al<sub>1-(r)</sub> und Au<sub>2</sub>Al<sub>1+(r)</sub>”, *Journal of Less Common Metals*, Volume 35, Issue 2, 1974, pp. 259 – 266.
- <sup>53</sup> Range K.-J. and Büchler H.: “Hochdrucksynthese und Kristallstruktur von Al<sub>3</sub>Au<sub>8</sub>”, *Journal of Less Common Metals*, Volume 154, Issue 2, 1989, pp. 251 – 260.

- <sup>54</sup> Range K.-J. and Büchler H.: “Zur Kenntnis des  $\beta$ -Mangan-typs: Hochdrucksynthese und strukturverfeinerung von  $\text{AlAu}_4$ ”, *Journal of Less Common Metals*, Volume 161, Issue 2, 1990, pp. 347 – 354.
- <sup>55</sup> Majni G., Nobili C., Ottaviani G., Costato M., and Galli E.: “Gold-Aluminum Thin-Film Interactions and Compound Formation”, *Journal of Applied Physics*, Vol. 52, No. 6, June 1981, pp. 4047 – 4054.
- <sup>56</sup> Ulrich C.M., Hashibon A., Svoboda J., Elsässer C., Helm D., and Riedel H.: “Diffusion Kinetics in Aluminum-Gold Bond Contacts from First Principles Density Functional Calculations”, *Acta Materialia* 59, 2011, 7634-7644.
- <sup>57</sup> Tamou Y., Li J., Russel S.W., and Mayer J.: “Thermal Ion Beam Induced Thin Film Reactions in Cu-Al Bilayers”, *Nuclear Instruments & Methods in Physics Research*, Vol. 64, 1992, pp. 130 – 133.
- <sup>58</sup> Yu Y.H., Wang Y.W., Appelt B.K., Lai Y.S., and Kao C.R.: “Growth of Cu-Al IMCs in Cu and Cu (Pd) Wire Bondings”, *IEEE Electronic Components and Technology Conference*, 2011, pp. 1481 – 1488.
- <sup>59</sup> Na S., Hwang T., Park J., Kim J., Yoo H., and Lee C.: “Characterization of Intermetallic Compound (IMC) Growth in Cu Wire Ball Bonding on Al Pad Metallization”, *IEEE Electronic Components and Technology Conference*, 2011, pp.1740 – 1745.
- <sup>60</sup> Black, J.R.: “Electromigration a Brief Survey and Some Recent Results”, *IEEE Transactions on Electronic Devices*, Vol. 16, No. 4, April 1969, pp. 338 – 347.
- <sup>61</sup> Black, J.R.: “Mass Transport of Aluminum by Momentum Exchange with conducting electrons”, 6<sup>th</sup> Annual Reliability Physics Symposium, Los Angeles, 1967.

- <sup>62</sup> Black, J.R.: “Electromigration Failure Modes in Aluminum Metallization for Semiconductor Devices”, Proceeding of the IEEE, Vol. 57, No. 9, September 1969, pp. 1587- 1594.
- <sup>63</sup> Nah J.W., Suh J.O., and Tu K.N.: “Effect of Current Crowding and Joule Heating on Electromigration-Induced Failure in Chip Composite Solder Joints Tested at Room Temperature”, Journal of Applied Physics, Vol. 98, 2005.
- <sup>64</sup> Middle East Technical University, Computer Simulation Laboratory, 2005: [www.cls.mete.metu.edu.tr/Electromigration/emig.htm](http://www.cls.mete.metu.edu.tr/Electromigration/emig.htm)
- <sup>65</sup> Lienig J., “Invited Talk: Introduction to Electromigration-Aware Physical Design”, International Symposium on Physical Design, 2006, pp. 39 – 46.
- <sup>66</sup> Lloyd J.R.: “Electromigration Failure”, Journal of Applied Physics, Vol. 69, No. 11, 1991, pp. 7601 – 7604.
- <sup>67</sup> Kirchheim R. and Kaeber U.: “Atomistic and Computer Modeling of Metallization Failure of Integrated Circuits by Electromigration”, Journal of Applied Physics, Vol. 70, No. 1, 1991, pp. 172 – 181.
- <sup>68</sup> Lloyd J.R. and Shatzkes M.: “A model for Conductor Failure Considering Diffusion Concurrently with Electromigration resulting in a current exponent of 2”, Journal of Applied Physics, Vol. 59, No. 11, 1986, pp. 3890 – 3893.
- <sup>69</sup> Kirchheim R.: “Stress and Electromigration in Al-lines of Integrated Circuits”, Acta Metallurgica et Materialia, Vol. 40, No. 2, 1992, pp. 309 – 323.
- <sup>70</sup> Korhonen M.A. and Borgesen P.: “Stress Evolution due to Electromigration in Confined Metal Lines”, Journal of Applied Physics, Vol. 73, No. 8, 1993, pp. 3790 – 3799.
- <sup>71</sup> Lloyd J.R.: “Black’s Law Revisited – Nucleation and Growth in Electromigration Failure”, Microelectronics Reliability, Vol. 47, 2007, pp. 1468 – 1472.

- <sup>72</sup> Zin E., Michaels N., Kang S.H., Oh K.H., Chul U., Cho J.S., Moon J.T., and Kim C.-U.: “Mechanisms of Electromigration in Au/Al Wire Bond and its Effects”, Electronic Components and Technology Conference, 2009, pp. 943 – 947.
- <sup>73</sup> Lienig J.: “Interconnect and Current Density Stress – An Introduction to Electromigration – Aware Design”, IEEE, 2005, pp. 81 -88.
- <sup>74</sup> Lloyd J.R., Clemens J., and Snede R.: “Copper Metallization Reliability”, Microelectronics Reliability, 1999, pp. 1595 – 1602.
- <sup>75</sup> Siewert T.A., Madeni J.C., and Liu S.: “Formation and Growth of Intermetallics at the Interface Between Lead-Free Solders and Copper Substrates”, NIST.
- <sup>76</sup> Xu H., Liu C., Silberschmidt V.V., Pramana S.S., White T.J., Chen Z., and Acoff V.L.: “Behavior of Aluminum Oxide, Intermetallics and Voids in Cu-Al wire bonds”, Acta Materialia, 2011, pp. 5661 – 5673.
- <sup>77</sup> Xu H., Liu C., Silberschmidt V., and Chen Z.: “Growth of IMCs in Thermosonic Copper Wire Bonding on Aluminum Metallization”, Journal of Electronic Materials, Vol. 39, No. 1, 2010, pp. 124 – 131.
- <sup>78</sup> Chen L.D., Huang M.L., and Zhou S.M.: “Effect of Electromigration on IMC Formation in Line-Type Cu/Sn/Cu Interconnect”, Journal of Alloys and Compounds, Vol. 504, 2010, pp. 535 – 541.
- <sup>79</sup> Mishler C., Ouvarov-Bancalero V., Chae S., Nguyen L., and Kim C.-U.: “IMC Growth and Stress Development in Al-Cu Diffusion Couple”, submitted to Journal of Materials Science for publication, 2016.



- <sup>80</sup> Xu H., Liu C., Silberschmidt V., and Chen Z.: “Growth of IMCs in Thermosonic Copper Wire Bonding on Aluminum Metallization”, *Journal of Electronic Materials*, Vol. 39, No. 1, 2010, pp. 124 – 131.
- <sup>81</sup> Tian Y., Hang C., Wang C., and Zhou Y.: “Evolution of Cu/Al IMCs in the Copper Bump Bonds During Aging Process”, *IEEE*, 2007.
- <sup>82</sup> Drozdov M., Gur G., Atzmon Z., and Kaplan W.D.: “Detailed Investigation of Ultrasonic Al-Cu Wire Bonds: I. Intermetallic Formation in the As-bonded State”, *Journal of Material Science*, Vol. 43, 2008, pp. 6029 – 6037.
- <sup>83</sup> Ratched P., Stoukatch S., and Swinnen B.: “Mechanical Reliability of Au and Cu Wire Bonds to Al, Ni/Au and Ni/PD/Cd Capped Cu Bond Pads”, *Microelectronics Reliability*, Vol. 46, 2005, pp. 1315 – 1325.
- <sup>84</sup> Murali S., Srikanth N., and Vath C.J.: “An Analysis of Intermetallic Formation of Gold and Copper Ball Bonding on Thermal Aging”, *Materials Research Bulletin*, Vol. 38, 2003, pp. 637 – 646.
- <sup>85</sup> Murali S., Srikanth N., and Vath C.J.: “An Evaluation of Gold and Copper Ball Bonds on Shear and Pull Testing”, *Journal of Electronic Packaging*, Vol. 128, September 2006, pp. 192 – 201.
- <sup>86</sup> Lu Y.H., Wang Y.W., Appelt B.K., Lai Y.S., and Kao C.R.: “Growth of Cu/Al IMCs in Cu and Cu(Pd) Wire Bonding”, *Electronic Components and Technology Conference*, 2011, pp. 1481 – 1488.
- <sup>87</sup> Murali S., Srikanth N., and Vath C.J.: “Grains, Deformation Substructures and Slip Bands Observed in Thermosonic Copper Ball Bonding”, *Materials Characterization*, Vol. 50, 2003, pp. 39 – 50.

- <sup>88</sup> Drozdov M., Gur G., Atzmon Z., and Kaplan W.D.: “Detailed Investigation of Ultrasonic Al-Cu Wire Bonds: II Microstructural Evolution During Annealing”, *Journal of Material Science*, Vol. 43, 2008, pp. 6038 – 6048.
- <sup>89</sup> Lum I., Jung J.P., and Zhou Y.: “Bonding Mechanism in Ultrasonic Ball Bonds on Copper Substrate”, *Metallurgical and Materials Transactions A*, Vol. 36A, 2005, pp. 1279 – 1286.
- <sup>90</sup> Chen J., Degryse D., Ratchev P., and De Wolf I.: “Mechanical Issues of Cu-to-Cu Wire Bonding”, *IEEE Transactions on Components and Packaging Technologies*, Vol. 27, No. 3, September 2004, pp. 539 – 545.
- <sup>91</sup> Kim H.J., Lee J.Y., Paik K.W., Koh K.W., Won J., Choe S., Lee J., Moon J.T., and Park Y.J.: “Effects of Cu/Al IMC (IMC) on Copper Wire and Aluminum Pad Bondability”, *IEEE Transactions on Components and Packaging Technologies*, Vol. 26, No. 2, June 2003, pp. 367 – 374.
- <sup>92</sup> Rajan K. and Wallach E.R.: “A Transmission Electron Microscopy Study of Intermetallic Formation in Aluminum-Copper Thin-Film Couples”, *Journal of Crystal Growth*, Vol. 49, 1980, pp. 297 – 302.
- <sup>93</sup> Tamou Y., Li J, Russell S.W., and Mayer J.: “Thermal and Ion Beam Induced Thin Film Reactions in Cu – Al Bilayers”, *Nuclear Instruments and Methods in Physics Research B64*, 1992, pp. 130 – 133.
- <sup>94</sup> Jang G., Duh J., Takahashi H., and Su D.: “Solid-State Reaction in an Au Wire Connection with an Al-Cu Pad During Aging”, *Journal of Electronic Materials*, Vol. 35, Issue 2, February 2006, pp. 323 – 332.
- <sup>95</sup> Bhadeshia H.: “Diffusion-Controlled Growth”, *Kinetics and Microstructure Modelling*.

- <sup>96</sup> Erickson K., Hopkins P., and Vianco P.: “Solid State IMC Growth Between Copper and High Temperature, Tin-Rich Solders – Part II: Modeling”, *Journal of Electronic Materials*, Vol. 33, Issue 8, August 1994, pp. 729 – 734.
- <sup>97</sup> Mei Z., Sunwoo A.J., and Morris J.W.: “Analysis of Low-Temperature Intermetallic Growth in Copper-Tin Diffusion Couples”, *Metallurgical Transaction A*, Volume 23, Issue 3, March 1992, pp. 857 – 864.
- <sup>98</sup> Schaefer M., Fournelle R., and Liang J.: “Theory for Intermetallic Phase Growth Between Cu and Liquid Sn-Pb Solder Based on Grain Boundary Diffusion Control”, *Journal of Electronic Materials*, Vol. 27, No. 11, 1998, pp. 1167 – 1177.
- <sup>99</sup> Vianco P., Hlava P., and Kilgo A.: “IMC Layer Formation Between Copper and Hot-Dipped 100In, 50In-50Sn, 100Sn and 63Sn-37Pb Coatings”, *Journal of Electronic Materials*, Vol. 23, No. 7, 1994, pp. 583 – 594.
- <sup>100</sup> Vianco P., Erickson K., and Hopkins P.: “Solid State IMC Growth Between Copper and High Temperature Tin-Rich Solders – Part I: Experimental Analysis”, *Journal of Electronic Materials*, Vol. 23, No. 8, 1994, pp. 721 – 727.
- <sup>101</sup> Kim H.K., Liou H.K., and Tu K.N.: “Three-Dimensional Morphology of a Very Rough Interface Formed in the Soldering Reaction Between Eutectic SnPb and Cu”, *Applied Physics Letters*, Vol. 66, Issue 18, May 1995, pp. 2337 – 2339.
- <sup>102</sup> Schaefer M., Laub W., Sabee J., and Fournelle R.: “A Numerical Method for Predicting Intermetallic Layer Thickness Developed During the Formation of Solder Joints”, *Journal of Electronic Materials*, Vol. 25, No. 6, 1996, pp. 992 – 1003.

- <sup>103</sup> Kim C.-U., Morris J.W., and Lee H.-M.: “Kinetics of Electromigration-induced Edge Drift in Al-Cu Thin Films Interconnects”, *Journal of Applied Physics*, Vol. 82, No. 4, 1997, pp. 1592 – 1598.
- <sup>104</sup> Chen C. and Hwang W.: “Effect of Annealing on the Interfacial Structure of Aluminum-Copper Joints”, *Materials Transactions*, Vol. 48, No. 7, 2007, pp. 1938 – 1947.
- <sup>105</sup> Lee W., Bang K., and Jung S.: “Effects of IMC on the Electrical and Mechanical Properties of Friction Welded Cu/Al Bimetallic Joints During Annealing”, *Journal of Alloys and Compounds*, 390, 2005, pp. 212 – 219.
- <sup>106</sup> Siewert T.A., Madeni J.C., and Liu S.: “Formation and Growth of Intermetallics at the Interface Between Lead-Free Solders and Copper Substrates”, *Proceedings of the APEX Conference on Electronics Manufacturing*, Vol. 23, No. 7, 2003, pp. 583 – 594.
- <sup>107</sup> Guuo, Y., Liu G., Jin H., Shi Z., and Qiao G.: “Intermetallic Phase Formation in Diffusion-Bonded Cu/Al Laminates”, *Journal of Material Science*, 2011, pp. 2467 – 2473.
- <sup>108</sup> Erickson K.L., Hopkins P.L., and Vianco P.T.: “Modeling the Solid-State Reaction Between Sn-Pb Solder and a Porous Substrate Coating”, *Journal of Electronic Materials*, Vol. 27, No. 11, 1998, pp. 1177 – 1192.

## 7. BIOGRAPHICAL INFORMATION

Patricia Aracelly Rodriguez – Salazar received her B.S. in Mechanical Engineering from the Polytechnic National School (Escuela Politécnica Nacional), Quito – Ecuador, in 1999 and her Masters of Engineering in Mechanical Engineering from Gannon University, Erie – PA in 2008. She joined the University of Texas at Arlington in 2010 in order to pursue her Ph.D. in Materials Science and Engineering. During her studies, she became a member in the Electronics Materials Laboratory where she worked in testing of electronic packaging reliability under electromigration and high temperature conditions as well as performing tasks such as mechanical and electrical design and manufacture and assembly of testing equipment.